U.S. Department of Transportation
Federal Aviation Administration

FINAL PROJECT REPORT

Form Approved:
O.M.B. No. 2120-0559
9/30/2013

PART I - PROJECT IDENTIFICATION INFORMATION

1. Institution and Address	2. FAA Program	3. FAA Award Number
Georgia Institute of Technology-ASDL	AJFE	13-C-AJFE-GIT – 063
270 Ferst Drive NW, Atlanta, GA 30332-0150	4. Award Period From 06/05/2020 To 02//29/2024	5. Cumulative Award Amount $533,333 (with Cost Share)

6. Project Title
ASCENT Project 059A: Jet Noise Modeling to Support Low Noise Supersonic Aircraft Technology Development

PART II - SUMMARY OF COMPLETED PROJECT (For Public Use)

This project sought to understand the degree to which a 2D supersonic inlet with variable geometry could mitigate thrust losses associated with the addition of jet noise reduction technologies, without overcoming the noise benefits from those technologies, during landing and takeoff (LTO) conditions. The work developed a supersonic inlet modeling capability to predict inlet impacts to performance and aerodynamics and then utilized a supersonic transport aircraft with mixed flow turbofan engine models using a multidisciplinary analysis code for supersonic aircraft, which couples the NPSS engine modeling code with several NASA codes for mission analysis (FLOPS), compressor map generation (CMPGEN), and noise prediction (ANOPP). The study modeled the fixed aircraft and engine with an added nozzle-based noise reduction technology in the form of chevrons, and fixed supersonic inlet model, and then performed follow on studies to understand how varying the inlet geometry with a variable geometry cowl lip and/or blow-in doors could improve mass flowrate availability at LTO conditions and it ' s effects on a selection of chevrons attached to the engine CD plug nozzle. Results showed that these inlet design features can mitigate thrust losses for LTO, while maintaining sufficient thrust to complete the mission. However, selection of inlet feature for mass flowrate increase and effects at different observed directivity angles vary.

PART III - TECHNICAL INFORMATION (For Program Management Uses)

1. **ITEM** (Check appropriate blocks)	NONE	ATTACHED	PREVIOUSLY FURNISHED	TO BE FURNISHED SEPARATELY TO PROGRAM	
				Check (X)	Approx. Date
a. Abstracts of Theses		✘			
b. Publication Citations	✘				
c. Data on Scientific Collaborators		✘			
d. Information on Inventions	✘				
e. Technical Description of Project and Results		✘			
f. Other (specify)					

2. Principal Investigator/Project Director Name (Typed)	3. Principal Investigator / Project Director Signature	4. Date
Mr. James D. Kenny, Jr.	James Kenny	04/21/2025

FAA Form 9550-5 (03-03) Supersedes Previous Edition

Project 059(A) Jet Noise Modeling to Support Low Noise Supersonic Aircraft Technology Development

Georgia Institute of Technology

Project Lead Investigators

Dimitri Mavris
Regents Professor
School of Aerospace Engineering
Georgia Institute of Technology
Mail Stop 0150
Atlanta, GA 30332-0150
404-894-1557
Dimitri.mavris@ae.gatech.edu

Jimmy Tai
Senior Research Engineer
School of Aerospace Engineering
Georgia Institute of Technology
Mail Stop 0150
Atlanta, GA 30332-0150
404-894-0197
jimmy.tai@ae.gatech.edu

University Participants

Georgia Institute of Technology (Georgia Tech or GT)

- P.I.s: Dr. Dimitri Mavris (P.I.), Dr. Jimmy Tai (co-P.I.)
- FAA Award Number: 13-C-AJFE-GIT-070
- Period of Performance: October 1, 2022, to December 31, 2023

Project Funding Level

The ASCENT Project 059(A) is funded at the following levels: Georgia Tech, $100,000.

Georgia Tech has agreed to a total of $100,000 in matching funds. This total includes salaries for the project director, research engineers, and graduate research assistants, as well as computing, financial, and administrative support, including meeting arrangements. Georgia Tech has also agreed to provide tuition remission for the students, paid for by state funds. During the period of performance, in-kind cost sharing is also obtained for cost share.

Investigation Team

Georgia Institute of Technology

Dimitri Mavris, P.I.
Jimmy Tai, Co-Investigator
James Kenny, Project Manager/Technical Lead, Primary technical developer, project manager, and student advisor
Jai Ahuja, Supporting Engineer, Supporting technical developer, aerodynamics subject matter expert (SME)
Students: Student technical support role involved completing various tasks to support completion of supersonic inlet code, actual tasks varied depending on timeframe support provided.
Noah Chartier, Graduate Research Assistant, Provided technical support from 2021 to 2022, co-developed majority of the inlet code with James Kenny
Andrew Tai, Undergraduate Research Assistant, Supported between late 2021 to early 2022

Sijian Tan, Graduate Research Assistant, Supported inlet code development from mid-2022 to end of period of performance.

Project Overview

The original purpose of this project was to develop and assess computational tools to simulate the flow and noise of civil supersonic aircraft engines and to identify novel methods for noise reduction. In addition to noise predictions, the impact of the noise reduction methods on overall engine performance would be assessed. The predictions would include consideration of the engine inlet, engine cycle, mixers and ejectors, and unsteady jet exhaust. Accurate prediction of the engine exhaust flow would enable the noise generated by the theoretical system to be computed. Predictions were to be assessed through comparison with available experimental measurements provided by ASCENT Project 059 research partners focusing on experimental methods.

In discussion with the Federal Aviation Administration (FAA), the overall direction of the project was changed in fiscal year (FY) 2022 of the project. Instead of developing and simulating jet noise reduction technologies, ASCENT Project 059(A) will provide an assessment of the benefits addressing the supersonic jet noise problem through a different approach—considering the supersonic inlet's effects on maintaining thrust while jet noise devices are employed on the engine nozzle, and ensuring a retention of jet noise reduction, precluding the necessitation of a higher throttle setting, which could potentially negate any benefits seen to thrust. To support this, models for inlet performance, a coupled engine and aircraft model, and jet noise technology models were required to be developed and integrated. Although the primary objectives anticipated for ASCENT Project 059(A) being supported by experimental data provided by other ASCENT Project 059 technical partners, including the work of jet noise experimentation teams, experimental data to be used in this simulation was not able to be generated by the technical partners due to technical difficulties. As such, the Georgia Tech team was required to perform extensive literature review and develop modeling capabilities to simulate jet noise reduction technology designs and their effects and integrate into their broader models.

As a result of this change, the research goal for the Georgia Tech team in Year 2 shifted to pursue means to identify a thrust–noise break-even relationships for arbitrary and real nozzle-based jet noise reduction technologies. In the final year of the project (Year 3), this objective was superseded by a more focused approach in modeling the effects of a parameterized family of supersonic chevrons applied to a fixed 65-passenger aircraft model with a design Mach number of 1.7, using a supersonic mixed-flow turbofan engine model with axisymmetric plug nozzle. The study seeks to understand if a custom-designed supersonic inlet, which functions acceptably well while installed on a vehicle for an entire supersonic transport (SST) mission profile would be able to recover the thrust lost due to chevrons applied to that fixed engine and aircraft configuration. If it were not, researchers sought to determine how much better variable geometry features applied to the same inlet could perform, again, attempting to minimize thrust loss and retain noise reduction properties provided by the chevrons. This study seeks to identify whether an improved and variable geometry inlet can recover thrust lost by the nozzle technology installed on an engine, while precluding the need to resize the engine, which would likely increase the likelihood of greater noise production due to increased thrust, and also precluding the need for the landing and take-off (LTO) throttle setting to be increased, having the same effect as an upsized engine. This slight modification to the scope of the previously defined primary research objective removes the ambiguity associated with coupling arbitrary sets of thrust loss values with noise reduction values in reasonable proportions to one another, which would be performed for a thrust-noise breakeven analysis, instead, pursuing designs which could actually be encountered by actual jet noise reduction devices applied to nozzles.

Also in Year 2, the goal of implementing low-fidelity, low-speed aerodynamics models to be implemented for the supersonic inlet and new variable-geometry models to determine whether any thrust lost by the addition of the jet noise technology can be recovered by sole use of inlet variable geometry (including the external compression inlet ramps or cone, a variable-geometry cowl lip, and potentially blow-in doors), without further manipulation of the throttle were to be developed. These tasks were retained and completed in the work presented below. In future work, higher-fidelity modeling capabilities may be incorporated into the zeroth-order inlet performance tool, if this area of study appears promising because of work completed here. Essentially, our team sought to identify and explore ways to facilitate rapid exploration of installed engine configurations, ensure that the selected nozzle-based jet noise technology does not degrade aircraft thrust to an extent that the technology is no longer beneficial, and to determine the effectiveness of off-design variable-geometry configurations for conditions of low speed/high inlet air demand conditions.

Project Introduction

As previously discussed, the main objectives of this research project in the first two years (Year 1 and Year 2) were twofold. First, to facilitate the capability to perform thrust-noise break-even studies for arbitrary nozzle-based jet noise technologies. Second, to develop capabilities to identify the impacts of supersonic inlet configurations and designs on thrust recovery—thus ultimately determining whether off-design supersonic inlet configurations can recover the thrust detriment from noise technologies used for jet noise regulation compliance. Because of the Georgia Tech team's departure from being coupled with Pennsylvania State University (PSU) researchers, and the modification of the overall project direction, the major project milestones for Years 2 and 3 were modified. Furthermore, as the Year 3 objective was redefined to explore the impacts of a specific jet noise reduction technology, chevrons, the project milestones listed below were modified even further and extended to capture the discrete sections of work completed to answer the research questions proposed.

Regarding earlier project milestones, such as Task 2.2 which was previously described as "Determination of boundary conditions from 'Vision SST Engine Cycle'," the replacement task for this period was to continue improvement of Task 2.1, "Assembly of zeroth-order methods to predict inlet performance." At the initially projected due date for Task 2.1, the supersonic inlet analysis tool developed during Year 1, although functional, was found to lack many capabilities necessary to analyze the installed inlet performance across the SST mission profile. While the project only sought to understand LTO performance, the design and installation of an advanced inlet configuration which would operate in a realistic SST mission profile, resulting in a realistic SST engine and aircraft design was sought out to serve as the baseline for this work. Some, but not all, of these lacking capabilities included the abilities to predict required inlet capture area, accurately calculate internal shock quantity and positioning and the associated losses for mixed compression conditions for a supersonic two-dimensional (2D) inlet to (1) predict and determine additive (pre-entry) drags and cowl lip suction forces, (2) predict the location and corresponding strength of the normal shock when swallowed, and (3) accurately predict the low-speed aerothermodynamic losses associated with conditions of low-speed and high-air-demand conditions (i.e., take-off). Furthermore, our team used all of Year 2 to improve the supersonic inlet analysis tool's user interface and perform debugging to achieve highly robust performance across a variety of supersonic inlet geometries and mission profiles—from external compression to mixed compression inlets, as well as from transonic design Mach numbers to low hypersonic values (1.2 to 5) and off-design cases. As a result of this work, the tool was found to be able to perform well in all explored and conditions compared to published inlet data. Additionally, the tool was integrated with the team's internal supersonic aircraft and engine sizing and synthesis tool (Flight Analysis for Supersonic Transports [FASST], also used for ASCENT Project 010), by converting the inlet code into a rapid-running executable. However, despite the development of an executable, it was determined that the creation of conventional inlet maps for use with the engine cycle and vehicle sizing tool was the best option due to runtime and flexibility—inlet map generation capability was developed late in Year 3.

From the outset of this project, a highly functional supersonic inlet analysis tool was found to be required to perform thrust recovery analyses, in accordance with the initial goal of the project. Therefore, the focus for the Year 1 and Year 2 was on the robust development of this capability. Although it was intended for continued development of the supersonic inlet tool to take a secondary role during the third and final year (Year 3) of this project, some improvements were required prior to the execution and facilitation of the jet noise reduction-break-even study. Specifically, the low-speed aerodynamic model and its validation were required, and this took several months of effort. As a result, the final project deadline and subsequent milestones were extended via a No-Cost Extension, which was requested for the project grant completion, and approved by the FAA. As a result, the final project deadline was shifted to February 29, 2024. Further work was required to perform code integration and ensure robust and reliable results, with the inlet performance data implemented in the engine cycle and noise analysis, and as such, the work proceeded well past the approved No-Cost Extension date, mentioned previously. Rationale and technical complications which necessitated this are outlined in the section titled "Comments on Schedule Modifications."

The integration of the supersonic inlet analysis and design code developed under this project, as well as the engine cycle code and noise prediction codes all needed to be integrated for the results in question to be determined. Additionally, a supersonic engine and aircraft needed to be selected and adapted to employ an inlet designed for the SST design mission, and the identification and selection of a reasonable jet noise reduction method with thrust and noise performance relationships needed to be performed. Lastly the installation of these models into the overall engine cycle needed to be performed and the study utilizing the fixed engine and aircraft with modifications to the nozzle and variable geometry inlet needed to be performed, for thrust degradation, and then noise impacts, using the cycle results to capture the jet stream thermodynamic properties. All these tasks comprise the overall objective of accomplishing an investigation into the

main research goals. These tasks are all captured, along with modified planned due dates and actual and projected completion dates in the Milestones table, below.

Project Milestones
The major milestones and planned due dates are as follows:

Task No.	Milestone	University	Planned Due Date	Planned/Actual Completion Date
1	Selection of initial geometry in coordination with other Project 059 Investigators	PSU and Georgia Tech	12/15/2020	12/15/2020
2.1	Final assembly of zero-order methods to predict inlet performance: Complete supersonic inlet analysis code	Georgia Tech	1/30/2023	9/15/2023
2.2	Determination of boundary conditions from "Vision SST Engine Cycle"—collaboration efforts: Identify engine and operating conditions for inlet studies to be performed	Georgia Tech	5/31/2023	10/30/2023
~~3~~	~~Internal and external modeling of jet exhaust flow for noise modeling~~	~~PSU and Georgia Tech~~	~~8/1/2022~~	~~Cancelled~~
~~4~~	~~Script construction for generation of ANOPP custom jet noise source~~	~~PSU and Georgia Tech~~	~~9/1/2022~~	~~Cancelled~~
5	Submission of 2022 Annual Report	Georgia Tech	12/1/2022	3/1/2023
6	Extension of zeroth-order methods for inlet performance to include low-speed aerodynamics	Georgia Tech	4/15/2023	10/30/2023
7	Establish overall modeling and simulation framework	Georgia Tech	6/1/2023	4/30/2024
8	Development of inlet variable geometry methods and models for improving LTO thrust	Georgia Tech	7/1/2023	2/15/2024
9	Development and design of SST inlet to be used as baseline model and off-design inlet maps	Georgia Tech	7/30/2023	3/30/2024
10	Development and implementation of nozzle-based jet noise reduction methods for engine cycle effects	Georgia Tech	8/30/2023	4/15/2024
11	Completion of the full thrust recovery and noise effects study	Georgia Tech	2/1/2024	11/15/2024
12.1	Submission of FY2023 Annual Report	Georgia Tech	2/1/2024	6/3/2024
12.2	Submission of interim final project report (intermediate results)	Georgia Tech	2/29/2024	6/3/2024
12.3	Submission of the final project report (completion of project)	Georgia Tech	2/29/2024*	11/22/2024

**Indicates planned date based on no-cost-extension, pushing official project end date to 2/29/2024*

Comments on Schedule Modifications

Based on the Project Milestone table and previously submitted annual reports, the project timeline has significantly deviated from the initially planned one. There are several factors which contributed to this large deviation in task completion, which are predominantly technical in nature. First, while the project was overall focused on the integration of inlet performance predictions into an installed engine cycle model, the development of zeroth-order inlet models which could capture any appreciable benefit to the engine cycle and noise model needed to be carefully developed and tested to ensure realistic performance and the ability to design a bespoke supersonic inlet for application to a selected engine cycle and aircraft. One reason for the prioritization of this task was due to the predicted sensitivity of the inlet performance predictions using the inlet design and analysis tool developed in this project, translating to thrust.

Since deviations from a baseline inlet at the LTO conditions would be studied primarily, the ability to discern even seemingly negligible performance benefits relating to the inlet pressure recovery was crucial to answering the primary research question of, "can the inlet recover sufficient thrust without compromising noise benefits to ensure that supersonic jet nozzle noise technologies are feasible?" As such, despite the low fidelity of the modeling efforts—which were pursued due to the desire for enabling rapid assessments without the use of complex computational fluid dynamics (CFD) analyses and high-fidelity inlet computer aided design (CAD) models and meshes to be developed for single analyses—accuracy was determined to be critical. To ensure accuracy, the inlet tool performance was validated against various inlet performance studies in the public domain, and gradually extended and improved, with component models being verified and validated using Inlet Performance Analysis Code (IPAC) case runs, where those component models are also used, and in the case of the addition of the low-speed aerodynamics model, validating with CFD runs performed by competent inlet designers and CFD experts. A detailed discussion regarding the process for this development will be discussed in Tasks 2.1 and 6; however, it can be summarized that this improvement took much longer than initially intended to ensure accuracy when compared to experimentally tested inlets and the execution of CFD runs to validate the low-speed aerodynamics models.

Due to the aforementioned factors, the time required to complete the inlet analysis tool, which was employed for the purposes of generating the baseline inlet in this study, and the variations of it utilizing variable inlet geometry, along with the addition of the capability of modeling the variable geometry, the tool development process took a disproportionate amount of time to complete, rendering the majority of the remaining study to be compressed into a much tighter schedule. As a result, the final study could not be completed by the initial deadline, despite the best effort of the researchers.

A second factor contributing to the delay in schedule was the requirement to effectively perform integration among the three tools required for the study. The study required the use of an engine cycle and aircraft modeling tool, FASST, developed in-house by Georgia Tech's Aerospace Systems Design Laboratory (GT-ASDL), which employs several National Aeronautics and Space Administration (NASA) tools, including CMPGEN[1] for compressor map generation, Numerical Propulsion System Simulation (NPSS) for cycle design and modeling, and FLight Optimization System (FLOPS), for aircraft optimization and mission profile analysis. The study also required use of the Aircraft Noise Prediction Program (ANOPP), NASA noise prediction module, which is coupled to Environmental Design Space (EDS) to allow for analysis of a designed engine and aircraft system. Lastly, the inlet design tool, Supersonic Inlet Performance Code (SIPC) was developed for this project and based in Python.® While it was clear that the tools could all be used together, the action of performing software integration and ensuring consistent cycle performance, and ultimately, noise predictions through the ANOPP, required the ability to create inlet performance inputs in a means compatible with FASST. Doing so required a significant amount of trial and error and presented a non-trivial learning curve for the researchers. In Year 2, an approach was pursued to package SIPC as an executable to be called upon each iteration of the execution of the engine model. This approach proved to be too complicated to ensure consistent results and could not be effectively integrated to ensure accurate inlet performance predictions for each run. As such, this process was abandoned for a simplified approach to generate supersonic inlet maps and install them into the engine cycle for rapid and seamless use when called by the cycle model. The understanding of how to generate inlet performance maps analytically required a notable amount of research, culminating in a discussion with a senior technologist at the Inlets and Nozzles Branch at the NASA Glenn Research Center (Dr. John Slater). As a result, this effort contributed to a push in the overall project completion timeline.

[1] CMPGEN is a modeling tool used to compute off-design performance of fans, booster, and compressors.
® Python is a registered trademark of Python Software Foundation, Beaverton, Oregon.

A third major factor contributing to research complexity and timeline shift was the need to accurately model nozzle noise technologies, along with their thrust and noise effects. In the first two years (Year 1 and Year 2) of the project, it was anticipated that other ASCENT Project A059 research partners would provide experimental data to correlate nozzle geometries and factors which could be replicated and modeled analytically by the engine cycle modeling code. However, at the end of Year 2, it was understood that it would not be possible to obtain these data from the partner researchers, and alternative means to achieve this task were sought out, due to its critical function in accomplishing the ASCENT Project 059(A) research goals. As a result, a deep literature review was performed to support this task, ultimately yielding the finding that a dearth of experimental data existed in the public domain explicitly coupling jet noise technologies to thrust loss and noise reduction. Some significant publications were identified which answered this question, but these were isolated to the exploration of these trends in chevrons on supersonic engines and nozzles. A set of experimental papers published by NASA nozzle experts were used, primarily by the late Dr. John Seiner, which explored the use of parametric families of chevrons on the F404 engine and axisymmetric converging-diverging nozzle (Seiner, 1995 and others). The studies found the noise and thrust impacts associated with take-off conditions and were thereby applicable for use in the research presented here, while some assumptions were made for compatibility and consistency of the use in the study, which are detailed in the sections below.

Lastly, the explicit procedures for using these tools, in concert with one another to answer the correct research questions, were not clear at the outset of the project, and took time well into the software integration phase to understand. The FASST operates by running several iterations of engine cycle model and vehicle model, finally converging to meet initial cycle and aircraft requirement inputs provided by the user. As such, it generates an inlet design for each iteration and performs an off-design analysis to identify whether the engine can meet the requirements provided by the user. The ANOPP is integrated into the FASST run scheme, to generate input files from FASST vehicle outputs, and then an ANOPP analysis is performed. Non-trivial modifications of the FASST code were necessary to ensure that the variable geometry inlet study could be performed as desired. This involved ensuring that the engine models could use the variable geometry inlet maps in the off-design conditions without modifying the engine design at all—as the engine and nozzle configuration were to remain fixed in order to answer the primary research question. Additionally, modifications of execution procedure and codes, and deeper research into capabilities of the ANOPP for use in the noise reduction study were performed, specifically, the addition of supersonic chevrons and their parametrized impacts on noise at LTO conditions.

In summary, it is with the deepest sincerity and humility that the researchers who are performing this work apologize for the late nature of the submission of this work and the final results and findings, which we believe will be of interest to the SST research community. While technical challenges were encountered and overcome, compliance with agreed-upon timelines is a priority and not taken lightly. It is hoped that the work presented here is notable enough to justify the tardiness of terminal reporting of it. The team is grateful for the understanding, patience, and support of the FAA.

Major Accomplishments

Year 1 and Year 2 of work largely comprised creating and developing the supersonic inlet analysis code and refining its capabilities. Year 1 of effort was focused primarily on the assembly of various zeroth-order methods to conduct this inlet analysis, whereas Year 2 efforts were focused primarily on making the tool useful and suitable for the ASCENT Project 059(A) research goals. Year 1 accomplishments included the following:

1. **Task 2.1 - Final assembly of zero-order methods to predict inlet performance**
    - Completed a simple parametric 2D analysis tool able to predict the following:
        - Pressure recovery between freestream and engine face
        - Oblique and normal shock predictions
        - Inlet geometry schematic for verification
        - Bleed, bypass, and spillage drags
    - Validated tool performance against several published 2D inlets.
        - Good agreement with mixed compression M_d = 5.0 inlet provided in an IPAC manuscript (Barnhart, 1998).
        - Good agreement with external compression M_d = 2.3 inlet in *Fundamentals of Aircraft and Airship Design* (Nicolai & Carichner, 2013).
        - Analysis and validation of Performance of Installed Propulsion System Interactive (PIPSI) "R2DSST" M_d = 2.3 mixed compression inlet; currently underway (Kowalski & Atkins, 1979).

During Year 2 of ASCENT Project 059(A) efforts, capability gaps were closed, and several capabilities were improved:

1. **Task 2.1 - Final assembly of zero-order methods to predict inlet performance**

- Identified and improved many capability gaps between the Year 1 supersonic inlet analysis tool and needs including:
  - Inlet–engine airflow matching → bypass mass flow determination
  - Inlet capture area sizing
  - Cowl lip suction and additive drag predictions
  - Nacelle wave drag predictions
- Improved mixed compression inlet performance prediction.
- Improved accuracy of location and strength of internal oblique shock train.
- Improved accuracy of location and strength of internal terminal normal shock.
- Completed the initial integration of supersonic inlet tool and supersonic engine and aircraft analysis and design tools (FASST).

Finally, many significant Year 3 tasks were completed, requiring the modification of the initial milestones and task list to facilitate answering the primary research questions proposed. Year 3 accomplishments include the following:

1. **Task 2.1 - Final assembly of zero-order methods to predict inlet performance**
   - Enabled critical spillage and spillage drag calculations at high supersonic Mach numbers into the SIPC.
   - Improved cowl lip suction calculations based on Crosthwaite et al. (1967).
   - Developed and inlet choking condition prediction and limitations into the SIPC.
   - Extended additive drag predictions to include detached normal shock conditions into the SIPC.
   - Improved subsonic diffuser duct loss prediction models into the SIPC.
   - Developed and added an automated mass flow sizing approach for user-defined normal shock position into the SIPC.
   - Developed and added capability to photographically scale inlet into the SIPC.
   - Developed and added angle of attack effects to inlet model into the SIPC.
   - Developed and added increased fidelity in the inlet model to capture external normal shock-oblique shock interactions into the SIPC.
   - Developed and added the ability to visualize oblique shock-normal shock interactions and a three-dimensional (3D) view of inlet configuration into the SIPC.
   - Developed and added the ability to run batches of inlet cases into the SIPC for design space exploration.
   - Added ram drag calculation into the SIPC.
   - Completed the inlet modeling tool for the project.
2. **Task 6 - Extension of zeroth-order methods for inlet performance to include low-speed aerodynamics**
   - Developed and added a low-speed viscous aerodynamic model into the SIPC and validated with CFD.
3. **Task 7 - Establish overall modeling and simulation framework**
   - Performed initial integration work using an example inlet, and the selected engine and aircraft design to be used in project studies.
   - Determined and evaluated an approach for coupling inlet, aircraft, and noise codes.
   - Identified the ANOPP noise modeling approach for use with chevrons.
4. **Task 8 - Development of inlet variable geometry methods and models for improving LTO thrust**
   - Developed and added ramp bleed ports and throat bypass models into the SIPC.
   - Developed and added blow-in door models into the SIPC.
   - Developed and added variable geometry cowl lip models into the SIPC.
5. **Task 9 - Development and design of SST inlet to be used as baseline model and off-design inlet maps**
   - Designed the baseline inlet model for selected M=1.7 65-passenger SST vehicle with the mixed-flow turbofan (MFTF) engine.
   - Adapted the baseline inlet model to use previously developed blow-in doors, variable geometry cowl lips, and ramp bleed and throat bypass models for off-design and verified functionality across the flight profile.
   - Developed process for analytically generating inlet maps for all off-design conditions using the standardized inlet map format presented in Kowalski (1979).
   - Developed inlet maps for baseline inlet, variable geometry cowl lip, blow-in doors, and hybrid (both).
6. **Task 10 - Development and implementation of nozzle-based jet noise reduction methods for engine cycle effects**
   - Performed a literature review to identify potential nozzle-based jet noise technologies to be modeled, which provided a thrust and noise relationship.

- Identified research papers with experimental and analytically derived data which correlated jet noise reduction to thrust loss using chevrons.
- Determined an approach for implementing chevrons into the cycle model to capture thrust losses and the impact to engine cycle, as well as the effects on jet noise in ANOPP.

7. **Task 11 - Completion of the full thrust recovery and noise effects study**
   - Integrated inlet maps, and fixed engine and aircraft models to ensure functionality and confirm study procedure.
   - Added chevrons for three parametrized designs defined in aforementioned reference into the NPSS nozzle element and ensured functionality.
   - Integrated inlet maps, fixed engine and aircraft models, and chevron models to ensure functionality and confirm study procedure.
   - Ran a baseline engine case and established the ANOPP performance values for baseline inlet, fixed engine and aircraft, and clean nozzle (no chevrons) for a comparison datum.
   - Determined the necessary chevron geometry and inlet variable geometry cases to be studied.
   - ***In-process:***
     - ***Completing studies and compiling data.***
     - ***Performing analysis of data and necessary model reruns.***

Task 1 - Select Jet Nozzle Geometry

Georgia Institute of Technology
Pennsylvania State University

Objective

The objective of this task was initially to unify and maximize the impact of work across relevant ASCENT projects; Georgia Tech and PSU will coordinate efforts to select an initial jet nozzle geometry. In work with Dr. Krishnan Ahuja, the experimental data from this standard geometry (gathered in ASCENT Project 059) will be used to inform the work of ASCENT Project 059(A).

Research Approach

The combined PSU and Georgia Tech research team will work together to identify promising geometries for use across the ASCENT projects. The selected geometry must be relevant to the project goals, and also achievable regarding experimental measurement, computational analysis, and other supporting tasks. Specific evaluation criteria may include jet velocity reduction and thrust loss.

This task was completed during Year 1 of work. Although the results of this effort were not used to complete the inlet analysis code, it was helpful in identifying and converging upon the ultimate objective of the project and establishing cooperative working relationships with other ASCENT Project 059(A) partners.

Milestone

- Selected a notional jet nozzle geometry. This project task was completed early in the project (Year 1). The nozzle geometry was superseded in Year 3 in favor of one which was employed on an engine and aircraft model which were designed initially for ASCENT Project 010.

Major Accomplishments

- Selected an initial nozzle configuration.
- Established a collaboration with Georgia Tech experimental lab and PSU.

Publications

None.

Outreach Efforts

None.

Awards
None.

Student Involvement
None.

Plans for Next Period
None.

Task 2 - Translate Installed Cycle Performance Requirements into Boundary Conditions
Georgia Institute of Technology

Objective
The objective of this task is to leverage engine cycle modeling capabilities to determine the installed thrust for an engine of interest that is appropriate for commercial SST. The thermodynamic properties across this mixed flow turbofan engine, alongside the install thrust value, are used to characterize the mixer exit, nozzle entrance, and nozzle exit operating conditions during take-off. Because the initial testing and high-fidelity simulations are not (yet) representative of a mixed flow turbofan, these operating conditions (i.e., total pressure, total temperature, mass flow, geometry, etc.) will inform the testing team regarding relevant testing conditions.

Research Approach
Task 2.0 - Determine Installed Thrust
To ensure that minimum thrust is lost during implementation of potential jet noise reduction technology, the installed thrust requirement must be determined, because it is directly proportional to jet velocity. A major contributor to installed thrust is inlet performance, which is highly dependent on how the engine is integrated with the vehicle. Therefore, the primary element of Task 2 is to investigate zeroth-order methods to predict inlet performance for different inlet designs and off-design configurations.

Task 2.2 - Generate Boundary Conditions
Initially, the objective of this task for Georgia Tech was to analyze the engine cycle developed by ASCENT Project 010 to estimate the best operating conditions for LTO to minimize certification noise levels. This task was updated to reflect the required boundary condition/experimental data generated by project partners, to be used in Tasks 7 and 8. Additionally, the timeline was updated to reflect when these data were required by the ASCENT Project 059(A) team. Some beneficial data for modeling will include mixer and nozzle conditions, i.e., total temperature, total pressure, and mass flow rate, as well as measured thrust vs. noise for each tested jet noise reduction technology or mixer type. This task was completed in Year 3.

Task 2.1 - Zero-order Methods to Predict Inlet Performance
A major contributor to installed thrust is inlet performance, which is highly dependent on how the engine is integrated with the vehicle. To capture thrust recovery due to improved inlet performance, the Georgia Tech team must develop a means to predict inlet performance across the SST flight envelope, particularly at low-speed conditions during which jet noise is most prominent (i.e., LTO).

During Year 1, the Georgia Tech team completed an initial the model development for the 2D inlet case, by developing a modular 2D supersonic inlet anlaysis tool (see Figure 1). In addition, the team has completed an initial validation of the 2D inlet case with satisfactory preliminary results (refer to Figure 2).

Table 1 compares the developed tool's predicted total pressure recovery to that produced by IPAC across the mission-relevant range of freestream Mach numbers (Barnhart, 1998). Here, the supersonic inlet is designed for a freesteam Mach number of 5, and evaluated across a range of lower "off-design" operating freestream Mach settings. The maximum and average error values were found to be 3.69% and 0.82%, respectively, across this range.

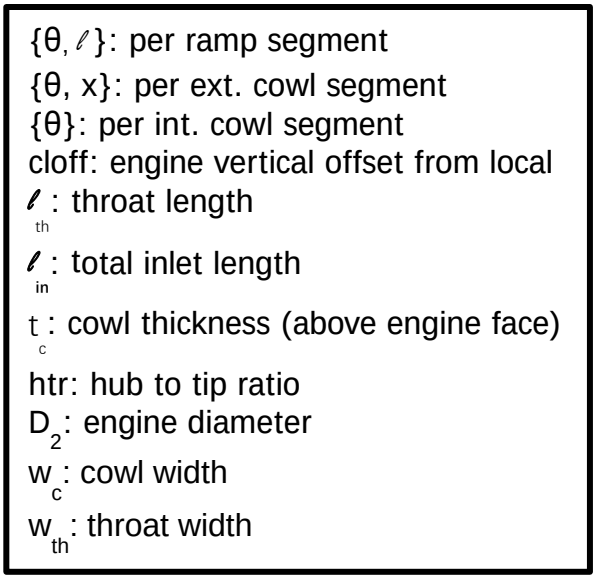

Figure 1. Geometry inputs to define inlet in Year 1 supersonic inlet analysis code.

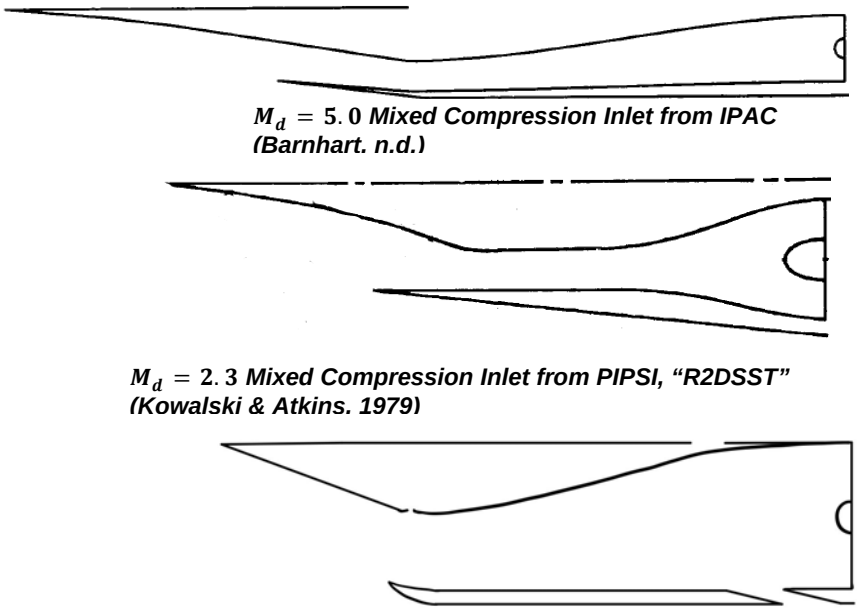

$M_d = 5.0$ ***Mixed Compression Inlet from IPAC (Barnhart. n.d.)***

$M_d = 2.3$ ***Mixed Compression Inlet from PIPSI, "R2DSST" (Kowalski & Atkins. 1979)***

$M_d = 2.3$ ***External Compression Inlet from Nicolai & Carichner (2013)***

Figure 2. Three 2D supersonic inlets used to validate the Year 1 inlet analysis tool; top inlet performance results are displayed in Table 1.

Table 1. Validation case: total pressure recovery.

Freestream Mach number	Modeled	Reference	Error (%)
0.01	0.9586	0.9608	−0.23
0.2	0.9586	0.9608	−0.23
0.4	0.9586	0.9608	−0.23
0.6	0.9586	0.9608	−0.23
0.8	0.9586	0.9608	−0.23
1.0	0.9586	0.9608	−0.23
1.2	0.9517	0.9539	−0.23
1.4	0.9404	0.9456	−0.55
1.6	0.9233	0.9285	−0.56
1.8	0.8767	0.8816	−0.55
2.0	0.8107	0.8153	−0.57
2.5	0.8591	0.8760	−1.97
3.0	0.7873	0.7875	−0.03
4.0	0.6618	0.6427	2.88
5.0	0.5349	0.5152	3.67

Table 2 compares the developed tool's predicted total drag coefficient and that produced by IPAC across the mission-relevant range of freestream Mach numbers (Barnhart, 1998). This drag term includes the contributions of spillage, bleed, and bypass drag on the engine inlet. Again, the supersonic inlet is designed for a freesteam Mach number of 5 and is evaluated across a range of lower "off-design" operating freestream Mach settings. The maximum and average error values were found to be 9.88% and 1.19%, respectively, across this range.

Table 2. Validation case: total drag coefficient.

Freestream Mach number	Modeled	Reference	Error (%)
0.01	0.0000	0.0000	0.00
0.2	0.0000	0.0000	0.00
0.4	0.1976	0.1799	9.88
0.6	0.3086	0.3024	2.05
0.8	0.3831	0.3811	0.53
1.0	0.4809	0.4797	0.25
1.2	0.6537	0.6617	−1.21
1.4	0.3953	0.3855	2.53
1.6	0.3264	0.3265	−0.01
1.8	0.3245	0.3250	−0.15
2.0	0.3426	0.3411	0.45
2.5	0.3007	0.3000	0.23
3.0	0.2994	0.2987	0.23
4.0	0.2315	0.2307	0.35
5.0	0.0175	0.0175	0.00

The developed inlet performance analysis tool is intended to help identify competitive supersonic inlet designs for overcoming negative performance impacts accompanying noise reduction nozzle technologies across the flight envelope and as identifying the resulting behaviors associated with low-speed performance and off-design ramp (and other variable geometry) configurations of the inlet. To this end, a sensitivity study was performed to evaluate inlet variable-geometry settings that may be capable of recovering thrust across off-design flight segments (i.e., LTO).

For Year 2, the inlet performance tool was extended to include several capabilities for performance modeling, as listed in the Major Accomplishments section. One simple capability added for Year 2 was a schematic showing the user where the external oblique shocks are located with respect to the external portion of the supersonic inlet (Figure 3). This schematic allows users of the supersonic inlet analysis script as a standalone tool (i.e., not coupled to an engine/airframe sizing and synthesis tool) to quickly identify whether an external shock system is attached to the inlet, or a detached shock system has been formed. In work for Year 3, the normal shock system, whether external or internal, will be included in the schematic. Additionally, the subsonic diffuser portion (the internal inlet section closest to the engine face) will reflect the actual curvature reflected in the model (here, it is straight, without curvature).

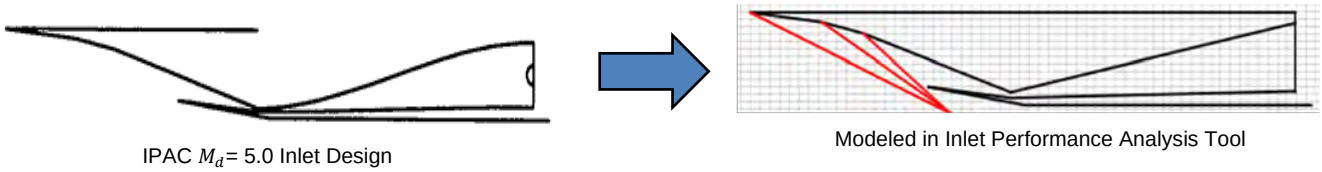

Figure 3. Inlet and shock schematic enabled in supersonic inlet tool during Year 2 work.

In addition to the modeling fidelity improvements listed in the Major Accomplishments section, many more stations and the physical properties of airflow at those stations can be modeled as a consequence of the Year 2 work. Instead of simply considering the total pressure recovery and drags, as displayed for the Year 1 work in Table 1 and Table 2, the work of Year 2 enabled a much closer examination of the supersonic inlet performance at each station. The performance of the inlet at each of these additional stations was compared with those from the published results of the M = 5.0 mixed compression inlet from IPAC (shown at top in Figure 2). Detailed results for the M = 3.0 off-design case of this inlet are shown in Table 3; the design case and other off-design cases down to M = 0.01 had similar performance results with respect to the validation error. As described previously, a greater level of fidelity regarding flow station performance and improvements in the accuracy of the model were achieved. Using the Year 2 inlet analysis tools, the team had found an improvement in accuracy regarding total pressure recovery (total pressure ratio across the entire inlet) as a consequence of the improvement in shock location predictions and internal reflected shock quantities.

Table 3. Validation results for IPAC M = 5.0 inlet and M = 3.0 off-design case.

Outputs	Local calculated	Local reference	Error (%)	Cowl lip calculated	Cowl lip reference	Error (%)	Throat calculated	Throat reference	Error (%)
Flow area (ft^2)	0.6905	0.6905	0.0000	0.3953	0.3955	0.0594	0.1600	0.1598	−0.1126
Mach number	3.0000	3.0000	0.0000	2.3982	2.3990	0.0335	1.3149	1.3140	−0.0700
Static pressure (lbf/ft^2)	156.7630	156.3000	−0.2962	390.6043	389.5000	−0.2835	1,960.9823	1,959.0000	−0.1012
Static temperature (R)	389.9700	390.0000	0.0077	508.6205	507.7000	−0.1813	812.6533	811.5000	−0.1421
Density (slg/ft^3)	0.0002	0.0002	−0.2490	0.0004	0.0004	−0.2472	0.0016	0.0014	−13.3433
Velocity (ft/s)	2,905.4154	2,904.0000	−0.0487	2,650.0449	2,649.0000	−0.0394	1,838.3284	1,835.0000	−0.1814
Total pressure (lbf/ft^2)	5,753.6784	5,743.0000	−0.1859	5,694.5814	5,684.0000	−0.1862	5,545.0869	5,534.0000	−0.2003
Total temperature (R)	1,093.6709	1,092.0000	−0.1530	1,093.6709	1,092.0000	−0.1530	1,093.6709	1,092.0000	−0.1530
Mass flow (lbm/s)	21.8556	21.8200	−0.1630	15.0913	15.0700	−0.1411	13.2882	13.2700	−0.1370
$\frac{P_{T_1}}{P_{T_L}}$	$\frac{P_{T_1}}{P_{T_{L\,REF}}}$	$\frac{P_{T_{TH}}}{P_{T_1}}$	$\frac{P_{T_{TH}}}{P_{T_{1\,REF}}}$	$\frac{P_{T_2}}{P_{T_{TH}}}$	$\frac{P_{T_2}}{P_{T_{TH\,REF}}}$	$\frac{P_{T_X}}{P_{T_Y}}$ (across normal shock)	$\frac{P_{T_X}}{P_{T_{Y\,REF}}}$ (across normal shock)	Number of internal shocks	Number of internal shocks (reference)
0.9897	0.9900	0.9737	0.9740	0.8164	0.8174	0.897	.8952	3	3

During Year 3 work, many significant progresses were made, and the overall completion of the inlet modeling tool was completed. First, critical spillage determinations and the ability to calculate drag forces for them was developed. While in Year 2, the ability to determine subcritical spillage was developed and added into the inlet model, critical spillage at higher

Mach numbers was not present. Critical spillage is experienced when the normal shock in a shock system is swallowed by a mixed compression inlet, but the oblique shocks are not converged upon the cowl lip. An example of this can be seen in Figure 4, from Barnhart (1998). It can be seen that since the oblique shocks do not converge on the cowl lip (i.e., the lower protruding surface), and streamtube area entering the inlet is less than the total capture area, denoted as A_c. This creates a spillage effect, since the overall mass flow which could be captured by the inlet is not able to be due to the oblique shock system, and a momentum drag is incurred. While this is only relevant to supersonic conditions, an inlet with realistic performance predictions for the entire SST mission profile needed to be designed, and this condition and capability needed to be added to the inlet model.

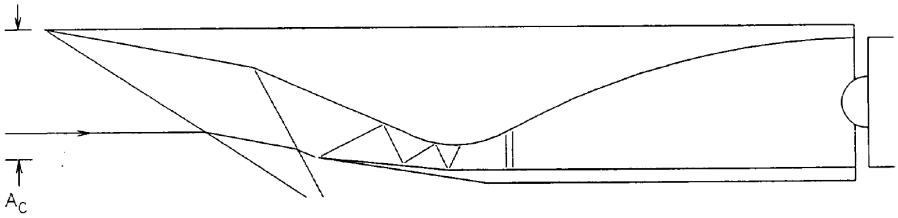

Figure 4. Critical spillage due to oblique shocks (Barnhart, 1998).

Another improvement to the inlet performance tool was the improvement of cowl lip suction calculations based on Crosthwaite et al. (1967), "Preliminary Design Methodology for Air-Induction Systems." Although the IPAC technical report (Barnhart, 1998) outlines a basis for cowl lip suction calculation based on this reference, the researchers could not achieve consistent performance for the cowl lip suction calculation using the equations provided by the IPAC report. In several cases, when running the IPAC example 2D inlet with a design Mach number of 5.0, cowl lip suction values varied from the reference calculations up to 5%. As a result, a simplified approach found in the original work from which the IPAC equations were derived was used, enabling agreement and improvement with highest error of 2% for the worst case in the validation dataset. Another improvement predicated on improving the physics modeling of the inlet code was to add a choking condition prediction for the different points of convergence inside the inlet duct and provide an error which would yield an invalid case run to the user. As a consequence of the conservation of mass and compressibility effects, the mass air flow through an inlet is limited by its smallest area. The inlet code requires a user (or engine deck) input for engine demand, bleed, and bypass—the components or sum of which can choke the inlet either at the cowl lip entrance, or later, at the throat (most likely). If this is the case, it is important for the user model the condition in which no more mass flow can be demanded by the engine, bleed ports (for boundary layer control), or bypass (for shock system stability control). As such, adding this functionality ensured a more accurate physical representation of the operation of an inlet across the mission profile of the vehicle, especially LTO conditions, at which extreme amounts of air are required to operate. This furthermore enabled the user to know when the inlet needed to be upsized for a condition, or variable geometry compression ramps needed to have their deflection angles changed.

In the case in which the inlet experiences a detached normal shock—one that is located in front of any compressed surface—also known as a bow shock, additive drag is still experienced. Additive drag is the sum of cowl lip suction forces, the low-pressure suction phenomenon due to air flowing in the reverse direction of the streamtube, over the inlet cowl lip, and drag due to spillage. While the drag due to spillage was developed, implemented, and validated for other operating conditions, it was added for the supersonic condition during which there is extremely low mass air flow demand into the inlet. This improvement, again, was to ensure the overall prediction of the inlet maps was physically accurate for overall mission modeling. For reference, the inlet generally used for component model validation is shown in Figure 5. In Year 3, as previously discussed, there were further modifications and improvements to the inlet modeling code which were performed, including the improvement of subsonic diffuser duct loss predictions. This task was identified as necessary, as the partial total pressure recovery which was calculated as the loss in total pressure between the inlet throat and the engine fan face was providing worse (lower) total pressure recovery values than those predicted by the IPAC code. As such, the source data employed by IPAC, found in Crosthwaite et al. (1967), were digitized, added to the code as a lookup table, and revalidated in order to ensure better agreement with IPAC output values.

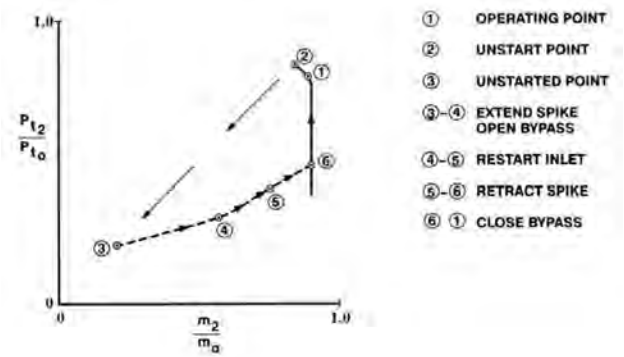

Figure 5. SR-71 inlet operation and operability chart on "Cane Curve" shows the effects of inlet unstart (Anderson, 2014).

In previous versions of the supersonic inlet design code, the prediction of the internal normal shock was limited to being defined by the user using a throat Mach number definition, assuming that the internal oblique shock train would eventually become detached after enough internal shock reflections in the converging inlet duct wall, terminating at the throat. However, this assumption did not reflect the physics of the problem particularly well, upon deeper examination of the problem, nor did it truly enable a full analytical physics-based approach to understanding the performance of the inlet. Specifically, the inlet normal shock position is a consequence of the backpressure provided by the engine and bypass demands. An example of a started mixed compression inlet shown in Figure 4, where the normal shock is swallowed into the inlet duct. As the converging duct is an unstable location for a normal shock to reside (position of high shock instability), the normal shock, if swallowed, will lie at the throat, or past it inside the subsonic diffuser duct (which is a diverging duct, and geometry much more amenable to keeping a shock in place) (Seddon & Goldsmith, 1999). In practical operation, if the inlet is in the started condition, this necessitates that the inlet is moving fast enough to form all external oblique shocks, and also that the engine and bypass demand are sufficiently high to retain the normal shock. If the demand (backpressure) is too low (high), the normal shock will pop out of the inlet duct and the system will be in what is known as an "unstarted" condition. Two examples of this can be found in Figure 5. Since the normal shock position is exclusively dependent upon the inlet-engine-aircraft system operating conditions, it was crucial to ensure that the position was a response due to these factors, and not an independent modeling input provided by the user. This model was defined based on compressible flow relationships defined in Seddon and Goldsmith's "Intake Aerodynamics" (Seddon & Goldsmith, 1999), and positions were defined not by axial coordinates, but rather inlet cross-sectional areas segmented between inlet stations defined commonly defined across various inlet literature sources and shown in Figure 6. This method was validated successfully and ensured accurate determination of the position of the normal shock when swallowed. Previous work to define the normal shock on the external ramps when the unstarted condition was completed and validated against IPAC outputs in Year 2 of work, so effects of normal shock positioning across the entire range of inlet operation were fully captured upon the completion of this task.

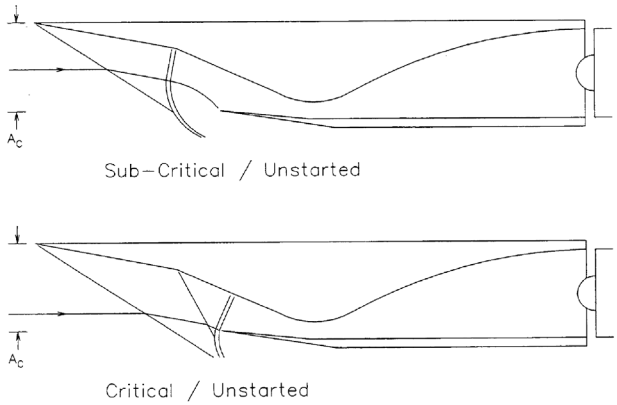

Figure 6. Examples of unstarted inlet conditions for mixed compression 2D inlet (Barnhart, 1998).

Additionally, a design analysis condition was defined to ensure that the inlet would remain in the started condition while performing analyses such as the generation of inlet performance maps. As will be described in later sections pertaining to the generation inlet performance maps for the selected inlet and engine models, inlet performance maps are generated for supersonic conditions assuming that the shock remains swallowed, since an unstarted inlet in a supersonic condition causes a highly unstable engine transient conditions, such as compressor stall or surge. This was a significant factor in the operability of the SR-71 axisymmetric inlet, which proved to be the most challenging feature of the entire aircraft design (Anderson, 2014).

As such, it was useful to automate two features to facilitate the retention of this condition in use of the analytical tool. First, a required mass flow rate for the inlet to retain the normal shock in the swallowed condition, and second, the ability to perform analysis keeping the normal shock fixed in a position defined by the user. For the first feature, Equation 1 defines the required mass flow for keeping the engine started condition, also assuming that the operating condition of the aircraft is sufficiently fast to create oblique shocks on all external ramps and a terminal normal shock after them. The maximum amount of mass flow ingested by the inlet at a given condition while the normal shock is swallowed is referred to as the critical mass flow ratio:

$$\frac{A_{0I}}{A_C}_{Critical} \quad \text{(Eq. 1).}$$

This value changes as the vehicle speed drops below the design Mach number for the inlet, as the geometry of the inlet is created to ensure a shock-on-lip condition, which prevents critical spillage from occurring. When the oblique shocks are no longer focused on the cowl lip, the oblique shocks are formed, starting on the compression ramps at a more shallow angle than in the design condition, and the streamtube of air which is able to be swallowed by the inlet is constrained by the compression of the streamtube as a result of the off-design compression of the external oblique shocks. An example of this can be seen in Figure 4, where the captured streamtube area is less than the forward-projected capture area defined by rectangle formed from the cowl lip to the bottom of the first compression ramp (and along the inlet sidewalls, not pictured in the axial cross section), and denoted as A_C. When the inlet (as shown) is operating at the design condition, the streamtube captured by the inlet (corresponding to the mass flow ingested by it) is in full flow and is equal to the capture area, since the external oblique shocks are concentrated on the cowl lip. So, to accomplish this task, it was necessary to identify a means to find the maximum ingested mass flow when the $\frac{A_{0I}}{A_C}_{Critical} \neq 1$ (where 1 represents the on-design condition and full flow). The total ingested mass flow is at the maximum when the following condition is met: $\frac{A_{0I}}{A_C} = \frac{A_{0_{eng}}}{A_C} + \frac{A_{0_{bld}}}{A_C} + \frac{A_{0_{byp}}}{A_C} = \frac{A_{0I}}{A_C}_{Critical}$. This was performed by calculating the streamtube area compression due to the oblique shocks moving backwards from the cowl lip, at each oblique shock intersection with the streamtube, to the inlet "local" position, which can be seen in the inlet position schematic in Figure 7. This approach needed to be parametric and conditional such that the $\frac{A_{0I}}{A_C}_{Critical}$ value could be determined across the entire flight regime. Again, it should be mentioned that while this particular task was not necessary for the determination of thrust benefit at LTO conditions, a new inlet, which worked for an installed engine on a vehicle performing an actual SST mission profile, needed to be defined for this task. To do this, performance at all mission points needed to be able to be ascertained. The second task listed above was to enable the fixing of the normal shock and understanding the resulting aerothermodynamic properties of the flow which result from these properties. This was notionally achieved in Year 2 of work with the model; however, the initial attempt at fixing the normal shock internally provided incongruous flow patterns between the first half (from freestream to throat) and the second half (from throat the engine fan face) of the inlet. The approach determined here allowed users to study the effects of the flow and perform the inlet design at off design configurations by modifying the ramp angles, and ensuring the normal shock was able to remain in a stable location for the off-design supersonic conditions.

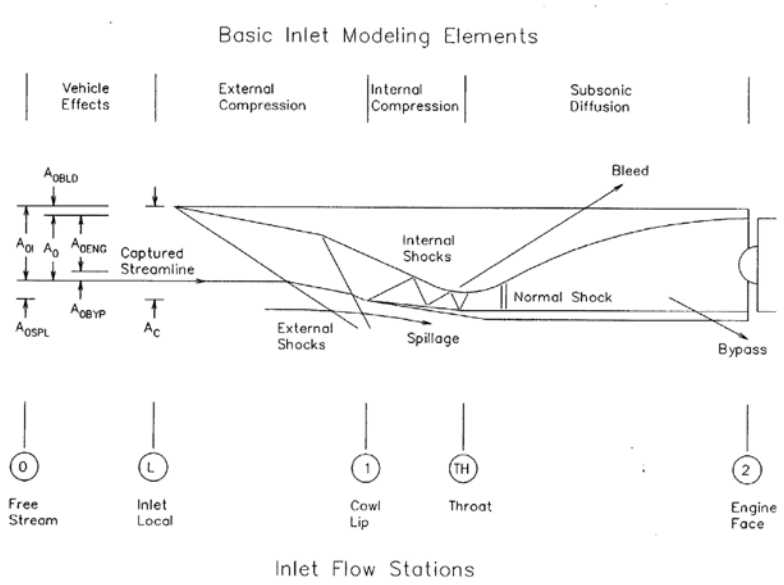

Figure 7. Commonly-defined inlet flow stations (Barnhart, 1998).

Another feature which was useful for the initial definition and design of the inlet to be used in the SST configuration for the study was the ability to size the inlet photographically. Previously, individual sizing parameters, such as ramp lengths, cowl lip width, engine fan diameter, and the like, were defined and would need to be redefined for each successive permutation of inlet design, even if a simply scaled-down or scaled-up version of the inlet was desired. This enabled the researchers to initially employ already-designed inlet models to various engines and have a baseline from which to begin inlet studies. An example of the scaling enabled by this step can be seen in Figure 8.

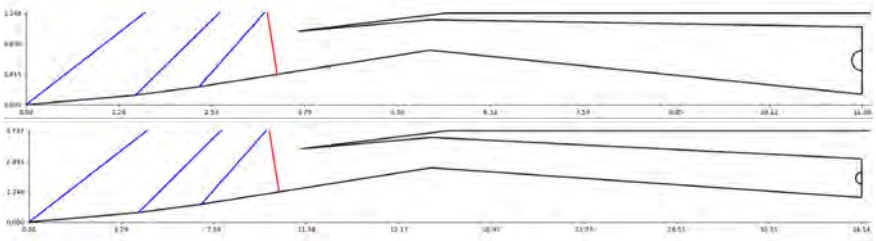

Figure 8. Identical inlets in off-design condition sized for different capture areas with same engine ($\mathrm{Ac} = 1\ (\mathrm{top}), \mathrm{Ac} = 3\ (\mathrm{bottom})$).

Yet another useful feature for understanding performance of the inlet across the SST mission profile was the addition of angle of attack effects in SIPC. While most inlet maps, and the IPAC inlet analysis code, do not account for inlet performance effects with modified angles of attack, it was important to account for this in the predicted inlet performance here, as a high angles of attack for SSTs are nearly inevitable for LTO conditions. While the plot generated by SIPC does not show the effects of modifications of angle of attack (see Figure 9). The external shock train prediction, due to the change in incident flow and position of the normal shock due to the ingested flow to the inlet, can be seen clearly in Figure 10. The normal shock in the top image shows the operation of the IPAC-defined $M_D = 5.0$ inlet at $\alpha = 0°$, while in the bottom image in Figure 9, where for the same inlet configurations and operating conditions, $\alpha = 8°$. It can be seen that the normal shock is positioned farther from the cowl lip due to less ingested airflow entering the inlet due to the oblique shock train, and the oblique shocks have a lower shock angle, despite maintaining the same ramp angle. These effects are further propagated to all following aerothermodynamic predictions at all stations and were able to be reflected in the inlet performance maps.

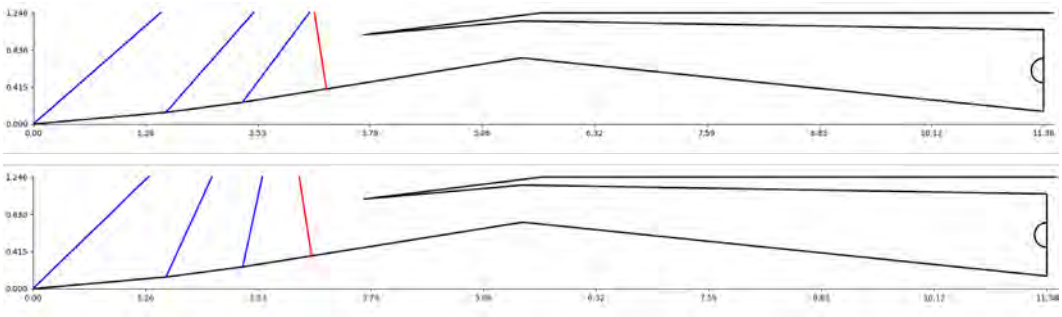

Figure 9. Effects of change in angle of attack: top α = 0°, bottom α = 8°.

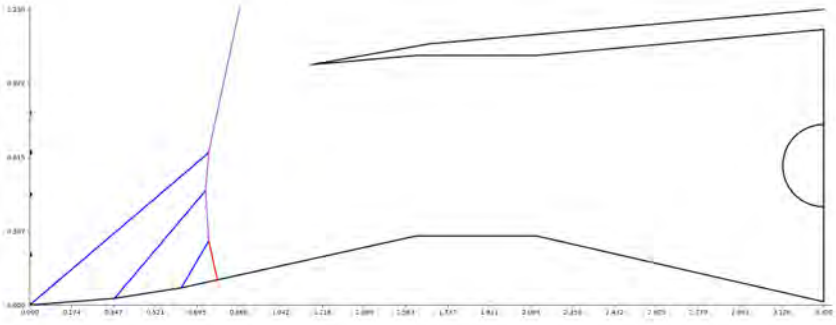

Figure 10. Example M=1.7 SST inlet experiencing external oblique-normal shock interactions (purple lines).

While in the previous year of work, it was assumed in off-design supersonic conditions, where the normal shock is not swallowed, that the normal shock and oblique shocks had no significant physical interaction. As such, any interaction between the two shock systems was not modeled. This was addressed by the team after some cursory CFD modeling was performed to better understand this phenomenon and if it was significant, and it was determined to be so. As such, an understanding of the compressible flow effects was sought, using in part, Seddon and Goldsmith (1999). Additionally, the explanation of the interactions of shocks was explained in Chapter 7.4 of Seddon and Goldsmith (1999). Seddon and Goldsmith (1999) indicates that instead of the weak oblique shocks which are seen in standard compression regimes at the ramp surface turning angles for supersonic flow, any interaction between normal shocks and oblique shocks would yield a strong oblique shock, rendering a stronger oblique shock instead of being replaced by the normal shock. As such, this effect was added to be modeled. In the weak oblique shock condition, the resulting flow after the shock remains supersonic, and only becomes subsonic after a terminal normal shock (which necessarily occurs). In a strong oblique shock condition, the flow which follows the shock becomes subsonic and no normal shock is experienced. Since the oblique shock equation has two solutions (supersonic and subsonic), the conditional to select which one in the root finder scheme was appropriately selected to model this phenomenon. Additionally, a visualization approach was developed and added to the code to show when this oblique-normal shock interaction occurs to the user (shown in Figure 11). The resulting strong shock can be seen as the purple line—and it can be seen that the oblique shocks modify the typically orthogonal shape of the normal shock (when measured from the compression ramp surface).

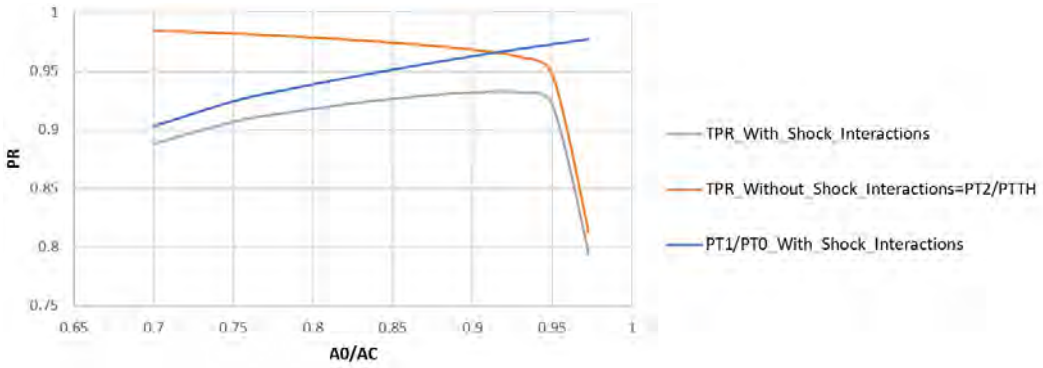

Figure 11. Total pressure recoveries for M=1.7 SST inlet comparing the modeling with and without shock interactions.

It can be seen in Figure 11, that the total pressure recoveries for an inlet at a fixed supersonic Mach number and in an off-design condition (since the normal shock is external to the inlet, and thus unstarted), the inlet performance "cane curve" shows nontrivial losses when only allowing the calculation of these normal-oblique shock interactions to take place. Here, for lower mass flow ratios ingested by the inlet, the difference in total pressure recovery from the non-interaction case is approximately 1%, while at higher mass flow ratios, it is closer to 0.25%. This affects the off-design performance of the inlet and likely, the overall design selected in the design phase.

To allow a better understanding of the inlet design, a 3D schematic generation was developed, which provides a movable 3D plot in the Python Matplotlib plot screen upon completion of the SIPC's execution. An example of this 3D print is shown in Figure 12.

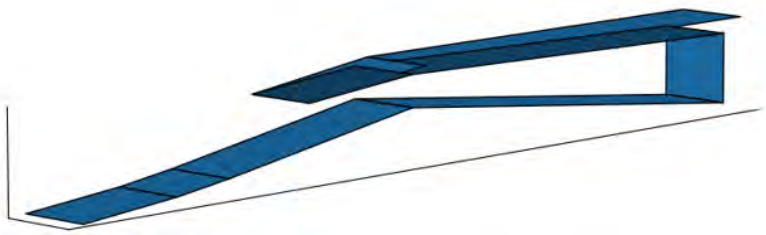

Figure 12. 3D schematic of M_D = 5.0 inlet.

To further illustrate the design variables and parametrization of the inlet, which is employed by the SIPC code, a schematic is provided in Figure 13. As can be seen, although the code is currently only capable of modeling 2D (rectangular cross-section) inlets, all possible geometric variables are considered and used in modeling. Another capability added to the inlet design and analysis code for this task was to enable the running of batches of inlet design cases, using a spreadsheet as the input file, for a user-defined quantity of inlet analysis cases. In the batch run capability, the code is able to vary any geometry variable, flight condition variable, or engine operating condition variable, and the results are collected and summarized in final comma separated value (CSV) file. A summary of the inlet user inputs is defined in Table 4 including units and variable descriptions. All of these variables are able to be varied in the input CSV file using the batch running capability, allowing for the running of many cases to generate inlet performance maps, or perform a design space exploration (DSE) for different geometries and configurations. The geometry variables which define the inlet are listed in Table 4, and are also shown in the schematic of the inlet in Figure 14. In addition to explaining the SIPC-defined lengths and angles mapped to a generic 2D supersonic inlet, the image captures the parameterization approach utilized in SIPC (see Table 4).

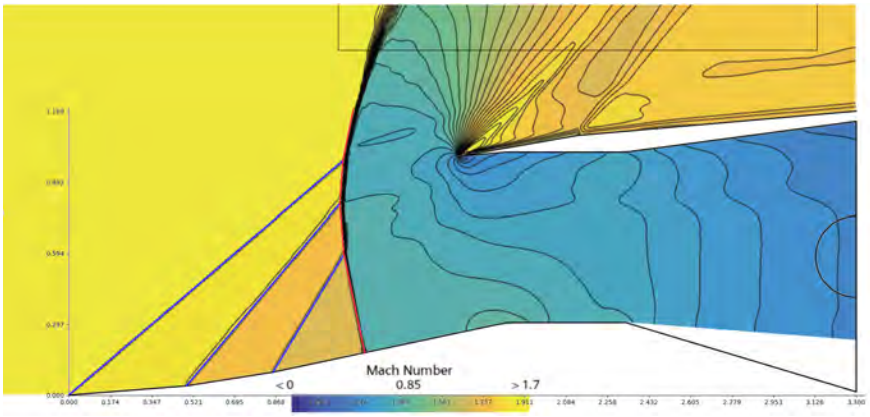

Figure 13. Reynolds-averaged Navier-Stokes (RANS) CFD model for SST inlet to validate external oblique-normal shock interactions.

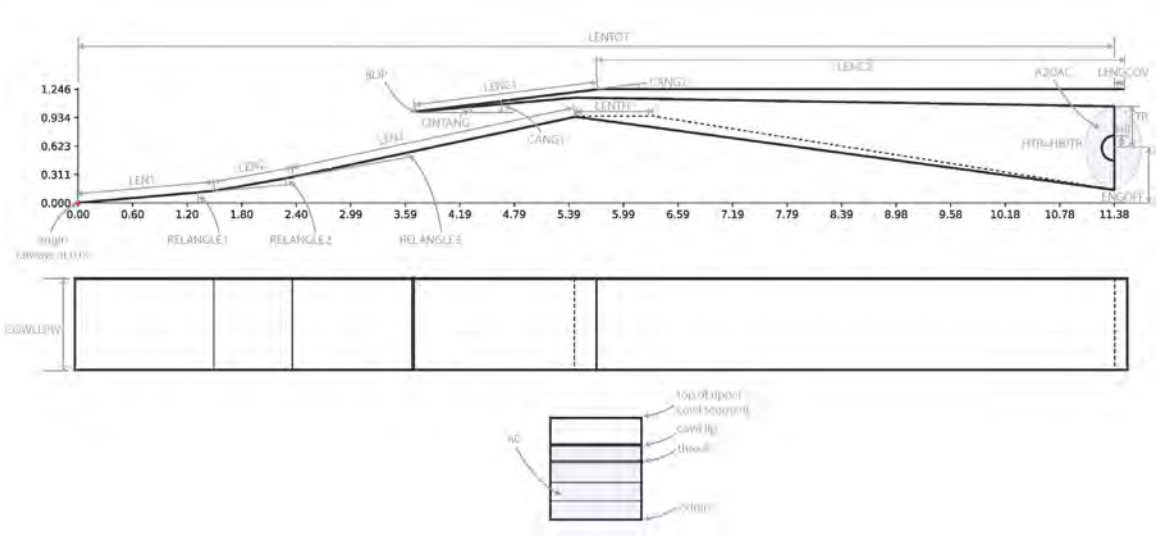

Figure 14. M_D =5.0 Inlet from IPAC report (Barnhart, 1998) defined using SI. PC variables Illustrating parameterization approach.

Table 4. SIPC input variables and units.

Variable Category	Variable Name	Description (Units)
AMBIENT	ALT	Altitude (ft)
	MACH	Freestream Mach number
	ALPHA	Angle of attack (degrees)
CAPTURE GEOMETRY	AC	Capture area (sqft)
	COWLLPW	Cowl lip width (ft)
FLOW CALCULATION	SET_AS	Flag to set normal shock position and keep there, if started
	AS_RATIO	Area ratio of normal shock position to throat area
	SIZED_FLOW	Flag to size the flow to keep mass flow equal to critical ingested mass flow rate
COWL GEOMETRY	NUMSEG	Number of cowl segments (ft)
	CANG1	Respective angles of the cowl lengths WRT horizontal (first one), then each other (relative) (ft)
	CANG2	Respective angles of the cowl lengths WRT horizontal (first one), then each other (relative) (ft)
	CINTANG	Internal cowl lip angles, relative after first angle (fron horizontal) (ft)
	LENC1	Length of each external cowl segment along the hypotenuse (ft)
	LENC2	Length of each external cowl segment along the hypotenuse (ft)
	RLIP	Lip Radius (ft) ;Sharp lip radius = 0
	LENTH	Length of throat section (constant area duct) (ft)
	LENTOT	Total inlet length, user-provided value by-design (ft)
EXTERNAL RAMP GEOMETRY	NRAMPS	Number of external ramps
	RELANGLE1	Angle of first ramp relative to previous (degrees)
	RELANGLE2	Angle of second ramp relative to previous (degrees)
	RELANGLE3	Angle of third ramp relative to previous (degrees)
	LEN1	Length of first ramp along the hypotenuse (ft)
	LEN2	Length of second ramp along the hypotenuse (ft)
	LEN3	Length of third ramp along the hypotenuse (ft)
ENGINE FACE GEOMETRY	A2OAC	Fan area ratio (Fan area/Capture area)
	HTR	Engine hub-to-tip ratio
	ENGOFF	Offset of the middle of the spinner (and engine) from the beginning of the ramps (i.e. y=0) (ft)
	LENGCOV	Length of the external cowl which is past the engine face (ft)
FLOW RATES	A0ENGOAC	Engine flow rate required as a fraction of catured flow
	ABLDOAC	Bleed flow rate as a fraction of captured flow
	ABYPOAC	Bypass flow rate as fraction of captured flow
SETUP	SDFRIC	Subsonic diffuser skin friction factor (real number)
	DEBUG	Debug print output off = 0, on = 1
	LIPLOSS	Lip loss calculations on = 1, off = 0
	PLOT	Plot inlet and resulting shock system on = 1, off=0
	SOL	Adjust ramp/cowl lengths for shock on lip/focus point (off = 0, on = 1)
	SOLOFF	Focal point above cowl lip for external shocks

Although a significant and disproportionate amount of time compared to other tasks was expended on Task 2, a great deal of improvements in modeling capabilities for the inlet were achieved because of it. At this point, it should be noted, that although NASA's IPAC was available to use for reference, it was not able to be used due to its restricted nature (only available to persons of the United States), while several graduate students which worked on the project over its course were international students. Additionally, the IPAC lacked several features which were desired to be used by the researchers, such as the shock visualization capability, shock interaction/strong oblique shock predictions, and low speed aerodynamic viscous models, among other things. Extensions of the IPAC would have been exceedingly difficult, if possible, even if not restricted, as the source code was not easily available to the researchers, and is a Fortran code, a language not regularly used by the researchers. As such, in order to design a bespoke inlet for this research effort, and to ensure that the inlet maps for use in later parts of this project to be accurate, work on the inlet design code was critical. Once completed, the inlet code, SIPC, allowed the researchers to complete the aforementioned tasks.

Milestones

- Completed the final assembly of zero-order methods to predict inlet performance.

Major Accomplishments

- Enabled critical spillage and spillage drag calculations at high supersonic Mach numbers into SIPC.
- Improved cowl lip suction calculations based on Crosthwaite et al. (1967).
- Developed and inlet choking condition prediction and limitations into SIPC.
- Extended additive drag predictions to include detached normal shock conditions into SIPC.
- Improved subsonic diffuser duct loss prediction models in the SIPC.
- Developed and added an automated mass flow sizing approach for user-defined normal shock position into
- Developed and added the capability to photographically scale the inlet into SIPC.
- Developed and added angle of attack effects to the inlet model in SIPC.
- Developed and added increased fidelity in the inlet model to capture external normal shock-oblique shock interactions in the SIPC.
- Developed and added the ability to visualize oblique shock-normal shock interactions and a 3D view of inlet configuration into SIPC.
- Developed and added the ability to run batches of inlet cases into SIPC for design space exploration.
- Added ram drag calculation into SIPC.

Publications

None.

Outreach Efforts

None.

Awards

None.

Student Involvement

Over the course of the work, several graduate students worked on the task of developing the inlet modeling capability. In total, this project funded the studies of four graduate students, for different proportions in the past three years, and all of them worked on this task.

Plans for Next Period

Task 2 is complete.

Task 6 - Extension of Zeroth-Order Methods for Inlet Performance to Include Low-Speed Aerodynamics

Georgia Institute of Technology

Objectives

The objectives of this task are for the completion the project, to capture the effects of the inlet operating at LTO conditions, and to facilitate low-speed aerodynamics modeling for the supersonic inlet, including the viscous effects encountered by supersonic inlets during LTO conditions. The initial inlet analysis model, used in Year 1 and Year 2 of the project, uses a simple viscous loss relationship, which is scaled depending on the freestream air Mach number and the sharpness and radius of the inlet cowl lip, taken from the IPAC publication's equations (Barnhart, 1998). This loss model does not account for the potential improvements achieved by modulating the variable geometry of the inlet to maximize airflow, and minimize the viscous effects incurred by incoming air when pulling around the cowl lip and sidewalls.

Research Approach

Several approaches were followed to identify computationally low-cost methods for determining low-speed aerodynamics over the supersonic inlet ramps, cowl lip, or compression center cone:

- Perform a literature review to identify analytical methods for modeling low-speed viscous flow over a flat ramp with varying angles of attack or incidence.
- Implement these methods within the script and compare results for validation against published sources and published experimental data.
- Perform flat-plate loss approximations and compare them with experimental data and the results achieved.
- Select the method yielding the best results with reasonable computation execution time.

As was mentioned in previous sections, it was important to ascertain any potential benefit or loss contributed by the inlet on the installed engine regarding thrust and impacts to noise. As such, the extension of the Task 2.1 effort, in adding a low-speed aerodynamic module to the supersonic inlet design and analysis code was anticipated to be important to achieving the overall research study. Several approaches were attempted to develop a low-cost low-speed aerodynamics module of the zero-order fidelity to integrate with the developed inlet code. These attempts employed flat-plate approximations, as well as more sophisticated approaches accounting for boundary layer skin friction losses and were validated by Reynolds-averaged Navier-Stokes (RANS) CFD runs performed by the researchers.

Viscous loss models associated with low-speed aerodynamics (below M=0.8) were developed and implemented in a viscous aerodynamics module and integrated into the inlet code. Several functions were developed from different references to model losses on the different sections and account for different phenomena and then integrated together. First, a model to capture the effects of skin friction driven total pressure losses on the external ramps was developed. The function computes the flat plate average turbulent skin friction coefficient on the external ramps using the Prandtl-Schlichting relationship for turbulent flow. This model also uses a relationship to add compressibility corrections to the skin friction equation, as most of the inlet code's compressibility effects were previously captured either through the prediction of shock effects, or compressible effects inside the inlet duct—prior to this effort, there were no viscous losses associated with the external compression ramps. The curves relating the Reynolds number of the flow to the incompressible turbulent flow before the compressible correction (Equation 4.3.7 from McLean [2012], shown in Figure 15) and is defined in McLean (2012) with the compressibility correction for skin friction.

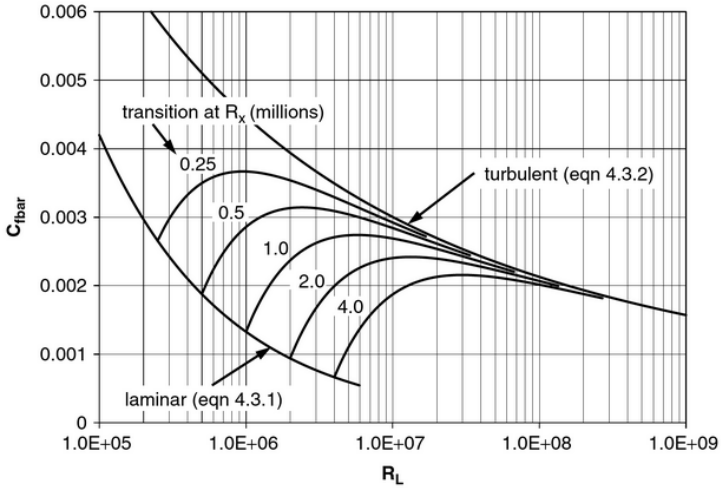

Figure 15. Prandtl-Schlicting relationship for incompressible turbulent flow (McLean, 2012).

The second relationship in the viscous flow module for external compression is similar to the previous one, except it is for the flow inside of the converging duct of the 2D inlet, and not the external compression ramps. This set of equations computes the turbulent skin friction coefficient in a 2D channel model of the internal converging duct utilizing the correlations identified in Dean (1978). As the rectangular duct loss model identified in Dean (1978) was for incompressible flow, the compressibility correction from McLean (2012) was employed here as well.

The third relationship identified for use in the low-speed viscous flow model is the calculation of total pressure losses on external ramps due to boundary layer skin friction. The model was derived from Seddon and Goldsmith's *Intake Aerodynamics* text, Equation 3.4 and employed using logic obtained from Chapters 2 and 3 (Seddon & Goldsmith, 1999). Here, an empirical factor defined by Seddon and Goldsmith (1999), the external wetted surface area, the ambient freestream dynamic pressure seen by the external ramps, and external skin friction values were calculated and used to find the change in total pressure due to boundary layer skin friction on the ramps, using Equation 3.4. Here, I is the duct integral, $q_\infty$is the freestream dynamic pressure, $\frac{A_\infty}{A_C}$ represents the ingested mass flow ratio, J is the position ratio defined by the surface area of the wetted flow divided by the inlet cross sectional area at the investigated location, and C_{fd} , C_{fa} are friction coefficients for the duct and the cross sectional area, respectively.

$$\frac{\Delta P}{q_\infty} = IC_{Fd}\frac{\rho_\infty}{\rho_c}\left(\frac{A_\infty}{A_c}\right)^2 + JC_{Fa}\left(\frac{A_c}{A_\infty}\right) \quad \text{(Eq. 2)}$$

The next relationship computes the incompressible flow and the critical flow ratio below which pre-entry losses due to boundary layer skin friction occur. it was derived from data taken from Seddon and Goldsmith (1999) (shown in Figure 16). This was adapted to application for compressible flow using Figure 16.

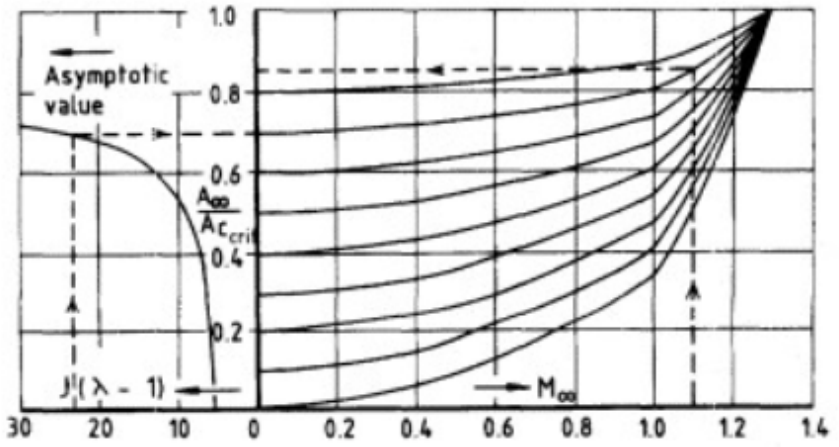

Figure 16. Critical flow ratio for pre-entry separation from intake aerodynamics (Seddon & Goldsmith, 1999).

The fifth relationship used in the viscous flow module computes the total pressure losses in the converging duct due to boundary layer skin friction—similar to the third viscous model described above, except adapted for the 2D duct. Lastly, a parametric model was developed to determine the separation losses for pre-entry flow due to boundary layer effects at low speed if the demanded flow ratio was less than the critical flow ratio. This model employed equations and approaches found in Seddon and Goldsmith (1999), Chapters 3 and 7.

The model was assembled and validated after several months of effort in attempting different approaches, and then it was validated using CFD runs, as previously discussed. The effects of pressure due to low speed aerodynamics validation can be seen using the final inlet design ($M_D = 1.7$), in Figure 17. The validation achieved across several runs for Mach 0.3 can be seen in Figure 18. It can be seen that the effects of the losses from the local position (ramp start location) to the throat (through converging duct) agree well for the baseline inlet model for pressure losses as the mass flow rate at the throat (WTH) is varied and normalized by the inlet height (depth in ft).

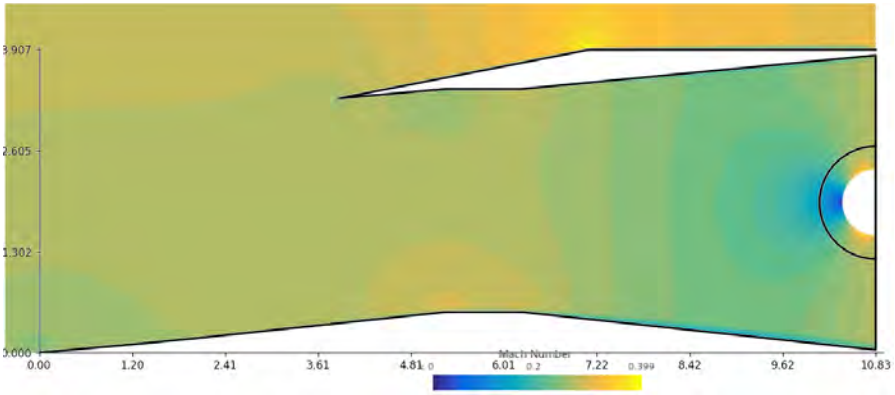

Figure 17. CFD run with the selected inlet design at M=0.2.

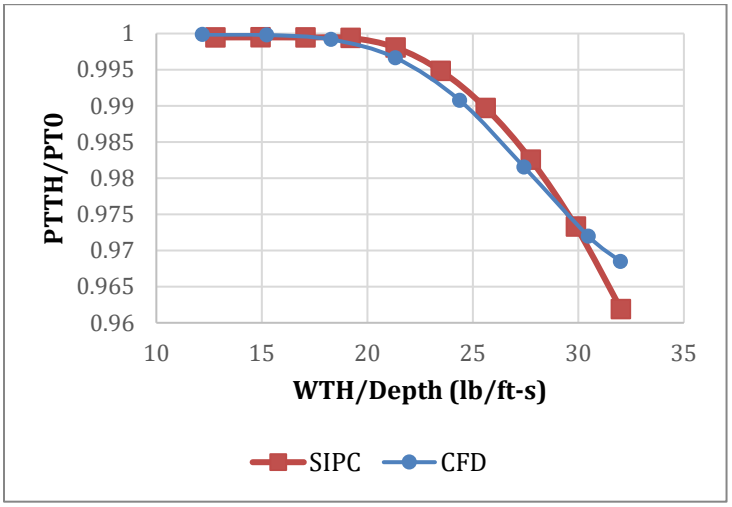

Figure 18. Validation of low-speed losses model in the SIPC vs. CFD run.

A similar study was performed for the larger capture area modification to the baseline inlet achieved using the variable geometry cowl lip (VGCL), which will be described in Task 8. This comparison proved the loss model performed with much worse agreement but nonetheless provided aggressive losses due to low-speed aerodynamics effects compared to the CFD run and thereby was retained as it provided a more conservative prediction of the overall inlet performance by underpredicting. The error between the SIPC and CFD models at the highest normalized throat mass flow rate was 2.2%, and the capture area was assumed to be 20% larger than the baseline inlet shown in Figure 18, which is shown in Figure 19.

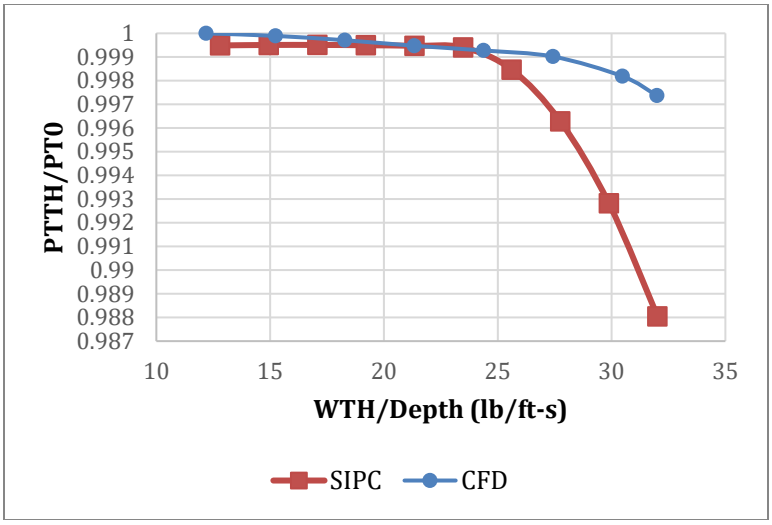

Figure 19. CFD validation results for the baseline inlet with variable geometry cowl lip (20% larger capture area).

The loss model was shown to have acceptable error when compared to CFD runs, which were used as a baseline truth model, and they were retained and used for the remainder of the study, specifically in the generation of the inlet maps.

Milestone

- Extended zeroth-order methods for inlet performance to include low-speed aerodynamics.

Major Accomplishments

- Developed and added a low-speed viscous aerodynamic model into the SIPC and validated with CFD.

Publications

None.

Outreach Efforts

None.

Awards

None.

Student Involvement

None.

Plans for Next Period

None.

Task 7 – Establish Modeling and Simulation Tool Integration

Georgia Institute of Technology

Objective

Since the research being pursued for the work described in this report was performed using analytical modeling and simulation approaches, it was necessary to identify suitable tools, however disparate, to accomplish the required tasks. The tasks to be accomplished by modeling and simulation tools were the following:

1. Inlet modeling: Needed to capture the effects of the inlet and generate performance data to be implemented into an engine cycle modeling tool.
2. Engine cycle model: Needed to capture the installed effects of the engine, including inlet and nozzle, along with jet noise reduction devices (chevrons).
3. Vehicle and mission model: Needed to capture system-level effects of installed engine during SST mission profile, specifically at LTO conditions.
4. Noise modeling: Needed to understand the potential benefits or degradations of an advanced inlet on an engine with adding variable geometry to an inlet and jet noise reduction technologies to the nozzle.

Research Approach

Several different tools were assessed to accomplish each of these tasks for the research effort, but the following were selected: (1) SIPC for inlet modeling, due to the flexibility of design, extensibility for future tasks, capability beyond IPAC in compressible flow modeling and low speed aerodynamics module, and the ability to be used by non-United States students, (2) FASST, an engine-vehicle sizing and synthesis code developed by GT-ASDL, which employs NASA's tools NPSS for engine cycle modeling, (3) CMPGEN for engine compressor map generation, (4) FLOPS for mission profile optimization and vehicle sizing and synthesis, and lastly (5) ANOPP, which is integrated into FASST, for noise prediction as a result of the engine and vehicle modeling results. A basic flowchart outlining the modeling framework utilized for this research is presented in Figure 20.

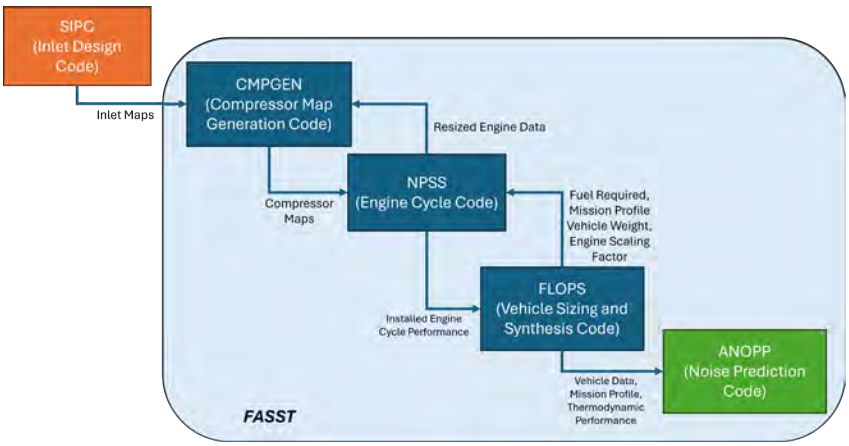

Figure 20. Flowchart of the modeling framework used in ASCENT Project 059(A).

Once the notional framework was determined, it was necessary to identify specific inputs and outputs provided by each section and connect them appropriately, in the correct format. For a first iteration testing of the framework and its component tools' integration, the tools in FASST were kept constant, which is to say, that they were not further modified for the purposes of the study at hand. This was in part due to the fact that necessary modifications to the iterative sizing process and software run order were not known or understood at the time of the initial framework integration. Modifications to the framework were identified after the specific inlet designed for the study was installed onto the selected engine and aircraft models, and the jet noise reduction methods were determined. These subtasks were performed in Task 11.

As shown in Figure 20, FASST is a supersonic vehicle sizing and synthesis tool which performs engine modeling, aircraft modeling, and mission profile optimization for the designed aircraft system. The tool utilizes user inputs to define criteria for engine and aircraft sizing, and initial guess points, such as maximum T4, turbomachinery calibration factors and map operating points, thrust targets for different segments (i.e., take-off, cruise, supersonic pinch point, top of climb and sea level static), mission profile altitudes, design mission range, and many others. Inputs used are passed initially to CMPGEN, which determines an initial set of turbomachinery compressor maps which are used in the first iteration of the engine code. After this first iteration is completed, the engine is resized to meet the demands of the required thrust in the NPSS model. After the engine is designed, the aircraft variables from the user input are utilized and the vehicle is modeled in FLOPS, with the installed engine for the design and off-design missions. After the vehicle has converged to an appropriate

size to fly with the designed cycle, meeting the requirements input by the user, it enters the "environmental off-design" analysis phase. In this phase, emissions and noise are determined, as well as detailed mission profile segments, such as take-off, approach, and landing. For the purposes of this project, only the noise module which utilizes ANOPP was run, as the other modules produced results which did not pertain to noise or thrust at LTO conditions.

Coupling the codes in the FASST was not necessary, as it was already performed as part of the code development, and used in several research projects, including ASCENT Project 010, where several SST vehicles and engines were developed and presented. It will be seen in the section describing Task 11, however, that FASST required modifications to achieve the objective of the research task sought here. Since the assembly of codes which defined FASST was already completed, the chief objective of this task was to determine a means to integrate inlet performance into the engine cycle and have those results propagated to final off-design performance and noise analysis. In Year 2 of work, researchers attempted to modify SIPC into rapidly running executable which could be called for each FASST iteration, changing the inlet design for each iteration. This task was notionally completed, but the variation in inlet design performed for each iteration could not be achieved with reliability.

It was found that the inlet code was not developed enough to allow for the prediction of normal shock position and redesign of the inlet variable geometry ramps with suitable accuracy to be utilized for the work at hand. Due to the desire to complete the project on time, the effort was abandoned, in favor of working on the development of SIPC to enable more robust predictions for off-design performance. Additionally, it should be noted that the executable-based approach for inlet performance prediction was initially sought due to the difficulty in understanding how to generate inlet performance maps, as there was a lack of any clear guidance in the literature. The pursuit of, and the accomplishment of, determining an inlet map generation process was completed by a deep literature review, independent research between several research engineers at the GT-ASDL (who were researchers on the project), and discussion with subject matter experts. This will be described in greater detail in Task 9.

As part of the inlet performance prediction integration into the overall modeling and simulation framework, it was determined that the use of conventional inlet maps was desired. In order to do this, the implementation of inlet maps into FASST had to be explored and developed, and the ability to generate maps using SIPC was also necessary. While a previously-defined set of inlet maps could have been used to perform a basic version of the study, the researchers determined that there was no reliable way to modify the models of experimental inlet data to attempt to add variable geometry, which is a key feature of the study presented in this document. As such, the inlet map integration exercise for this step was performed with an inlet from the PIPSI software, described in reference (Kowalski, 1979). An example of an inlet map, one of eight, shown in Figure 21. The eight-map format defined by PIPSI utilizes maps to describe all of the off-design operating conditions of the inlet, with several factors being implicit in them, and opaque to the user—specifically inlet geometry and ramp angles at off-design conditions.

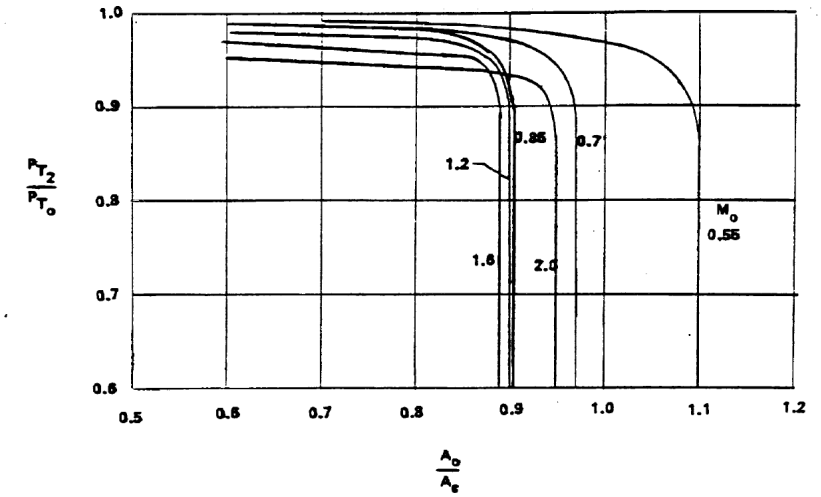

Figure 21. Inlet total pressure recovery map for ATS2 inlet from PIPSI (Kowalski, 1979).

A list of the maps defined for each inlet modeled in FASST, and used together to achieve a full picture of the inlet performance across engine cycle design and off-design points, is summarized as the following:

1. Inlet Recovery vs. A0/AC & Local Mach (TABLE 2A) → Cane curves to find Total Pressure Recovery of inlet
2. Buzz A0/AC vs. Local Mach (TABLE 2D) → Operability check of required inlet mass flow vs. buzz limit (lower bound)
3. Distortion A0/AC VS. Local Mach (TABLE 2E) →Operability check of required inlet mass flow vs. distortion limit (upper bound)
4. CD Spill vs. A0I/AC & Local Mach (TABLE 3) →Determination of spillage drag
5. CD Bleed vs. A0Bleed/AC & Local Mach (TABLE 4) →Determination of bleed drag
6. CD Bypass vs. A0Bypass/AC & Local Mach (TABLE 5) → Determination of bypass drag
7. A0Bleed/AC vs. A0/AC & Local Mach (TABLE 6A) →Determination of required bleed mass flow
8. A0Bypass/AC vs. A0Engine/AC & Local Mach (TABLE 7) →Determination of required bypass mass flow

The order of table lookups associated with the inlet installation using the PIPSI maps will be explained here. The engine mass flow demand is determined by the engine cycle model and then the required bypass mass flow, which was experimentally determined to be necessary for retaining a normal shock to stay "started" (if any), is determined from Table 7 (as defined in list above). Once the engine and bypass mass flow demands are known, these values sum to determine the value of $\frac{A_0}{A_C}$, which is a primary feature used for determining other flows. Then, the value of $\frac{A_0}{A_c}$ is then checked against Tables 2D and 2E (as defined in list above) for possible buzz and distortion effects due to mass flow through the inlet, which is too high, or too low. Buzz occurs in the inlet subsonic diffuser when the mass flow passing through it is too low, and an oscillatory behavior creates a harmonic oscillation which can potentially cause a compressor surge or stall (Seddon & Goldsmith, 1999). On the other end of the spectrum of inlet operability allowance, distortion is the effect seen when too much mass flow is passed through the inlet and creates uneven pressure distributions at the compressor (fan, in this case) face. This can have similar effects to buzz and could be detrimental to engine performance in off-design conditions (Seddon & Goldsmith, 1999). These values, like the others included in the inlet maps from PIPSI, were derived experimentally. If the $\frac{A_0}{A_C}$ values for the operating point under consideration are between the buzz and distortion limits, then Table 6A (as defined in PIPSI workflow list, above) is used to find the required boundary layer bleed mass flow ratio. The sum of $\frac{A_0}{A_C}$ and bleed mass flow rate yields the total ingested mass flow rate, $\frac{A_{0I}}{A_C}$, which determines the amount of spillage experienced by the inlet at any condition. As such, then Tables 3, 4, and 5 (as defined in PIPSI workflow list, above) enable the drag coefficients of spillage, bleed, and bypass to be determined. This is performed by the engine code each time the engine model is run. The means of installing the inlet performance determined SIPC was found to be best performed using inlet maps, and an example inlet map from PIPSI (Kowalski, 1979) was used to check this integration prior to the execution of the actual study.

As the final part of this task, it was sought to establish the functionality of ANOPP and its integration with FASST in a way that was usable in the study at hand. ANOPP is a NASA noise prediction code with many nuanced modules, requiring an expert to fully understand and utilize all of its capabilities. Furthermore, the tool's capabilities continue to grow regularly, being continually developed by NASA researchers. A GT-ASDL researcher who serves as a noise analyst and ANOPP expert was able to assist in ensuring that ANOPP was set up to study jet noise at LTO conditions. This involved a modification in the user inputs to switch on the jet noise so as to not be confounded by other noise sources. Additionally, the employment of chevrons was selected due to the ability to model their noise effects in ANOPP, and their effects on the engine cycle in NPSS. ANOPP has a chevron-specific noise prediction function which is based on empirical regressions using the "Stone 2" jet noise prediction module, which enables the study of jet noise effects based on the parametric scaling of the ratio of the wetted perimeter of the nozzle exhaust to the wetted perimeter of the chevron exit. With some geometric studies and comparison, these values were easy to ascertain from the selected chevron geometries selected for study in Task 10 but were performed for an arbitrary nozzle perimeter ratio for the completion of this initial task. Once this was completed, the task was considered complete.

Milestone

- Established modeling and simulation tool integration—engine cycle, inlet design, and noise analysis tools.

Major Accomplishments

- Performed initial integration work using example inlet, and selected engine and aircraft design to be used in studies.
- Determined and evaluated an approach for coupling inlet, aircraft, and noise codes.
- Identified ANOPP noise modeling approach for use with chevrons.

Publications

None.

Outreach Efforts

None.

Awards

None.

Student Involvement

None.

Plans for Next Period

Task 7 is complete.

Task 8 – Development of Inlet Variable Geometry Methods and Models for Improving LTO Thrust

Georgia Institute of Technology

Objective

The objective of this task was to find new ways to potentially enable the recovery of thrust when jet noise devices were added to the nozzle of the SST engine, by adding new ways for the inlet to function in the off-design condition. While it is possible that the baseline advanced inlet made for the selected 65-passenger SST with MFTF engine could provide sufficient thrust recovery, it was sought to determine how much more thrust from the baseline inlet model, variable geometry permutations of it could.

Research Approach

The capability to add several variable geometry configurations to a baseline inlet was sought in order to determine if these new configurations would allow for greater performance at high mass flow demand conditions, such as those seen at LTO. The variable geometry capabilities investigated by the researchers included a VGCL and blow-in doors; a third configuration in which both the VGCL and blow-in doors were manipulated was sought to be modeled. Variable geometry is typically employed in 2D supersonic inlets, but it is primarily used for the control of oblique shocks and the variation of the throat area to prevent mass flow restrictions and choking, thereby improving engine operability at supersonic speeds. After several iterations of design, the inlet designed here only used variable geometry for LTO conditions as described in this task, and no variable geometry. The purpose of this was to reduce weight and complexity when compared to highly complex inlet designs for SSTs such as the Concorde inlet. As such, the two variable geometry modeling additions described here were the only means utilized for the final study to modulate mass flow apart from the engine demand, bypass doors, and boundary layer bleed.

First, in order to facilitate a study into how to appropriately use bleeds, bypass and blow-in doors for a SST inlet without using variable geometry external compression ramps, the ability to draw bleed from ramps was added to the model, as well as bypass from the throat. As seen in Figure 7, boundary layer bleed is typically considered to be taken from the throat, while the bypass is taken from just forward of the engine face at station 2. Due to the decision to use a fixed inlet (no variable geometry external compression ramps), these options were needed in addition to the conventional positions of the bleed and bypass doors to prevent choking and improve operability. This was completed by replicating the bleed and bypass stations in SIPC in their new positions, ensuring that the mass flow ejected from them experienced the

appropriate friction losses, and ensuring that the downstream flow resulting from the mass flow extraction was appropriately modeled.

Second, a model to simulate blow-in doors was added to the inlet code. Blow-in doors are spring-loaded devices which have been employed on subsonic commercial transports for many years but were ultimately rejected despite their improvement in performance due to the increase in mass flow provided when the differential pressure between inlet and ambient static pressures were significant enough, due to noise problems (Marsh et al., 1983; McPike, 1972; Little & Russell, 1976; Aviation Stack Exchange, 2021). While this could clearly provide a potential problem for supersonic engines, which operate with much greater thrust than the subsonic engines referenced in Marsh et al. (1983), McPike (1972), Little & Russell (1976), and Aviation Stack Exchange (2021), this modeling option was desired to be explored in the case that technological improvements in noise shielding could potentially counteract this for future SST vehicles. Additionally, it can be seen in a schematic of the Concorde inlet in Figure 22, that blow-in doors were used for their ability to improve take-off mass flow rates (Slater, 2020). In combination with the first inlet modeling improvement subtask listed under this task, the blow-in doors were able to be modeled at the throat, as well, which could potentially provide a practical improvement in noise reduction over the aft-mounted blow-in doors on the Concorde inlet, which are much closer to the engine face. No SIPC schematic was developed to illustrate the blow-in doors, so it is not shown, here.

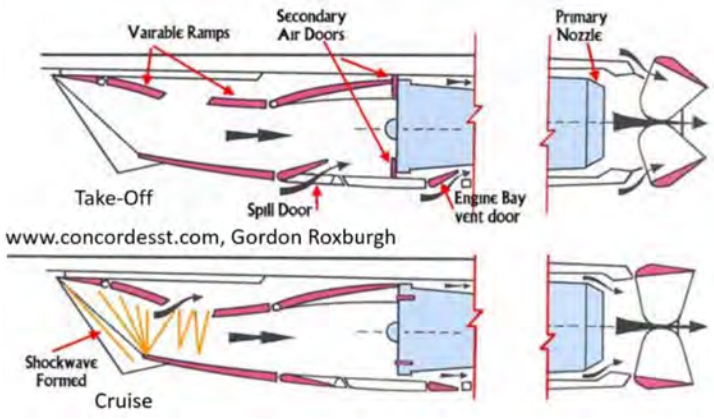

Figure 22. Schematic of Concorde inlet operation at take-off and cruise; spill/blow-in door used for take-off (Slater, 2020).

The last subtask for this task was to develop a model for the increase of capture area by allowing for a VGCL. Although initially conceived by the researchers as a novel concept, this design was found to have been implemented in several cases in actual vehicles for the purpose of increasing air quantity at take-off conditions. An example can be seen in the Eurofighter Typhoon EF2000, where the rectangular pitot inlet utilizes VGCLs for its bifurcated inlet design, seen in Figure 23 (Aircraft Recognition Guide, 2018). This concept was mirrored and implemented into the SIPC, enabling a pivot of the cowl lip just forward of the throat, and increasing the capture area 20%. This concept was evaluated and proved to show a large increase in capture area, with a decrease in friction losses compared to the baseline inlet. The SIPC-generated schematic of the VGCL superimposed upon the baseline inlet used for this study is shown in Figure 24. The improvements here assisted in the overall completion of the project by adding the ability to consider new ways to increase mass flow provided to the engine for thrust compensation. The results of this implementation will be shown in later sections.

Figure 23. Eurofighter Typhoon VGCL inlet (Aircraft Recognition Guide, 2018).

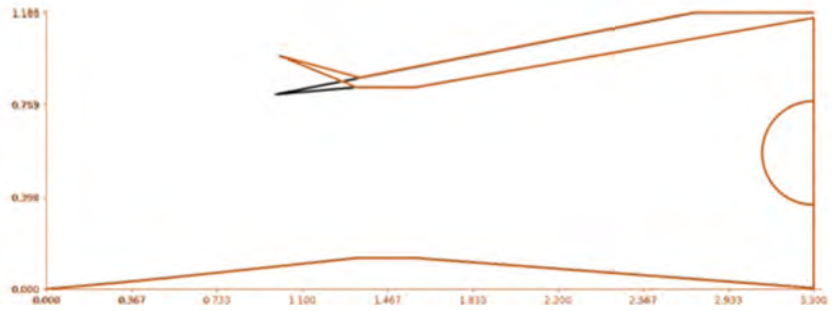

Figure 24. M=1.7 SST inlet used in study: Baseline inlet (black) vs. VGCL geometry activated (orange).

Milestone

- Completed the development of inlet variable geometry methods and models for improving LTO thrust.

Major Accomplishments

- Developed and added ramp bleed ports and throat bypass models into SIPC.
- Developed and added blow-in door models into SIPC.
- Developed and added VGCL models into SIPC.

Publications

None.

Outreach Efforts

None.

Awards

None.

Student Involvement
None.

Plans for Next Period
None.

Task 9 – Development and Implementation of SST Inlet to be used as Baseline Model and Off-design Inlet Maps
Georgia Institute of Technology

Objective
The objective of this task was to (1) identify and select the engine and vehicle to be used as the baseline for the thrust-noise study executed in Task 13, (2) design an inlet specifically for the vehicle selected from subtask 1, (3) understand how to analytically develop inlet maps, and (4) generate inlet maps for the inlet designed in subtask 2. These objectives were accomplished as part of three subtasks.

Accomplishing these specific tasks would enable a baseline installed engine to be developed from which the chevron and variable geometry inlet models could be compared with regards to thrust recovery and noise impacts.

Research Approach
The first task required to proceed with the analysis of jet noise reduction using inlet geometries was to select an engine and airframe to be used in the FASST as the basis for the nozzle and inlet study. A supersonic vehicle which could utilize a supersonic inlet and converging-diverging supersonic nozzle was required. As those components would be required for any SST design to which the study may apply. Beyond this, the details of the vehicle class and engine size were inconsequential, as the study here seeks to determine benefits of the inlet from an established baseline. As such, several engine and aircraft models developed by the GT-ASDL were considered, but the 65-passenger SST with a design Mach number of 1.7 was selected due to its extensive testing, model robustness across many operating conditions tested, and the fact that it had already been presented and investigated by ASCENT Project 010. A schematic of the vehicle is shown in Figure 25.

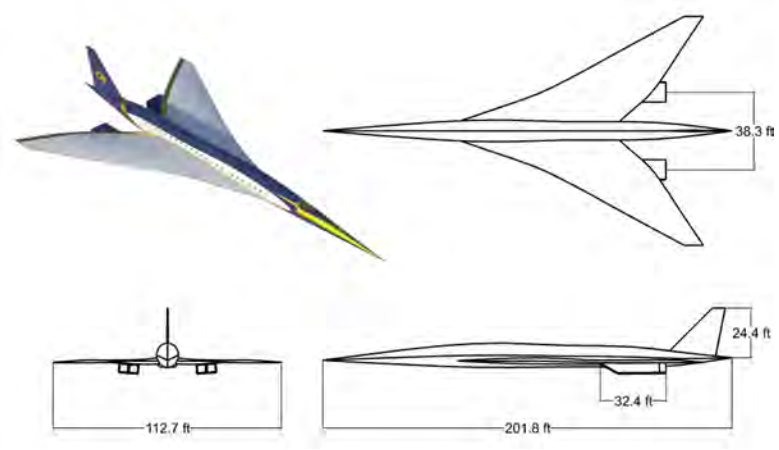

Figure 25. GT-ASDL SST (initially presented in ASCENT Project 010).

The GT-ASDL vehicle was developed using the FASST and several aerodynamics tools; the researchers used RANS CFD for aerodynamic shaping of the fuselage and outer mold line, along with multi-fidelity and parametric polar drags generated with tools developed in-house and used RANS CFD for LTO drag estimation. The propulsion cycle was modeled in NPSS using parametric loss models and multi-design point sizing, sizing for the supersonic pinch point, and satisfying operating

criteria for cruise, take-off, top of climb and sea-level static conditions. A summary of the vehicle performance data is in Table 5.

Table 5. Summary of GT-ASDL 65-passenger SST.

Passengers	65
Design Range	4,250 nmi
Cruise Mach	1.7
Max Take-off Field Length	11,000 ft
Approach Speed	165 kts

The engine developed for the ASCENT Project 010 and used here was a mixed-flow turbofan architecture which was designed in NPSS. The engine design parameters considered were the fan pressure ratio, overall pressure ratio, design turbine rotor inlet temperature, bypass ratio, and max turbine rotor inlet temperature. These parameters were varied to meet the design point and simultaneously meet the criteria of the aforementioned satisfaction points in a simultaneous multi-design point sizing approach. The engine utilizes two controls in order to affect thrust and noise conditions, fuel flow to affect the speed and thermodynamic states of the turbomachinery, and the nozzle throat, to affect the jet stream thermodynamic properties. A schematic of the engine layout as defined in NPSS is shown in Figure 26.

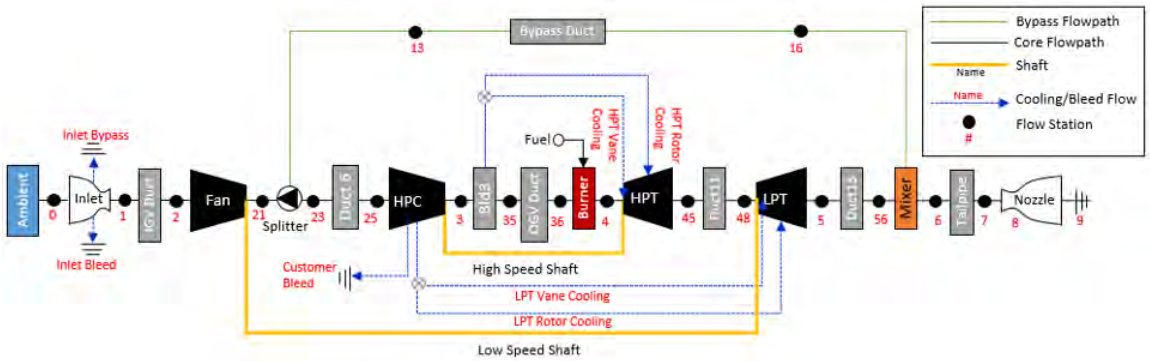

Figure 26. Schematic of NPSS Model of non-afterburning MFTF used on 65-passenger vehicle.

Ultimately, the vehicle designed could perform a 4,250 nmi mission with 13,650 lb of payload, using 156,611 lb of block fuel, and requiring 10,832 ft to take-off and 10,442 ft to land, with a cruise thrust-specific fuel consumption (TSFC) of 1.023. The vehicle employed a predefined inlet utilized from the PIPSI installation volume (Kowalski, 1979), ATS2 inlet, for each engine. This approach enabled a quick modeling of the inlet performance of the vehicle, but when it was developed, an inlet design capability to generate maps and utilize them in the FASST did not exist. As such, it was a suitable experiment to develop a new inlet for the 65-passenger GT-ASDL SST for the performance of this study.

The inlet was designed to be a 2D supersonic inlet with non-variable geometry and only utilizing external compression for the shock train management. This design selection was based on guidance from Seddon and Goldsmith's "Practical Intake Aerodynamic Design" (Seddon & Goldsmith, 1993) and Kowalski's guidance from the PIPSI documentation in Kowalski (1979). A chart of this guidance is shown in Figure 27. Investigating this chart in Figure 27, from early research and implementation on vehicles, up until the development of PIPSI (circa 1979), many different inlets were developed for use across a spectrum of design Mach numbers. The trend of increased numbers of oblique shocks corresponding to an increase in operating Mach number can be seen—this is used to mitigate the strength of the normal shock when it occurs in the inlet. It can also be seen here that it is recommended for the design of a supersonic inlet to be used at M=1.7 to use between two shocks and three shocks, and external compression. It can also be seen that this flight regime corresponds to a recommendation of variable geometry, but as this is at the initial stages of the supersonic regime, that recommendation can be seen as flexible. The driving factor in inlet design, as guided by Figure 27, is to minimize complexity and length of the inlet insofar as one can gain benefit from the simplest design. As such, variable geometry should be avoided for the low supersonic operating conditions since it adds a significant amount of weight and can add potential for failure in flight.

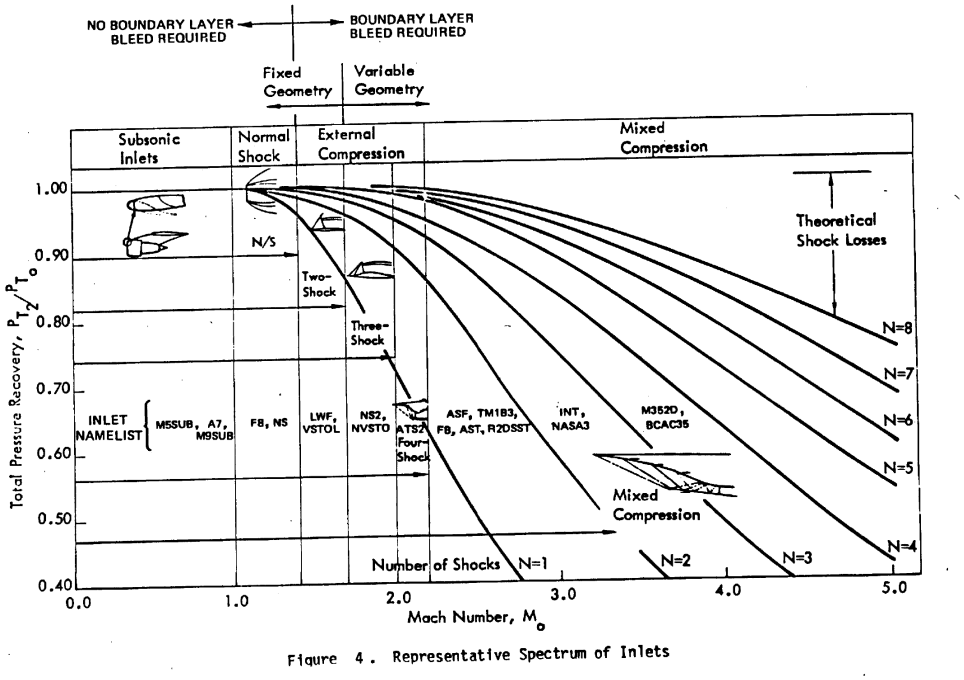

Figure 4. Representative Spectrum of Inlets

Figure 27. Recommended inlet designs for Mach numbers 0 to 5 (Kowalski, 1979).

Using this as guidance, the inlet design pursued for this study to be implemented on the GT-ASDL vehicle utilized three short fixed external compression ramps and was developed to be as short as possible to minimize weight, while still trying to take advantage of the benefits of the length of a subsonic diffuser, which slows down the flow of the ingested air just prior to the compressor face, and uses an isentropic diffusion surface to try to reduce the amount of pressure lost across it. In order to determine the appropriate size of the inlet, the uninstalled engine was run in NPSS. An engine deck was developed to identify the maximum mass flow required at all points of the previously defined SST mission. Once this was determined, the capture area was sized and the external ramp angle was determined based on maximizing total pressure recovery, and the condition that the external oblique shock had to meet the cowl lip at the cruise condition, to minimize the critical drag experienced there. A non-scaled model of the resulting inlet operating at the cruise condition, as generated by the SIPC shown in Figure 28. It can be seen that three oblique shocks form on the turning surfaces of the external compression ramps, converging at the cowl lip above them. A normal shock is formed and is positioned at the cowl lip, which serves as the critical operating condition for external compression ramps. Lastly, a strong oblique shock results at the cowl lip as a result of the normal shock-oblique shock interactions there. It can also be seen that a small, straight channel exits past the cowl lip, which serves as a safety region in the case of transients during which the normal shock may be swallowed.

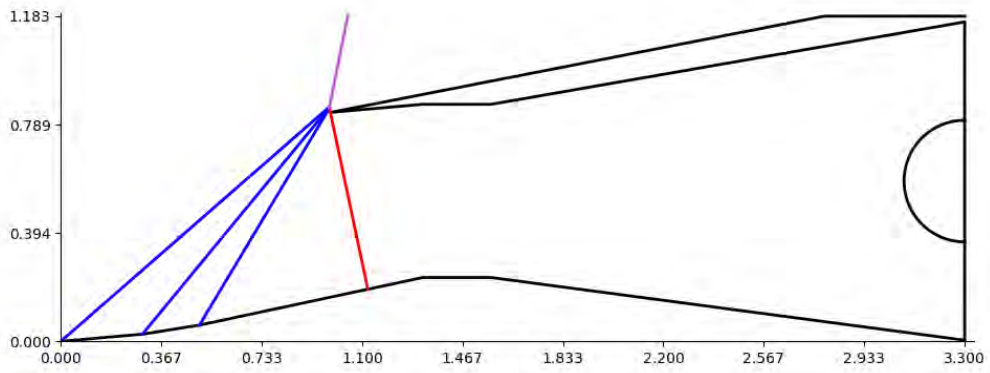

Figure 28. M=1.7 SST Baseline inlet at cruise condition (M=1.7).

After the inlet was designed, the variable geometry options developed in the prior task were evaluated and implemented at take-off conditions between M=0.01 and 0.3, based on the SST mission profile. The VGCL modification can be seen in Figure 24, and the aerothermodynamic effects of increasing mass flow and the associated were seen in the SIPC output files for the LTO conditions, as well. The bypass doors and VGCL each enabled a maximum mass flow to increase at LTO conditions of 20% of the capture area. As such, the baseline inlet capture area was assumed to be 1.2, and with both VGCL and blow-in doors activated, the inlet could use an effective capture area of 1.6 in the LTO regime. The inlet was modeled with functions actuated closed after rotation to minimize drag effects.

The process for generating inlet maps using the analytical inlet analysis tool then had to be determined and applied to get maps for the baseline inlet (no variable geometry), the VGCL case (only VGCL actuated), the blow-in doors case (only blow-in doors actuated), and then the hybrid case (both VGCL and blow-in doors actuated). The four different inlet maps used at the different conditions all employed the same inlet performance data in the operating regions outside of M=0.01 to M=0.3, as they were modeled to represent exploratory variations of the same inlet. The basis for inlet map generation took a significant amount of time (three months) and required input from subject matter experts and several papers and textbooks. Of note, Seddon and Goldsmith's texts (Seddon & Goldsmith, 1999; Seddon & Goldsmith, 1993) were of tremendous help, as was the paper describing the operation of the SR-71 inlet by Anderson (2014). Additionally, credit should be given to Dr. John Slater, the head of inlet design and analysis at NASA Glenn Research Center, who assisted in the researchers' understanding of map generation and provided validation of the approach.

Inlet maps are used to form a functional picture of the operational performance of an inlet for any point in the sky for which it was designed. In this way, inlet maps seek to inform the engine or aircraft designer about the predicted effects of installing a specific inlet design in all potential points which the inlet could see in flight. The primary inlet maps generated using the PIPSI format (Kowalski, 1979) describe the inlet's total pressure recovery, required mass flows for bypass and bleed, and drags associated with spillage, bypass, and bleed, along with reference maps which show the ideal performance case for each Mach number. The generation of the inlet maps, therefore, is akin to also performing the off-design control logic of the inlet and in the case of variable geometry ramps. However, in the case of fixed geometry, the maps are generated using variation of the engine mass flow at each Mach number from the lowest required mass flow to the highest required mass flow in the uninstalled engine deck as a guide for what would be required by the inlet. Additionally, bleed schedules need to be determined, using similar PIPSI maps as a guide, since these are typically generated experimentally. In this case, no bypass was used for internal shock positioning control, since the normal shock is not intended to be swallowed but was used to ensure external normal shock positioning to retain it at the cowl lip position and ensure minimized critical drag. Summaries of some of the inlet performance maps are shown in Figures 29 through 32, where they are compared side-by-side with a similar external compression inlet (ATS2 from PIPSI [Kowalski, 1979]) to illustrate the similarity in shape and numerical value.

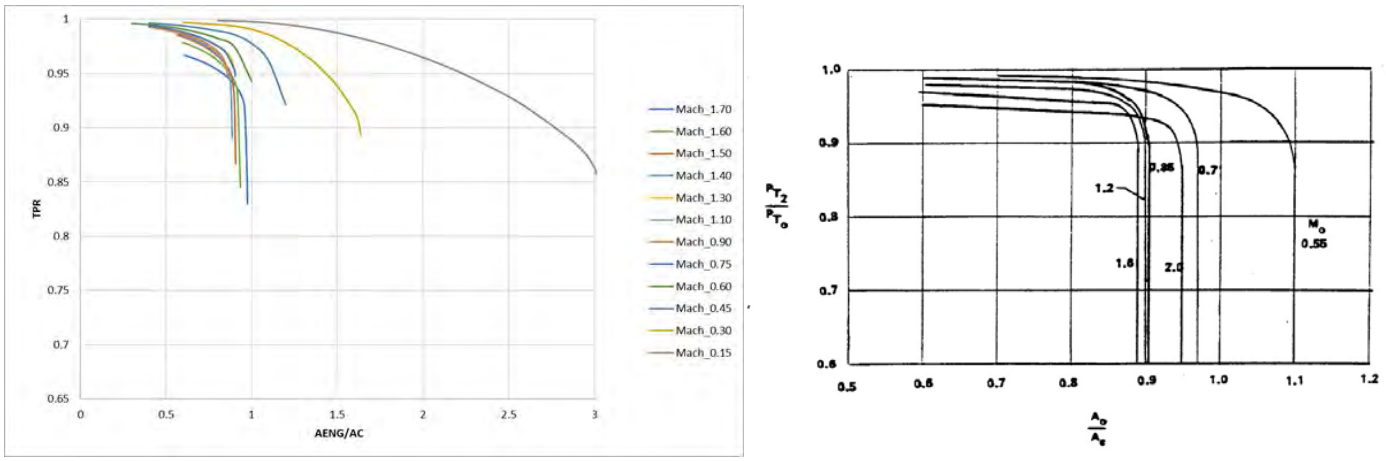

Figure 29. Total pressure recovery vs. mass flow ratio vs. Mach number (Kowalski, 1979).

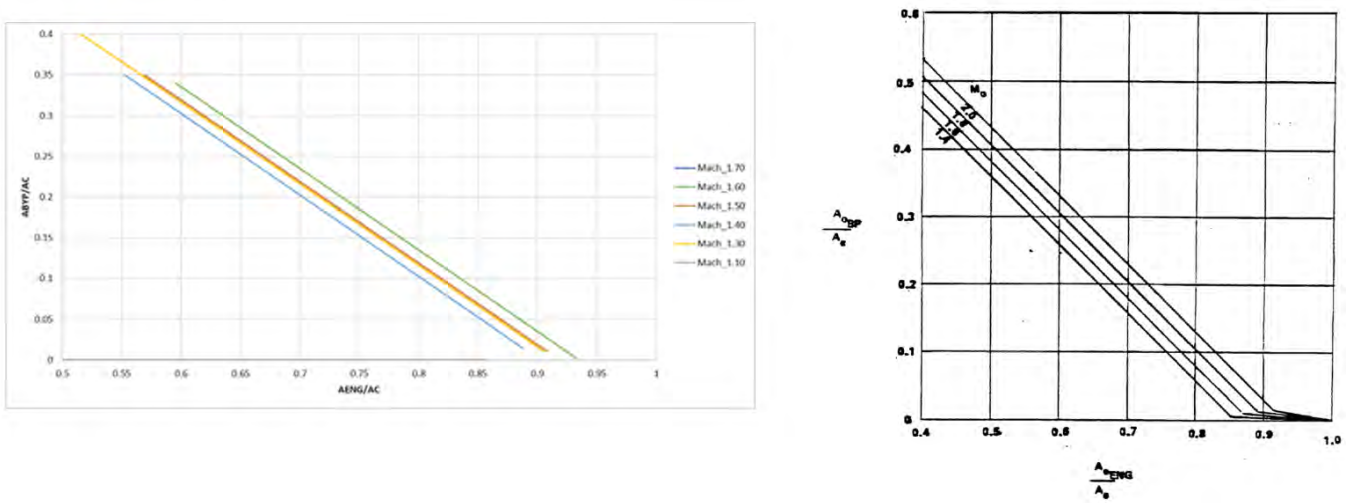

Figure 30. Engine mass flow ratio vs. required bypass mass flow ratio (Kowalski, 1979).

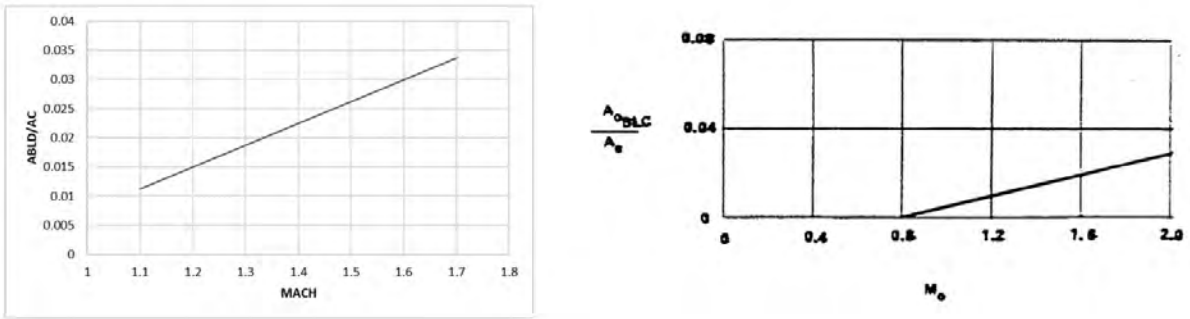

Figure 31. Required bleed mass flow ratio vs. Mach number (Kowalski, 1979).

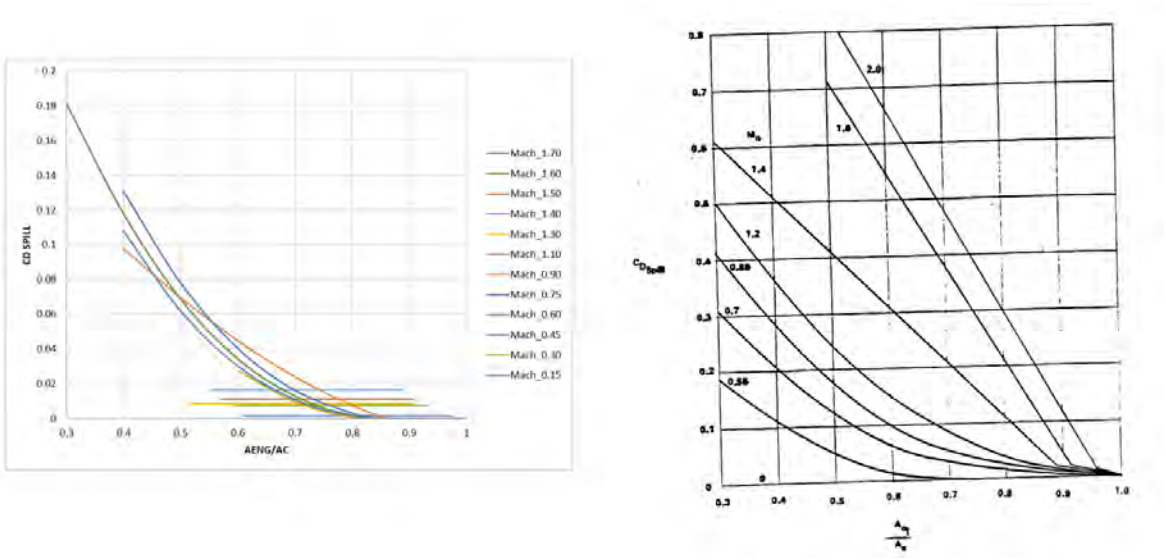

Figure 32. Spillage drag vs. mass flow ratio (Kowalski, 1979).

Finally, the inlet maps were generated for the variable geometry cases (i.e., baseline, VGCL, blow-in doors, and hybrid) defined previously and added to separate map files to be used in the FASST with integration with the GT-ASDL SST vehicle. Results for the cane curve (characteristic curve) map for the M=0.3 condition comparing the four cases can be seen in Figure 33. It can be seen that any means to increase capture area benefits the performance of the inlet for high mass flow ratios (engine demands), which are typically seen in the take-off condition. These maps account for viscous losses seen at low-speed conditions and the additional losses experienced by the air as a consequence of needing to move around the cowl lip due to the mass flow ratio being larger than 1 (implying that the streamtube area is larger than the capture area). Additionally, it can be seen that even if noise due to the implementation of blow-in doors is potentially an issue, significant benefit can still be achieved by only using the VGCL to increase airflow. Furthermore, an alternative to increase the area change due to the VGCL exists, as only one VGCL geometry was considered for this study.

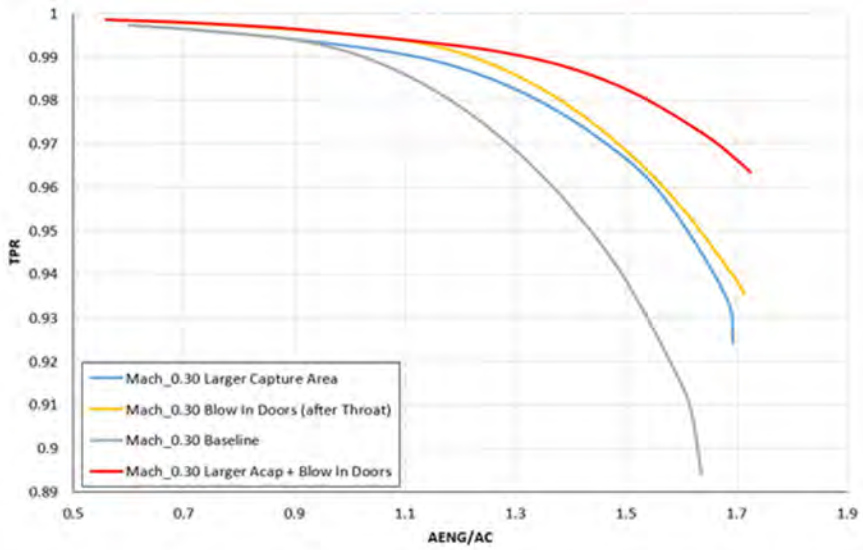

Figure 33. Cane curves for variable geometry inlet cases at M=0.3 take-off condition.

Milestone

- Completed the development and design of the SST inlet to be used as the baseline model and off-design inlet.

Major Accomplishments

- Designed the baseline inlet model for the selected M=1.7 65-passenger SST vehicle with MFTF engine.
- Adapted the baseline inlet model to use previously developed blow-in doors, VGCL, and ramp bleed and throat bypass models for off-design and verified functionality across the flight profile.
- Developed a process for analytically generating inlet maps for all off-design conditions using the standardized inlet map format presented in Kowalski (1979).
- Developed inlet maps for baseline inlet, VGCL, blow-in doors, and hybrid (both).

Publications

There are currently no publications for this effort; however, the researchers are pursuing a conference paper at 2025 AIAA Propulsion and Energy Forum to explain the development of the SIPC and analytical process for generating inlet maps.

Outreach Efforts

None.

Awards

None.

Student Involvement

None.

Plans for Next Period

None.

Task 10 – Development and Implementation of Nozzle-based Jet Noise Reduction Methods for Engine Cycle Effects

Georgia Institute of Technology

Objective

The objectives of this task are to determine a means to analytically model these features for several jet noise technologies and determine the metrics of interest (thrust loss and jet noise level) for them. This task was critical to model the effects of jet noise technologies on a supersonic engine to determine if the inlet can recover the thrust degraded by the nozzle technologies applied. As such, the jet noise technology modeling needed to account for thrust losses, effects on the exhaust stream, and the levels of noise resulting from the nozzle exhaust.

Research Approach

A key enabler for the completion of this research is a relationship between a jet noise technology's functional approach and effectiveness for noise reduction (mixing, noise insulation, etc.) and its effects on thrust losses. While many novel concepts have been investigated in the annals of aerospace research regarding reducing jet noise, and descriptions of the physical phenomena which contribute to noise reduction, it was found by the researchers that it is uncommon for those investigations into noise effects to be similarly investigated with corresponding effects on net thrust. As many technologies could be conceived which perform this function effectively, and have been implemented, many of them would generate losses in thrust which would render the device without net benefit to the installed engine. As such, for the purposes of this study, a means to couple these factors needed to be identified.

For the first two years (Year 1 and Year 2) of the project, it was anticipated that other ASCENT Project 059 partners would be able to experimentally or computationally derive relationships of thrust loss and noise benefit for unique nozzle-based jet noise technologies. After these relationships were determined experimentally, they would be provided to the ASCENT Project 059(A) team for use in the modeling and simulation described here. However, in Year 3, it was found that this

would not be possible, and an approach for modeling these behaviors would need to be found and implemented independently. To do this, a large literature review was performed, looking at a wide variety of jet noise technologies including chevrons (Bridges & Brown, 2004), contour shaping of the nozzle (Karon & Ahuja, 2017) , corrugations (Tinney et al., 2020), microfluidic injection (Morris et al., 2013), microvortex generators (Lui, 2021), and others.

More than 20 papers on the subject were carefully examined for potential use in this application, but their references are omitted for brevity. Ultimately, while some of the papers showed some relationships between thrust and noise benefits (very few, however), none also provided a scalable geometric or other factor which could be parameterized and implemented into the modified FASST framework used for this project except one paper, "An Aerodynamic and Acoustic Assessment of Convergent-Divergent Nozzles with Chevrons," by Frate and Khavaran (2011). This paper provides a means to parametrically define the chevron geometry using penetration depth, length and effective width as a percentage of base width and uses a RANS CFD code to find comprehensive results of thrust loss and noise benefit for installation on a modeled F400 series C-D nozzle. A parametric design of experiments based on these different chevron design parameters was developed and CAD models of the chevrons were generated for use in the CFD modeling. An illustration of the chevron parameters is shown in Figure 34, as well as the full matrix of their design of experiments (DOE) for the parameterization of the chevron geometries (Table 6), and the resulting performance values (Figure 35).

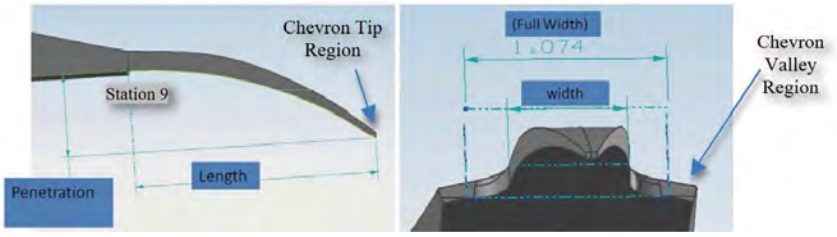

Figure 34. Parameterization of chevron geometries from Frate and Khavaran (2011).

Table 6. Chevron geometry DOE matrix from Frate and Khavaran (2011).

Serial	Configuration	Penetration (inches)	Length (inches)	Width (% of max)
1	P05L13W08	0.45	1.25	80
2	P03L08W06	0.3	0.75	60
3	P03L08W10	0.3	0.75	100
4	P03L18W06	0.3	1.75	60
5	P03L18W10	0.3	1.75	100
6	P06L08W06	0.6	0.75	60
7	P06L08W10	0.6	0.75	100
8	P06L18W06	0.6	1.75	60
9	P06L18W10	0.6	1.75	100
10	P02L13W08	0.2	1.25	80

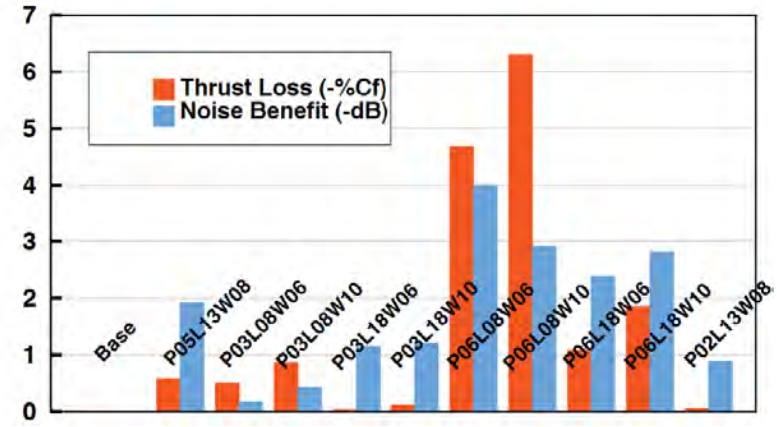

Figure 35. %Cfg loss and noise benefit for each tested chevron geometry in Frate and Khavaran (2011).

After this information was found, a sufficient set of data was determined to be in possession for the sake of performing the thrust-noise study. The means for modeling this experimental data and implementing them into the modified FASST framework was outlined in Task 7. The thrust losses for each nozzle technology were adapted to be modeled in the cycle modeling as a scalar on the gross thrust of the nozzle, using the gross thrust coefficient. Then, the effects on the jet noise and jet exhaust were modeled using the Stone 2 Jet Noise module within the ANOPP, which provides experimentally determined relationships for chevron noise benefits using a geometric relationship between the chevron nozzle wetted perimeter and the clean nozzle wetted perimeter, in a variable named "PER1." The geometries of the chevrons were scaled to the GT-ASDL SST MFTF engine nozzle size as they were normalized by the diameter of the F404 nozzle and rescaled to fit the GT-ASDL nozzle, assuming the performance remains similar when changing size, calculated on a spreadsheet. Once the effectiveness of this approach was determined by experimentation, the task was considered complete. The specific details regarding the chevron geometries selected and a comparison against the performance of similar chevron configurations are described in the task and section following this one.

Milestone

- Completed the development and implementation of nozzle-based jet noise reduction methods for engine cycle effects.

Major Accomplishments

- Performed a literature review to identify potential nozzle-based jet noise technologies to be modeled, which provided a thrust and noise relationship.
- Identified research papers with experimental and analytically derived data which correlated jet noise reduction to thrust loss using chevrons.
- Determined an approach for implementing chevrons into the cycle model to capture thrust losses and impact to engine cycle, as well as effects on jet noise in ANOPP.

Publications

None.

Outreach Efforts

None.

Awards

None.

Student Involvement

None.

Plans for Next Period

Task 10 is complete.

Task 11 – Completion of the Full Thrust Recovery and Noise Effects Study

Georgia Institute of Technology

Objective

The objective of this task is to integrate the products of all the previously completed tasks into the modified FASST modeling framework and ensure that the analysis methodology was sound. This involved modifying the FASST code even further to achieve the desired outcome for the study, which had been briefly mentioned previously. Additionally, it required manipulation and further adjustment of input data, such as the inlet maps and chevron nozzle parameters to ensure accurate modeling. A run matrix of experiments was compiled to understand the effects of the chevrons and inlets on noise and thrust, and analysis will be performed to identify the net effects of these devices on a baseline system. Upon completion of this task, the overall project was completed.

Research Approach

Introduction

Developing a suitable study to explore the topic at hand was difficult, due to the exclusively analytical approach and novelty of the effort. As such, several permutations of the study were investigated over time, and contributed to the tardiness of the submission of the final project results and findings. The approach in previous years to accomplish the primary research objectives was to investigate the necessary throttle push amount required to meet the take-off thrust requirements in spite of the installation of jet noise technologies added to the nozzle, and then proceed to see if the inlet could make up the difference in thrust push, precluding its necessity. Furthermore, this study was to be completed for a set of arbitrary nozzle technologies without any mapping to geometry or physical characteristics, since experimental data could not be ascertained. However, after attempting to model this, it was found that a simpler approach could be used to address the same research objectives in a more direct way. This modified approach was to:

1. Develop a baseline installed engine model with an unmodified inlet and clean nozzle (no chevrons).
2. Run the baseline installed engine model and aircraft in the FASST (and ANOPP) to obtain the baseline datum for comparison.
3. Add parameterized chevron geometries and thrust effects, as well as the record effects and run in the FASST/ANOPP to obtain losses due to chevrons.
4. Perform step 3 with variable geometry inlet settings.
5. Record and analyze data to understand the net effects of the inlet on jet noise.

Performing these steps would enable the same understanding as what was previously proposed, but in a much more straightforward manner. As such, it was important to develop a matrix of runs to execute, which can be seen in Table 7.

Table 7. Off-design Installed Engine FASST Run Matrix.

Run	Nozzle Model	Inlet Map
1	Round	Baseline
2	Chevron 1	Baseline
3	Chevron 2	Baseline
3	Chevron 3	Baseline
4	Round	VGCL
5	Chevron 1	VGCL
6	Chevron 2	VGCL
7	Chevron 3	VGCL
8	Round	Blow-In
9	Chevron 1	Blow-In
10	Chevron 2	Blow-In
11	Chevron 3	Blow-In
12	Round	Hybrid
13	Chevron 1	Hybrid
14	Chevron 2	Hybrid
15	Chevron 3	Hybrid

Modeling and Simulation Environment

The standard version of FASST utilizes many iterations of runs to ensure that the vehicle is sized to meet the requirements set by the user in the input file; this process was described in detail in Task 7. However, for FASST to run a selected off-design inlet and nozzle configuration and provide that data to ANOPP for a congruous noise output, it was necessary to identify a means for modeling a fixed engine, converging in a single iteration, and enabling the modification of the nozzle and inlet performance in the off-design study, only. Performing this task required that baseline vehicle did not resize itself to minimize block fuel burn after the installation of new inlet maps, but rather that the final 65-passenger vehicle model was achieved on the first run of the code.

By modifying the FASST code slightly, this was achieved, and the baseline engine and vehicle system results could be consistently obtained through a single run. Then,FASST needed to be prevented from resizing when an improved inlet was installed, as the sizing algorithm consistently wanted to downsize the engine and vehicle due to improved thrust.
The addition of the ability to prevent downsizing was beneficial in that improved inlet maps (from the baseline) could be added the model and run in the off-design condition to achieve the desired result, while maintaining the same initial baseline engine. To the knowledge of the researchers, this effort had not been considered with the FASST framework prior to this work, and it required substantial trial and error to ensure consistent results and the final off-design cycle data passed through to ANOPP for the noise performance prediction.

The primary tool utilized to model jet noise in the context of this research is the Stone Jet Noise module (hereafter referred to as ST2JET), developed by the NASA Glenn Research Center as an adjunct module to predict jet noise and suppression device effects outlined in a technical manual, found in reference (Stone et al., 2009). The Stone Jet Noise module was developed over several years, using a combination of experimental and analytical techniques, serving effectively as a hybrid predictive noise model to provide detailed suppressed jet noise predictions for subsonic and supersonic applications. Additionally, the module has provision for plug nozzles, which is what was selected for use in the SST vehicle which was employed in this study.

Since the model was able to model supersonic nozzle flow, plug nozzles, and had a parametric chevron suppression model, and integrated directly with NASA's ANOPP tool, it served as the ideal jet noise prediction environment to perform the studies presented here. Earlier versions of the Stone Jet Noise model, which were carried over into the most recent

version, ST2JET, included the initial development of jet noise prediction models which would serve to predict noise suppression based on the previously described wetted perimeter ratio and specific noise components. These components include mixing noise components (i.e., intermediate scale, large scale and small scales), and shock noise components (i.e., inner and outer streams), merged mixing noise, and plug separation noise. It should be noted that not all of these effects are seen by all aircraft. For example, inner stream plug separation noise only appears for high bypass ratio and low mixed jet velocity nozzles and operating conditions, so likely not applicable for most small SSTs (Stone et al., 2004). Additionally, certain elements, including plug and downstream shock noise are mitigated entirely by the presence of suppression modification to nozzle exit planes (Stone et al., 2004). Many different nozzle configurations for single and dual-flow nozzles with chevrons were compared against supersonic and subsonic experimental data produced for NASA (Janardan et al., 2000), with good agreement across the ranges of operation which were considered.

Chevron Modeling Approach

It should be noted that the primary objective of the work presented here was to determine if supersonic 2D inlet configurations with variable geometry provisions would be able to provide sufficient increased mass flowrates with minimal separation losses during the LTO conditions, when chevrons or other noise suppression devices are added, such that they can overcome the loss of thrust introduced by the suppression devices, while maintaining the noise benefit gained by them at the proposed conditions. In this work, other types of noise are neglected, and only jet noise is analyzed for impact with regards to chevron and inlet installation on the previously described engine and vehicle system. Since this was the chief objective, it was determined that the precise modeling and matching of specific chevrons and their performances was not necessary. However, it was necessary to select and model jet noise suppression devices in a way that affected both jet noise and thrust proportionally. For example, if an arbitrary jet noise reduction device was selected to be implemented which created jet noise benefit but introduced no thrust degradation. It is likely that the laws of physics were somehow violated. Similarly, if too large a thrust degradation was introduced for a jet noise reduction model, with too little of a jet noise benefit, it is unlikely that such a device would ever be selected as a candidate to be installed on an SST to begin with. As a result, it was crucial to identify some nozzle-based jet noise reduction models which captured behavior between these two extremes. To do this, the public literature regarding jet noise reduction devices was extensively reviewed to ensure that thrust loss and noise benefits obtained by the chevron types selected and described in the previous section were (a) reasonable with regards to the thrust degradation and noise benefit ratio and (b) could be modeled reasonably with the tools available. The development of the ST2JET noise model regressions is well developed and explained in references (Stone et al., 2009; Stone et al., 2004; Stone et al., 2003; Stone, 2001), but are extensive and are thus beyond the scope of the study presented here.

The chevron geometries selected to modify the round plug nozzle employed by the GT-ASDL SST engine to achieve a realistic noise-thrust relationship were based primarily on the Frate and Khavaran geometries also described in the previous section. Although those chevrons were adapted to a fighter jet converging-diverging nozzle, the NASA and Office of Naval Research/Naval Research Laboratory efforts to identify jet noise reduction methods for F404 engines were the only chevron-based experiments found in public literature with clear geometry schematics and definitions, thrust degradation and noise reduction performance results, and experimental operating conditions. Several extensions of initial studies by Henderson and Bridges (2010), using the F404 style supersonic tactical nozzle can be seen in Lui (2021), Frate & Khavaran (2011), Liu et al. (2022), and Rodriguez et al. (2022). The general chevron parametrization scheme incorporates penetration depth and length as fractions of round nozzle diameter, and width scaled by the width of the nozzle facet. An example of an experimental chevron nozzle used in this series of studies is shown in Figure 36. While these chevrons were created for use on an F404 converging-diverging nozzle of a smaller scale, their performance values and geometries were selected to be used and adapted for use on the GT-ASDL SST nozzle, which uses a different configuration—a converging-diverging plug nozzle. Although these nozzles utilize different architectures, the nozzle area ratios seen by converging-diverging nozzles and the plug nozzle used in this study are very similar in the take-off condition in which the nozzle jet is overexpanded.

Figure 36. Chevron nozzle with removable chevrons from experimental study (Henderson & Bridges, 2010).

Some modeling limitations when adapting the Frate and Khavaran chevrons were experienced. First, the chevrons employed in the F404 studies impinged on the jet stream, which is commonly seen across the F404-style chevron studies, which can be seen in the studies listed previously. This creates a smaller effective exit area, which influences jet velocity, and likely, thrust. Although a parametric modification to the effective A_9 to simulate the impingement of the chevrons was attempted to be modeled, it was not able to be achieved within the time required for the completion of the work presented here. However, the nozzle area ratio (A_9/A_8) was found to be similar for the overexpanded cases during take-off, which likely would result in little effect from the impingement effects with regards to effects on expanded jet velocity and thrust.

Additionally, the plug nozzle employed in the GT-ASDL SST model utilizes a translating plug which attempts to achieve perfect exhaust expansion across most operating conditions. As such, when the area was reduced during the work to modify the throat area due to chevron addition, the plug would consistently translate to maintain an area that would yield a similar overexpansion condition of the jet during take-off. To determine the effects of chevron impingement fully, future work would need to be completed to affect the throat area, A_8, and the nozzle effective exit area, A_9, and determine the second-order effects which propagate from it.

However, some slight impingement can be observed in the installation of chevrons within the Stone Jet modeling documentation (this can be seen in one of the schematics of a validation case nozzle configuration used in Janardan et al. [2000], shown in Figure 37), and thus to some extent it can be assumed that a reduction in area introduced by chevrons is already incorporated into the semi-empirical relationships developed in Stone et al. (2003) and Stone (2001). Here, it is stated that the model assumes the chevron contour "is a smooth continuation upstream of the original exit plane" (Stone, 2001), and in the same paragraph, the authors briefly discuss how penetration (impingement) of the chevrons are proprietary in their model, but "acknowledged to be in the order of boundary layer thickness" (Stone, 2001). Due to this linguistic ambiguity, it is somewhat unclear whether the penetration effects are fully captured in the ST2JET chevron models. While the penetration utilized in the model presented here is much more significant, it is only notional in the sense that it is only reflected in the model by the PER ratio (an overall perimeter ratio), and as such can simply represent a longer, and not deeper penetrating chevron. As a result, this limitation is assumed to have a negligible effect, unless trying to precisely match the performance of the F404 chevrons presented by Frate and Khavaran. The definition of the PER ratio utilized by the researchers and applied in the ST2JET module using Equation 3, assuming the nozzles described in both the numerator and denominator have the same round (baseline) geometry, and chevrons serve as an addition or augment. While generalized equations to determine the PER value are found in Stone et al. (2009), the relationship can be simply defined as such:

$$PER = \frac{Perimeter\ of\ chevron\ nozzle\ including\ plug\ perimeter}{Perimeter\ of\ round\ nozzle\ including\ plug\ perimeter} \quad \text{(Eq. 3)}$$

Another modeling limitation can be seen in the fact that the chevrons in the nozzle configuration employed in the study here were attached to the throat (see Figure 37). Chevrons in the F404-style converging-diverging nozzle types are attached at the nozzle exit, which likely produces a different effect in both noise benefit and thrust degradation; however,

since the models implemented by the experiments which informed and validated the ST2JET module utilized throat-attached chevrons in their installation, it was assumed that such a configuration for the supersonic plug nozzle is both acceptable and standard. The primary concern regarding this limitation is that the chevrons from Frate and Khavaran utilized for the study cannot be explicitly matched, which is a similar problem to the first limitation.

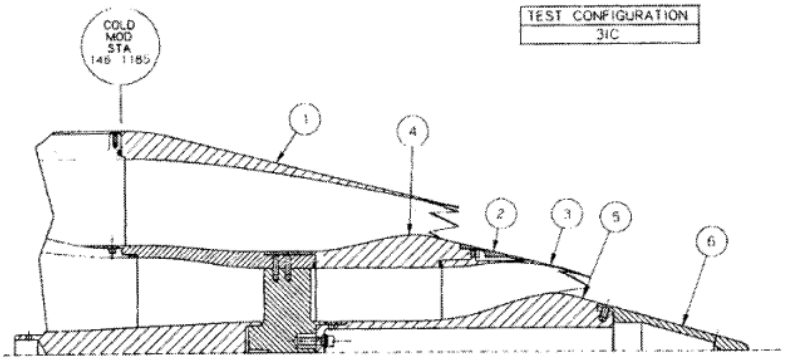

Figure 37. Chevron nozzle test configuration 3IC from Janardan et al. (2000), used in validation for Stone et al. (2004).

Since these modeling limitations exist, and the chevron geometry which was employed in this study cannot match a published model precisely, it was necessary to perform a comparison against other chevrons. This was primarily to understand the chevrons' performance and installation-level impacts on thrust and noise, and to understand whether the chevron models employed in the study here were reasonable and would yield sufficient insight when installed in a broader system level analysis. These comparison results are presented in Figure 38, after the results of the study are shown, for a clear comparison of reasonability. Further discussion regarding the limitations and their effects is provided in the next section.

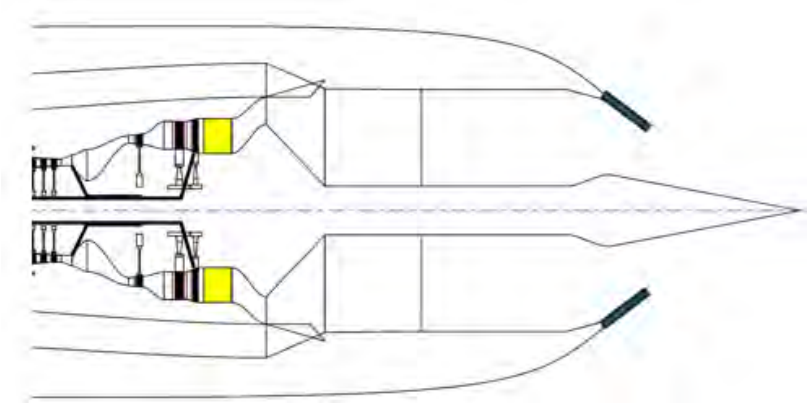

Figure 38. WATE++[2] Schematic of GT-ASDL plug nozzle with notional chevrons for visualization.

Chevron Model Development

As previously discussed, the selection of chevrons to be implemented into the study presented here required the satisfaction of several factors. First, the chevron model needed to be adaptable to the round (clean) plug nozzle under consideration and shown, in the manner presented in Figure 37. While the placement of the chevrons at the plug nozzle throat did not affect the flow area or downstream thermodynamics, as mentioned as a modeling limitation, the throat is the functionally correct position for the chevrons on this nozzle design, and as such, this needed to be utilized for the determination of the PER variable. Second, the chevron PER ratio could not exceed 1.5 as discussed in Stone et al. (2009).

[2] WATE++ is an object-oriented computer code for gas turbine engine weight analysis.

The documentation for the ST2JET module claims that while the model can provide nominal accuracy in prediction up to PER=2.0, the values between 1.5 and 2.0 are extrapolated from experimental data. As a result, chevron sizes needed to provide a wetted chevron to round nozzle (inclusive of plug circumference) perimeter ratio of less than 1.5. Additionally, the chevron models to be adapted for the purposes of this study needed to have results for thrust loss (to be employed in the study as a C_{fg}factor) and noise reduction values (for comparison and verification with the study results which used the ST2JET module). Lastly, the geometry in the literature accompanying the chevron performance data needed to provide a facet width to properly parameterize and scale the chevron width based on the nondimensional values provided.

Of all of the literature surveyed and described in the previous section, the chevron models from Frate and Khavaran were selected to be adapted to the full-scale model used on the GT-ASDL SST engine. The chevron geometries from Frate and Khavaran (2011) were normalized by round nozzle exit diameter and scaled to the GT-ASDL SST nozzle size. In the study, 12 chevrons were used, each placed on a standard facet of the F404 nozzle, with a small gap introduced by the variable geometry nozzle, referred to as a facet gap. This gap needed to be included in the overall calculation of the PER value in order to arrive at an accurate noise reduction value. As a note, ST2JET does not model chevron gaps, and assumes the chevrons are placed flush against one another—supersonic chevrons in this configuration could not be ascertained, so the chevron gaps were included in the PER calculation, despite the inevitable introduction of some deviation from noise reduction performance seen by the Frate and Khavaran chevrons. This was deemed acceptable in the adaptation of these chevron models for two reasons. First, since the only geometry variable seen by the NPSS and ANOPP model is the PER value, it can be understood that the chevrons modeled by the ST2JET module are of a similar shape, but individually smaller, to cover the overall gaps which are seen in the Frate and Khavaran nozzle configurations. As a result, this will lead to a lower noise benefit calculation, which was deemed acceptable, since the concern in adapting an experimental model to the model at hand was potentially having a disproportionately large noise benefit. Second, the chevrons adapted for the models presented here for the thrust recovery study only need to be similar in performance to the experimental ones, and an exact match between the two models was not possible to begin with.

After the geometries of the Frate and Khavaran chevrons were scaled to the size of the GT-ASDL SST nozzle, the PER values inclusive of plug perimeter were calculated, and a gross thrust coefficient, C_{fg}, were calculated for all the scaled chevron models. A summary of the baseline chevron geometries and the related geometry and performance values are seen in Figure 4, along with the scaled versions of the same chevron designs, denoted as “scaled.” Inclusive of the plug circumference (which is specified in the ST2JET documentation, as well as in Stone et al. [2009]), the PER values for all these chevrons are nearly all above 1.5, except for two, P03L08W06 and P03L08W10, which are highlighted in Table 8; these were selected to serve as the basis for the chevrons utilized for the inlet thrust recovery study. As can be seen here, gross thrust coefficients are assumed to be constant with an increase in size (which will be discussed in a later section), and the PER values are constant, since the chevron geometries were normalized by the nozzle exit diameter and a plug was included using the same hub-to-tip ratio as the GT-ASDL SST nozzle.

Table 8. Frate and Khavaran adapted chevron geometry values and scaled to GT-ASDL SST nozzle size (Frate & Khavaran, 2011).

Chevron Name	Penetration [inches]	Length [inches]	Width [%D_9]	Width [inches]	Chev. Leg Length [inches]	Chevron Perimeter Each [inches]	Total Perimeter of Chevrons [inches]	Total Perimeter with Plug [inches]	PER1 no plug	PER1 with Plug	C_{fg}
P05L13W08	0.45	1.25	80	0.8592	1.3218	2.7925	33.5104	41.7694	2.2952	1.9752	0.9842
P03L08W06	0.3	0.75	60	0.6444	0.8163	1.7393	20.8719	29.1310	1.5015	1.3775	0.9850
P03L08W10	0.3	0.75	100	1.0740	0.9224	1.9400	23.2796	31.5387	1.6527	1.4914	0.9814
P03L18W06	0.3	1.75	60	0.6444	1.7794	3.6091	43.3086	51.5677	2.9107	2.4385	0.9897
P03L18W10	0.3	1.75	100	1.0740	1.8305	3.7099	44.5190	52.7780	2.9867	2.4958	0.9889
P06L08W06	0.6	0.75	60	0.6444	0.8163	2.0261	24.3137	32.5728	1.7176	1.5403	0.9434
P06L08W10	0.6	0.75	100	1.0740	0.9224	2.2008	26.4095	34.6685	1.8493	1.6394	0.9274
P06L18W06	0.6	1.75	60	0.6444	1.7794	3.7557	45.0684	53.3274	3.0212	2.5217	0.9793
P06L18W10	0.6	1.75	100	1.0740	1.8305	3.8527	46.2327	54.4917	3.0943	2.5768	0.9716

Chevron Name	Penetration [inches]	Length [inches]	Width [%D_9]	Width [inches]	Chev. Leg Length [inches]	Chevron Perimeter Each [inches]	Total Perimeter of Chevrons [inches]	Total Perimeter with Plug [inches]	PER1 no plug	PER1 with Plug	C_{fg}
P02L13W08	0.2	1.25	80	0.8592	1.3218	2.6736	32.0834	40.3425	2.2056	1.9077	0.9896
P05L13W08 Scaled	3.77	10.48	80	7.2018	11.0790	23.4070	280.8840	350.1115	2.2952	1.9752	0.9842
P03L08W06 Scaled	2.51	6.29	60	5.4014	6.8421	14.5790	174.9484	244.1758	1.5015	1.3775	0.9850
P03L08W10 Scaled	2.51	6.29	100	9.0023	7.7318	16.2608	195.1299	264.3573	1.6527	1.4914	0.9814
P03L18W06 Scaled	2.51	14.67	60	5.4014	14.9151	30.2511	363.0130	432.2405	2.9107	2.4385	0.9897
P03L18W10 Scaled	2.51	14.67	100	9.0023	15.3436	31.0965	373.1584	442.3859	2.9867	2.4958	0.9889
P06L08W06 Scaled	5.03	6.29	60	5.4014	6.8421	16.9831	203.7976	273.0250	1.7176	1.5403	0.9434
P06L08W10 Scaled	5.03	6.29	100	9.0023	7.7318	18.4470	221.3644	290.5918	1.8493	1.6394	0.9274
P06L18W06 Scaled	5.03	14.67	60	5.4014	14.9151	31.4803	377.7631	446.9906	3.0212	2.5217	0.9793
P06L18W10 Scaled	5.03	14.67	100	9.0023	15.3436	32.2935	387.5225	456.7500	3.0943	2.5768	0.9716
P02L13W08 Scaled	1.68	10.48	80	7.2018	11.0790	22.4103	268.9232	338.1506	2.2056	1.9077	0.9896

An examination of the contents of Figure 39, which shows the relationship between PER ratio and thrust degradation in comparison to the round nozzle, while relationships exist that correlate the two metrics, the relationship between PER and thrust is not linear. Rather, linear relationships exist within subsets of families of chevron types when grouped by penetration and length. Intuition would dictate that a higher perimeter ratio would yield a higher thrust loss, but this is not the case. Despite this, because of the observed relationship within similar penetration and length families, this PER- C_{fg} relationship was used to develop the extrapolated family of chevrons for the study presented here.

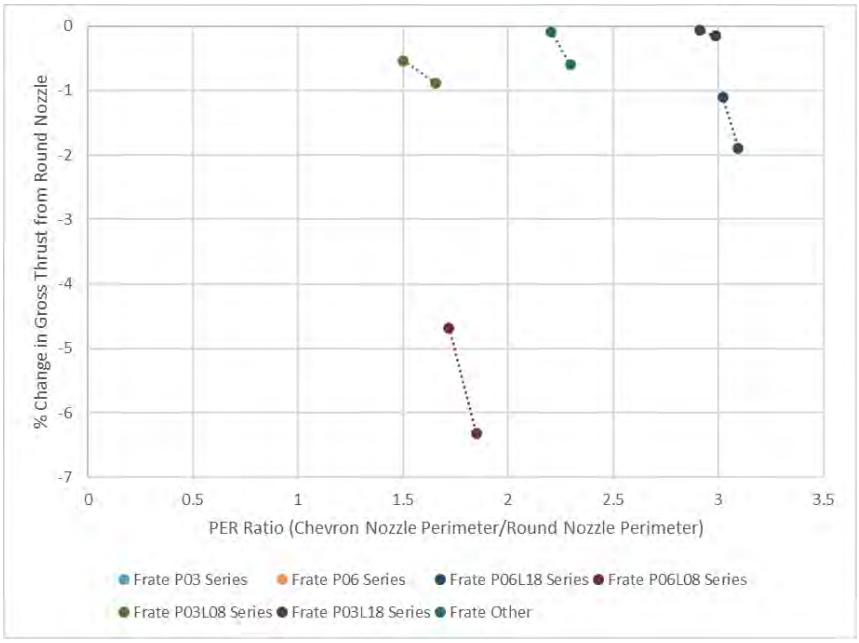

Figure 39. PER vs. change in gross thrust from baseline nozzle for unscaled Frate and Khavaran chevrons.

Using the geometry and performance data generated in the previously described step, two notional chevrons models with lower PER values were generated by linear extrapolation. The only objective with this step was to ensure that chevrons with lower PER values were obtained and evaluated with the GT-ASDL SST engine and nozzle configuration, due to the limitation

of the ST2JET module requirements for PER and the limited experimental data found in published literature pertaining to supersonic chevrons. A summary of the chevron inputs developed from the previously described steps can be seen in Table 9 and Figure 40, along with the baseline chevron. Note that the baseline nozzle is assumed to have a gross thrust coefficient, and as such, a scalar was employed to achieve the desired overall gross thrust degradation seen in the experimental data. The values in Table 9 match the selected geometry and performance values shown in Table 8.

Table 9. Summary of chevron inputs.

	PER1With Plug	CFG Scalar	CFG
Baseline	1.0000	1.0000	0.9900
Chevron 1	1.3775	0.9949	0.9850
Chevron 2	1.4914	0.9914	0.9814
Chevron 3	1.2500	0.9991	0.9890
Chevron 4	1.3000	0.9975	0.9875

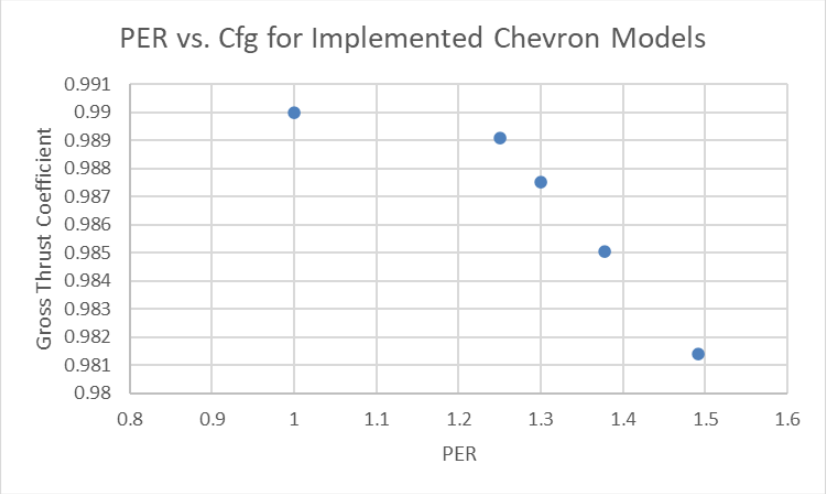

Figure 40. PER vs. C_{fg} for chevron models used in Installation study.

Baseline Chevron Installation Results, NPSS Modeling Setup, and Comparison

Upon completion of the development of the chevron models to be used in the broader study, these results needed to be evaluated against those seen in published data. As such, the chevrons were each installed on the previously described GT-ASDL SST engine with the baseline M=1.7 2D inlet with no variable geometry implemented. These individual cases serve as the baselines from which the variable geometry inlet cases were performed and compared against. After a significant amount of pre-processing to determine reasonable baseline chevron values, they were added to the NPSS and ANOPP models in the forms shown in Figure 40. The PER value is added in the FASST environment by the user, and it propagated through the runs to be used in ANOPP after the engine and vehicle performance is determined by the preceding parts of FASST (CMPGEN for compressor map generation, NPSS for engine cycle modeling and engine deck creation, and WATE++ for engine flow path calculation). The C_{fg}value is used in an off-design script, after the baseline, fixed engine and vehicle are run in the primary FASST run, in order to ensure each run uses the same engine and vehicle, with only inlet and chevron parameters changing, for a clear “apples-to-apples” comparisons between the configurations outlined in Table 7.

The ANOPP configuration selected for this study was to only consider jet noise resulting from the ST2JET module, with the ability to model shock noise turned on. The take-off model was taken from the Cutback-Approach (CBAP) output file

generated from the ANOPP after running, since it provided the most detailed take-off noise performance results with take-off conditions matching those generated by ANOPP. A custom take-off script which runs NPSS in off-design was created to model the take-off conditions defined in the FLOPS file for the baseline GT-ASDL SST vehicle. From this, the inlet and chevron nozzle inputs are added and modify the baseline engine solved earlier in the FASST run, affecting the take-off model with the desired inputs defined in the experiment run matrix in Table 7. These performance data are used in the calculation of the state tables for the ANOPP noise prediction, and as such, the take-off script performance output and the ANOPP jet noise prediction of the modified engine configuration are coupled. Due to the modeling setup as described, only $C_{fg}$and PER were required to define in the framework used for the study. While it is likely that higher fidelity models could improve jet noise prediction, the level of fidelity provided by this integration was deemed acceptable due to the validation of ST2JET with similar nozzle configurations, the proven reliability of NPSS and the FASST environment in previous studies, and their physics-based coupling.

After the baseline chevron data (seen in Table 9) were generated, they were input into the FASST modeling environment as described previously. Then, the systems-level metrics sought for this study, namely change in decibel noise reduction from the baseline round nozzle using overall sound pressure level (OASPL) at a selected 110° of directivity (a common angle presented in literature used for validation), and percent change in installed thrust from the baseline round nozzle. A summary of these values can be found in Table 10, highlighted in dark gold; the corresponding Frate and Khavaran (2011) chevron performance results are provided in light gold above them. These values are placed in the same table as a similar family of chevrons from the selected F404-style chevron nozzle studies, seen in Frate & Khavaran (2011), Liu et al. (2022), and Rodriguez et al. (2022). In the cases of the chevrons from Liu et al. (2022) and Rodriguez et al. (2022), detailed geometry was not provided regarding facet width and facet gap width.

Table 10. GT-ASDL and example F-404 style chevron geometry and performance results.

Run	Penetration [$\%D_9$]	Length [$\%D_9$]	Width [$\%L_F$]	PER	NPR	D_9 [in]	L_f [in]	$\%\ \Delta F_g$	ΔdB OASPL @110°	Reference
P06L20W100	6	20	100%	2.57	2.7	1.450	0.3072	-0.7600	-0.1764	Rodriguez [29]
P06L20W100	6	20	100%	2.57	3.0	1.450	0.3072	-0.61%	-1.6294	Rodriguez [29]
P08L20W100	8	20	100%	2.60	2.7	1.450	0.3072	-1.3900	-1.1764	Rodriguez [29]
P12L20W100	12	20	100%	2.70	2.7	1.450	0.3072	-3.2000	-0.7794	Rodriguez [29]
P08L20W80	8.9	25	80%	2.60	2.7	1.450	0.3072	-1.0400	-1.2277	Rodriguez [29]
P10L20W100	10	20	100%	2.08	2.7	3.167	0.6711	-2.2000	-0.67702	Liu [28]
P06L20W100	6	20	100%	1.98	2.7	3.167	0.6711	-0.76	-0.8575	Liu [28]
P06L20W100	6	20	100%	1.98	3.0	3.167	0.6711	-0.61%	-0.4436	Liu [28]
P08L20W100	8	20	100%	2.02	2.7	3.167	0.6711	-1.39	N/A	Liu [28]
P05L13W08	8.87	24.66	80%	2.29	3.0	5.068	1.074	-0.6047	-1.9330	Frate [22]
P03L08W06	5.91	14.79	60%	1.50	3.0	5.068	1.074	-0.5345	-0.1835	Frate [22]
P03L08W10	5.91	14.79	100%	1.65	3.0	5.068	1.074	-0.8855	-0.4427	Frate [22]
P03L18W06	5.91	34.53	60%	2.91	3.0	5.068	1.074	-0.0647	-1.1663	Frate [22]
P03L18W10	5.91	34.53	100%	2.98	3.0	5.068	1.074	-0.1511	-1.2203	Frate [22]
P06L08W06	11.83	14.79	60%	1.71	3.0	5.068	1.074	-4.6814	-3.9956	Frate [22]
P06L08W10	11.83	14.79	100%	1.84	3.0	5.068	1.074	-6.3120	-2.9157	Frate [22]
P06L18W06	11.83	34.53	60%	3.02	3.0	5.068	1.074	-1.1015	-2.4028	Frate [22]
P06L18W10	11.83	34.53	100%	3.09	3.0	5.068	1.074	-1.8952	-2.8185	Frate [22]

Run	Penetration [$\%D_9$]	Length [$\%D_9$]	Width [$\%L_F$]	PER	NPR	D_9 [in]	L_f [in]	$\% \Delta F_g$	ΔdB OASPL @110°	Reference
P02L13W08	3.94	24.66	80%	2.21	3.0	5.068	1.074	-0.0918	-0.8963	Frate [22]
Chevron 1	0.05	0.1479	60%	1.37	2.0	42.48	9.002	-0.5100	-5.1	GT-ASDL
Chevron 2	0.05	0.1479	100%	1.49	2.0	42.48	9.002	-0.8684	-6.1	GT-ASDL
Chevron 3	Notional	Notional	Notional	1.25	2.0	42.48	9.002	-0.0910	-3.7	GT-ASDL
Chevron 4	Notional	Notional	Notional	1.30	2.0	42.48	9.002	-0.2520	-4.3	GT-ASDL

Frate, F., & Khavaran, A. (2011, January 4-7). *An aerodynamic and acoustic assessment of convergent-divergent nozzles with Chevrons* [Conference paper]. 49th AIAA Aerospace Sciences Meeting including the New Horizons Forum and Aerospace Exposition, Orlando, Florida. https://doi.org/10.2514/6.2011-976

Liu, J., Khine, Y. Y., Saleem, M., Rodriguez, O. L., & Gutmark, E. (2022, June 14-17). *Comparison of the Thrust-Based Noise Reduction Performance between Micro-vortex Generators and Chevrons* [Conference presentation]. 28th AIAA/CEAS Aeroacoustics Conference, Southampton, United Kingdom. https://doi.org/10.2514/6.2022-2970

Rodriguez, O. L., Saleem, M., Gutmark, E., & Liu, J. (2022, January 3-7). *Implementation of chevrons as a noise reduction system for a supersonic tactical nozzle* [Conference presentation]. AIAA SciTech 2022 Forum, San Diego, California, & virtual. https://doi.org/10.2514/6.2022-0682

As a result, the detailed geometry from Frate and Khavaran (2011) was utilized to obtain a related PER value for comparison. As the same nozzle configuration (i.e., axisymmetric, 12-facet, variable geometry, converging-diverging F404 style nozzle) with a similar schematic, is shared across the aforementioned studies, it was assumed this was an acceptable approach. In comparing the GT-ASDL chevron geometries to the published ones, a significant increase in noise reduction is achieved, despite the PER value being notably smaller than most of the other chevrons listed, while the thrust loss is more or less in family with the other chevrons shown. This result can be seen in Table 10 and Figure 41. There are several potential explanations for this phenomenon. First, the difference in size from the nearest nozzle, used by Frate and Khavaran (2011), is nearly 8.5 times smaller than the full-size nozzle used in the study presented here. By investigation into the studies which presented the results in Table 10 and Figure 41 it can be found that operating conditions, nozzle size, and experimentation setup likely all have an effect on predicted sound level.

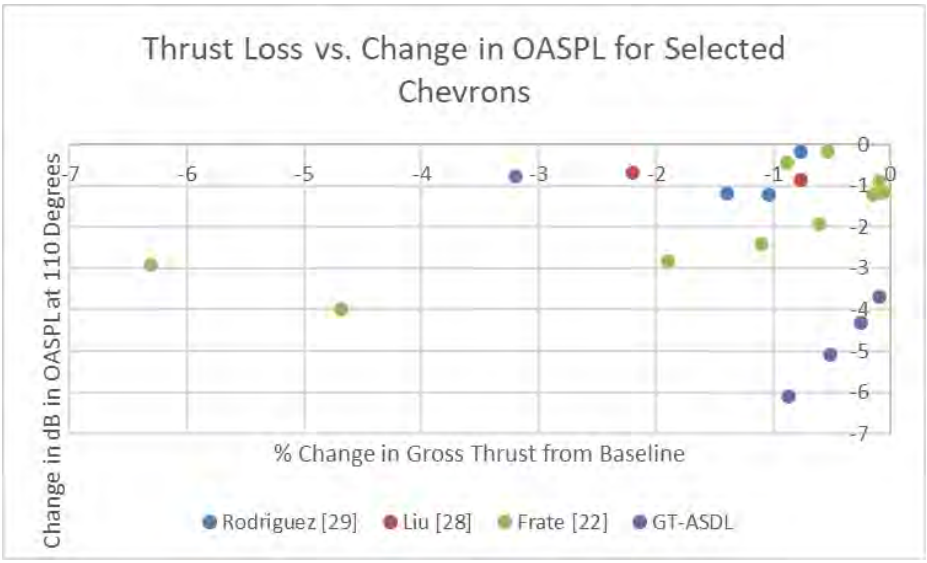

Figure 41. Thrust loss vs. change in OASPL at 110° for selected chevrons.

For identical chevron configurations defined in Rodriguez et al. (2022) and Liu et al. (2022) for the P06L20W100 chevron nozzle, it can be seen that variations occur in OASPL measured at 110° of directivity, when the nozzle pressure ratio (NPR) and nozzle diameter are measured. These experiments are an excellent comparison point to try to understand the basic effects of geometry and operating conditions on chevrons, since both experiments (1) use the same chevron parametrization for length, width, and penetration, (2) use the same NPR, NTR, freestream Mach number operating conditions, (3) use identical nozzle area ratios between the throat and nozzle exit areas, and (4) they are attached to an identical format, but different sized nozzle. It should also be noted that these studies both utilized large eddy simulations (LES) for determination of thrust loss, but Rodriguez et al. (2022) employed an acoustic test rig for physical experimental data. As such, those data are trusted more when considering the effect of change of NPR on the OASPL reduction values. Regardless of accuracy, it can be seen that for identical models, significant differences in OASPL reduction can be seen both as a function of nozzle size, and operating conditions, namely NPR. Conversely, when comparing these papers, the difference in gross thrust for the different sized nozzles in these studies remains the same. The observations discussed here can be gleaned in Figure 42.

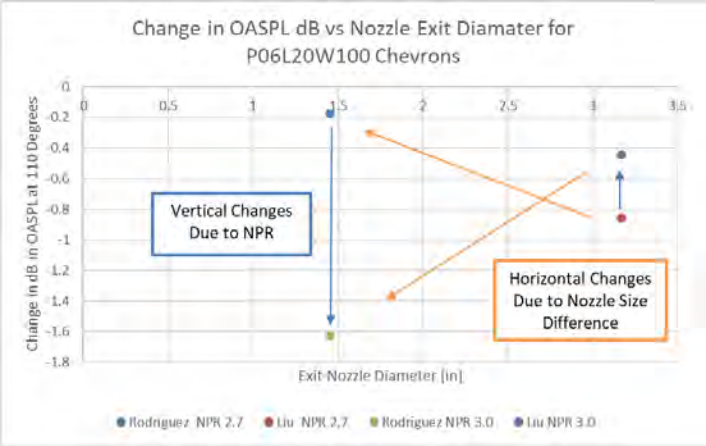

Figure 42. Noise reduction vs. nozzle exit diameter for P06L20W100 chevrons of the two studies performed, comparing Liu and Rodriguez based chevron designs.

Upon further inspection of the results presented in Table 10, it can be postulated that nozzle size is a key driver in jet noise reduction. As mentioned previously, the GT-ASDL chevron nozzles achieve substantially better jet noise reduction performance than smaller nozzles; it is not immediately clear if noise reduction is heavily dependent on nozzle exit area and overall scale effects. For this reason, a normalized metric was sought to determine if the noise reduction levels from literature and those found from the study at hand related to primarily to nozzle size, and secondarily to chevron geometry and size (both of which are related parameters). It is shown in Figure 43 that each group of chevrons (including the previously analyzed families of Frate chevrons, shown in Figure 39) generally yields a trend of increasing normalized jet noise reduction with increasing values of PER. The trend has outliers, and this is typically because (a) in the case of the best-performing Frate chevrons, the PER values are very low and it can be seen that higher values of penetration with shorter length affects the flow at the exit plane more significantly than other chevron geometries in the group, and (b) potential experimental deviations seen in the directivity trend seen in Liu et al. (2022), seen in red in Figure 43. Another observation is that the GT-ASDL chevrons selected, while lower in PER values compared to the other chevrons, yield a similar normalized jet noise reduction level to several other chevrons. In this way, our team has effectively confirmed that the chevrons which were modeled here are both acceptable in thrust degradation and jet noise reduction performance, when size effects are considered. Lastly, to confirm the validity of the noise reduction model, we will consider two other performance trends of the chevron nozzles utilized for the study at hand, noise composition breakdown, and an OASPL directivity comparison against other many other chevrons to identify some trends and close the book on verification and comparison of the GT-ASDL chevron models.

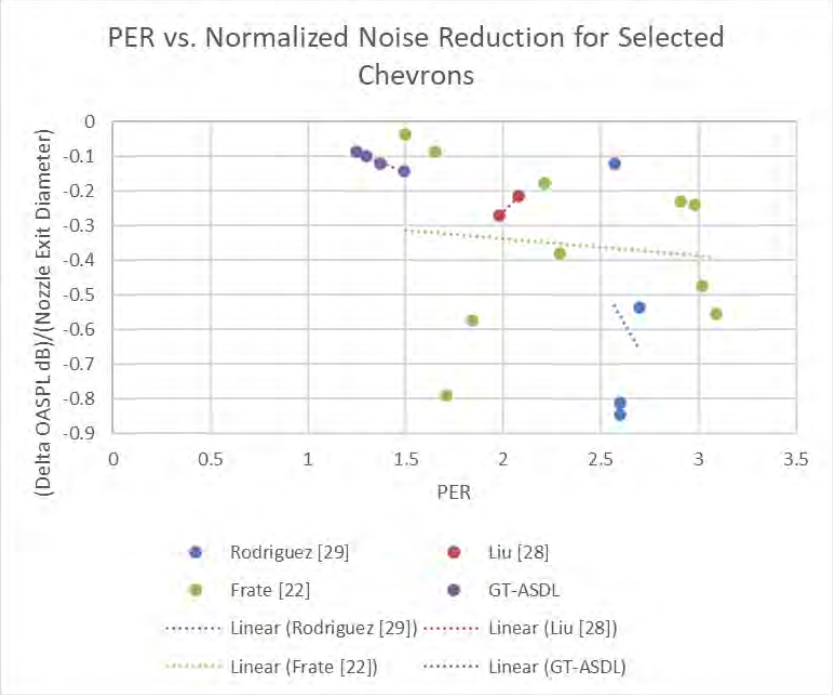

Figure 43. Normalized Jet Noise Reduction vs. PER.

An examination of a standard directivity angle vs. OASPL noise reduction plot is shown in Figure 44. While not initially obvious, the chevron trends for the GT-ASDL chevrons (labeled chevrons 1-4) are roughly similar to those of Liu et al. (2022), with a delayed dip in performance. The trends in Liu et al. (2022) were recorded at a smaller set of directivity angles, which prevents more comprehensive understanding of the trends. Additionally, the curves from Liu et al. (2022) dip lowest towards the standard observation angle of 110°, where the experimental ones are lowest closer to 0°. A final observation is from the supersonic jet from Chen et al. (2024). Despite employing an unrelated chevron geometry (on a supersonic cold conical nozzle), the magnitudes of noise reduction are fairly similar to a median of what was obtained through chevrons 1-4 (see Figure 44). Additionally, with Chen et al. (2024) and Liu et al. (2022), their Mach numbers at the nozzle exhaust plane are 1.2 and ~1.5, respectively. They also both experience shocks—as will be discussed here, the Mach number in the nozzle exhaust plane for the experimental chevrons with plug nozzle is, on average, very close to 1.01 and has no shock noise component for take-off from the ANOPP predictions. As such, the difference in chevron and nozzle geometry and operating conditions can also likely be attributed to the lack of shock in the experimental nozzle results.

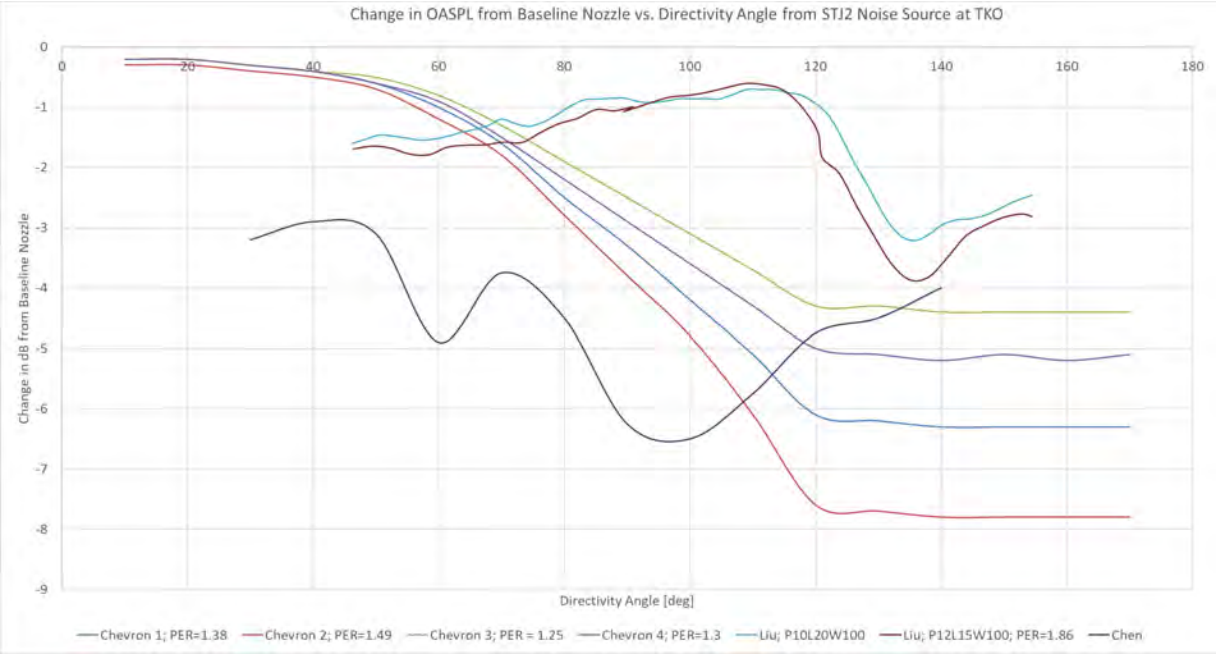

Figure 44. Directivity angle vs. OASPL noise reduction for a selection of chevrons.

After sufficient investigation and comparison, it was determined that the chevron models utilized for the GT-ASDL SST engine and vehicle models were reasonable and deviation from nearest points of comparison were justifiable. It was found that the normalized baseline chevron jet noise reduction values were similar in magnitude to experimental values, thrust loss magnitudes correspond well to other chevron nozzles even of different scales and operating conditions, variations in operating condition and size contributed most to deviation. Most importantly, it was determined that the differences from (deltas) across chevron performance data need to be reasonably accurate, which it seems to be.

Inlet Thrust Loss Mitigation Study

Recall from the initial discussion in earlier sections of this report that the primary objective of the research was to identify whether a variable geometry supersonic inlet which performs well at cruise could potentially mitigate the drawbacks associated with jet noise reduction devices at LTO (effects on other segments not considered here). To do this, an inlet was designed with three modes of variable geometry which could allow for higher mass flow into the engine with lower duct and separation losses at low speeds—a VGCL, blow-in doors, and a hybrid mode which enabled both. Separate inlet maps were created using a process defined by SIPC, an inlet design and analysis tool developed for the completion of this task. Nozzles were modeled and added to the NPSS and ANOPP models to model the effects of chevrons on noise and thrust, and the installed combinations of these inlets and nozzles were implemented and modeled in the FASST integrated modeling environment to obtain results comparing noise and thrust degradation compared to a round nozzle with the baseline inlet using no variable geometry (the baseline case). Some important results of the study are shown in Figure 45.

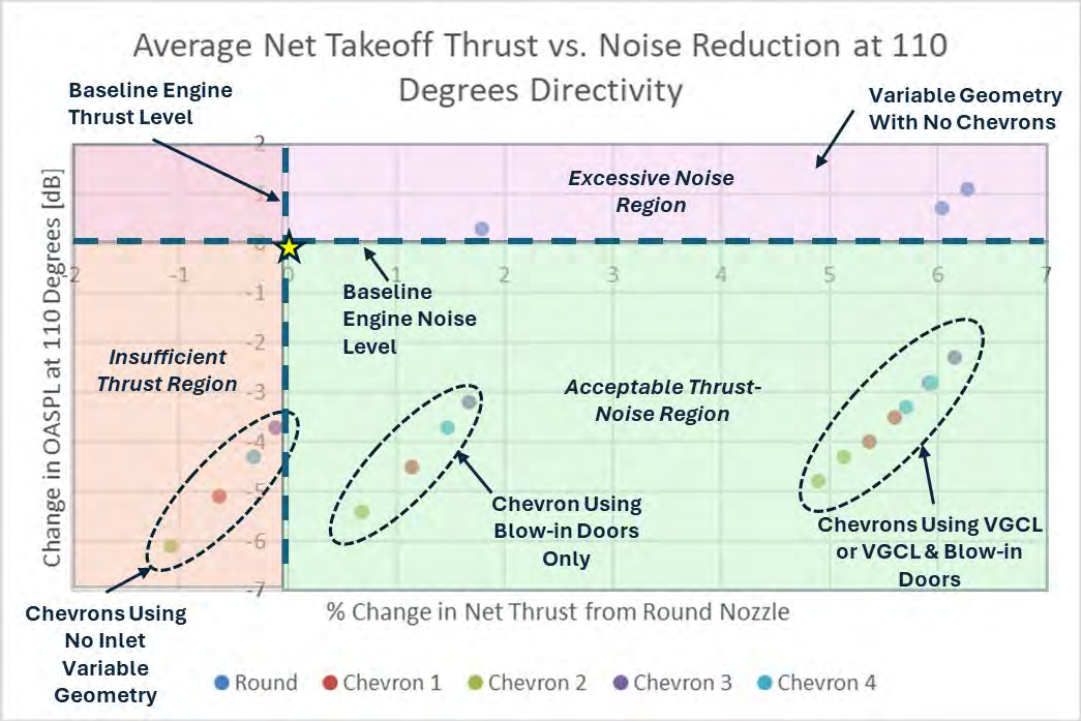

Figure 45. Average net take-off thrust vs. noise reduction at 110° directivity.

In Figure 45, the percent change in average installed (gross thrust – inlet ram drag – inlet drags) net thrust compared to change in OASPL at 110° directivity in decibels is presented. Several visual overlays have been added to the basic chart to aid in explaining the results. The results of thrust-noise relationship points were color-coded by the chevron type and their respective inlet types are grouped and identified using arrows. It can be seen here that the pink-shaded area above 0 dB change in OASPL is labeled the excessive noise region; this is because, if chevrons are being implemented on SST, achieving worse noise performance is unacceptable. Similarly, the orange-shaded area to the left is the insufficient thrust region, which is to the left of the 0% change in net thrust from round nozzle line (vertical axis). If an installation performs worse than the baseline case, it is an unacceptable configuration for the aircraft. A star marks the origin simply for quick reference since the axes are not bright due to the region overlays. We can see that, as predicted, for the cases in which engine has chevrons installed, but the inlet is not using any variable geometry, the noise reduction is excellent, but the thrust introduced by the chevrons cannot be overcome. Similarly, some points appear in the excessive noise region, and upon investigation, these are the variable geometry cases which employ no chevrons to mitigate increased jet noise as a result of increased mass flow into the engine. The remaining points exist within the acceptable thrust-noise region in which thrust degradation and noise benefit is equal to or greater than the baseline configuration. On the lower left side of the acceptable thrust region, the four cases which use blow-in doors only have good noise befit compared to the baseline, but only slight improvement in thrust over it. This follows logically, since the blow-in doors were limited in the inlet model to take in a small amount of air to prevent excessive noise which can be introduced by inlet blow-in doors positioned near the fan face. Lastly, a mix of chevron cases which use either the VGCL alone, or VGCL and blow-in doors together are observed. They provide significant improvements in thrust and maintain nearly the same noise level as the blow-in door cases.

Similar graphics were developed for the net take-off thrust vs. noise reduction at 60° and 90° of directivity as shown in Figure 46 and Figure 47. However, in these charts, the results are more complicated. While the regions previously defined remain intact, and the relative improvement in net take-off thrust has remained the same, the level of noise reduction has reduced dramatically, and as a result, most of the VGCL and hybrid VGCL/blow-in door cases are in the excessive noise region at this angle of directivity. At this angle of observation, only the chevron cases with blow-in doors are operating in the acceptable noise region.

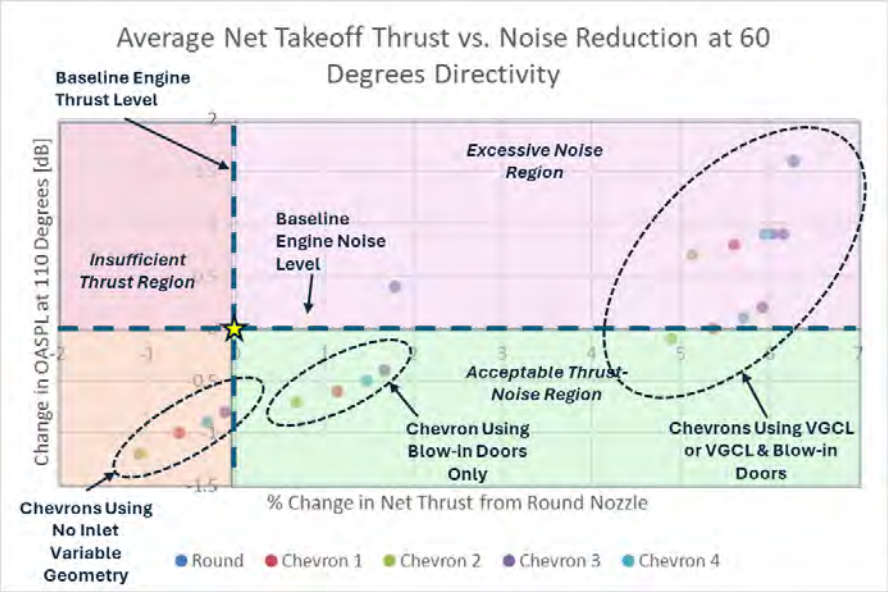

Figure 46. Average net take-off thrust vs. change in jet noise at 60° directivity.

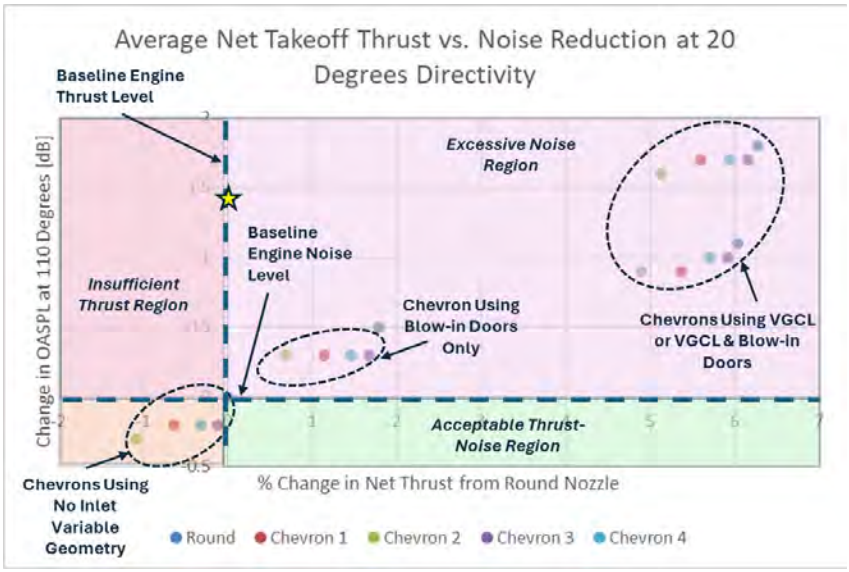

Figure 47. Average net take-off thrust vs. change in jet noise at 20° directivity.

Similarly, we see an even more interesting result in Figure 47 for the same study for 20° directivity. Here, the noise reductions, even with the chevrons, are not sufficient to break even with the baseline case if they use inlet variable geometry. And the cases which use chevrons, but no inlet variable geometry produce acceptable noise benefit, cannot produce sufficient thrust to enable the vehicle to take-off (break even with the baseline case). This trend of seeing worse noise benefit as the directivity angle decreases towards zero is shown in Figure 48, which shows the change in OASPL at various directivity angles for the different cases examined in this study. As Figure 44 shows, the general trend for the nozzle with jet stream noise benefit increases as directivity angle increases. Most inlet and nozzle combinations have worse noise performance than the baseline case for directivity angles between 10° and 60°. The linear-shaped results

above the noise breakeven line are attributed to the cases which utilize variable geometry inlet configurations with no chevrons and should be ignored when determining thrust-noise behavior of the proposed engine installations.

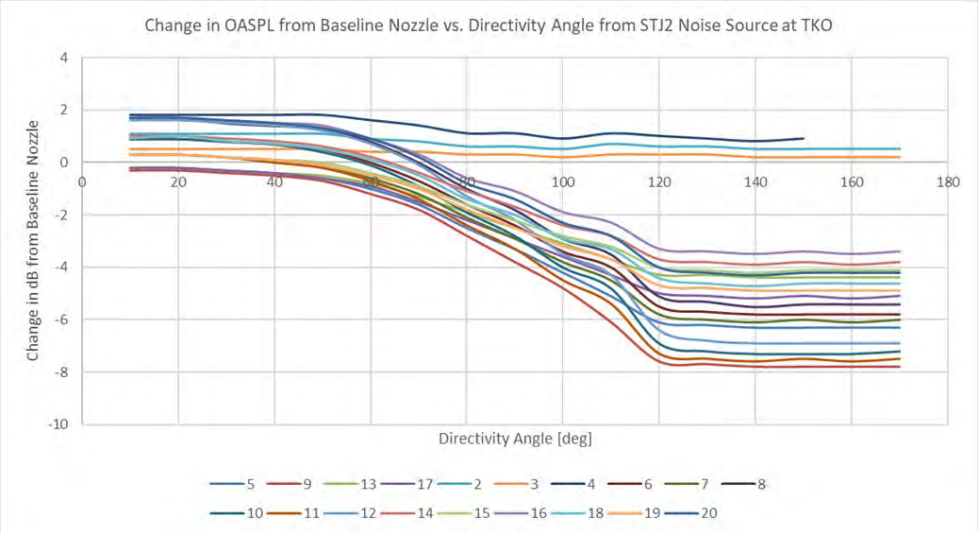

1	Baseline	Round
2	VGCL	Round
3	BlowIn	Round
4	BlowInVGCL	Round
5	Baseline	Chevron1
6	VGCL	Chevron1
7	BlowIn	Chevron1
8	BlowInVGCL	Chevron1
9	Baseline	Chevron2
10	VGCL	Chevron2
11	BlowIn	Chevron2
12	BlowInVGCL	Chevron2
13	Baseline	Chevron3
14	VGCL	Chevron3
15	BlowIn	Chevron3
16	BlowInVGCL	Chevron3
17	Baseline	Chevron4
18	VGCL	Chevron4
19	BlowIn	Chevron4
20	BlowInVGCL	Chevron4

Figure 48. Change in OASPL from baseline nozzle [dB] vs. directivity angle θ for all tested installation configurations.

Discussion and Conclusions

Based on the results shown in Figures 45 to 48, several takeaways can be identified:

- Variable geometry inlet configurations are capable of overcoming the losses introduced by a notional set of chevrons added to a supersonic engine nozzle at take-off conditions.
- The blow-in door model maintains a strong noise reduction performance and still ensures sufficient thrust benefit to break even with the losses introduced by the chevrons (in most cases, perform slightly better).
- The VGCL and VGCL/blow-in door hybrid configurations of inlet variable geometry produce high levels of thrust improvement, but at the expense of noise increase.
  - The rate of increase in noise (decrease in noise benefit) seen with these configurations was better than anticipated (low decrease in noise benefit for much higher thrust).
- As observed in Figures 46 to 48, nearly all inlet/chevron configurations experienced noise degradation from the baseline for directivity angles between 10° and 60°.
  - It is unclear whether this quality would render the inlet variable geometry incapable of performing the task of overcoming the thrust and enabling a breakeven with the baseline noise performance (i.e., the louder nozzle across 50° of directivity is acceptable and the other directivity angles are more important (or the inverse could be true, as well).
  - Investigation into this could be accomplished with future work.
- Since the chevron models and variable geometry models implemented are notional and based on studies into published literature and engineering assessments, it is possible other better performing chevrons or better performing installation combinations exist which could fully mitigate the effects seen in the lower directivity angles.
- Chevron models were only adapted from literature because of the inability to obtain relevant jet noise and thrust relationships from other ASCENT Project 059 partners, as initially anticipated—future work should incorporate the addition of experimental data with new jet noise reduction techniques.
  - Literature has been published regarding microvortex generators and tab devices which could also be modeled at low effort to perform a similar but lower fidelity function.
- The noise analysis was performed at a single point ~9 ft in altitude from the lift-off point of the aircraft—further analysis could be completed to identify a more comprehensive set of data.
- The development of the inlet design and analysis code proved to be the most demanding component of the project, taking nearly two and a half years to complete; the proper adaptation of chevron models and their

justification and comparison to those in published literature, as well as the development of the overall study framework was a close second in complexity

Parting Thoughts
The Georgia Tech team would like to thank the FAA ASCENT community and leadership for their support, guidance and understanding in the completion of this project over the last four years. This project has supported several students through their graduate careers and ultimately turned one into a full-time research engineer at Georgia Tech. We are grateful for the opportunity to work on this project and attempt to contribute to the field of civil aviation and supersonics.

Milestone

- Completed the full thrust recovery and noise effects study.
- Completed the presentation and analysis of the final results.

Major Accomplishments

- Integrated inlet maps, and fixed engine and aircraft models to ensure functionality and confirm study procedure.
- Added chevrons for four parametrized designs defined in aforementioned reference into the NPSS nozzle element and ensured functionality.
- Integrated inlet maps, fixed engine and aircraft models, and chevron models to ensure functionality and confirm the study procedure.
- Ran a baseline engine case and established ANOPP performance values for the baseline inlet, fixed engine and aircraft, and clean nozzle (no chevrons) for a comparison datum.
- Determined necessary chevron geometry and inlet variable geometry cases to be studied.
- Performed thrust-noise degradation studies.
- Performed a comparison and analysis of selected/designed chevron nozzle models with those found in published literature.
- Identified a relevant jet noise model and parameters for inclusion in the study and performed analysis of the results.

Publications

The ASCENT Project 059(A) will seek to publish these findings at AIAA SciTech 2026 with the acknowledgement of the FAA ASCENT team's support.

Outreach Efforts

None.

Awards

None.

Student Involvement

None.

Plans for Next Period

None.

References

Aircraft Recognition Guide. (2018). *Eurofighter Typhoon*. https://www.aircraftrecognitionguide.com/eurofighter-typhoon

Anderson, J. T. (2014, May 1). *How supersonic inlets work: Details of the SR-71 mixed compression inlet geometry and operation* [Conference presentation]. 11th Aircraft Engine Historical Society (AEHS) Convention, San Diego, California. https://www.enginehistory.org/Convention/2014/SR-71Inlts/SR-71Inlts.shtml

Aviation Stack Exchange. (2021). Why do the 737-100's JT8Ds, and no others, have suck-in doors. https://aviation.stackexchange.com/questions/70316/why-do-the-737-100s-jt8ds-and-no-others-have-suck-in-doors

Barnhart, P. J. (1998). *Inlet performance analysis code developed*. NASA Research and Technology. https://ntrs.nasa.gov/search.jsp?R=20050177169

Bridges, J., & Brown, C. (2004, May 10-12). *Parametric testing of chevrons on single flow hot jets* [Conference paper]. 10th AIAA/CEAS Aeroacoustics Conference, Manchester, Great Britain.

Chen, B., Li, W., Fei, W., & Zhengwu, C. (2024). Experimental study of the noise suppression of supersonic impinging jets with chevrons. *Applied Acoustics, 221*.

Crosthwait, E. L., Kennon, I. G., & Roland, H. L. (1967). Preliminary design methodology for air-induction systems (SEG-TR-67-1). Systems Engineering Group, Research and Technology Division, Air Force Systems Command, Wright-Patterson Air Force Base, Ohio.

Dean, R. B. (1978). Reynolds number dependence of skin friction and other bulk flow variables in two-dimensional rectangular duct flow. *Journal of Fluids Engineering, 100*, 215–223.

Frate, F., & Khavaran, A. (2011, January 4-7). *An aerodynamic and acoustic assessment of convergent-divergent nozzles with Chevrons* [Conference paper]. 49th AIAA Aerospace Sciences Meeting including the New Horizons Forum and Aerospace Exposition, Orlando, Florida. https://doi.org/10.2514/6.2011-976

Henderson, B., & Bridges, J. (2010, June 7-9). *An MDOE investigation of chevrons for supersonic jet noise reduction* [Conference paper]. 16th AIAA/CEAS Aeroacoustics Conference, Stockholm, Sweden. https://doi.org/10.2514/6.2010-3926

Janardan, B.A., Hoff, G. E., Barter, J. W., Martens, S., Gliebe, P. R., Mengle, V., & Dalton, W. N. (2000). *AST critical propulsion and noise reduction technologies for future commercial subsonic engines: Separate flow exhaust system noise reduction concept evaluation* (NASA/CR-2000-2100039). General Electric Aircraft Engines and Allison Engine Company. https://ntrs.nasa.gov/api/citations/20010061345/downloads/20010061345.pdf

Karon, A. Z., & Ahuja, K. K. (2017, June 5-9). *Reduction of jet noise by the nozzle-exit boundary layer* [Conference paper]. 23rd AIAA/CEAS Aeroacoustics Conference, Denver, Colorado. https://doi.org/10.2514/6.2017-3859

Kowalski, E. J. (1979). *Computer code for estimating installed performance of aircraft gas turbine engines, Vol 1: Final report.* NASA Lewis Research Center. https://ntrs.nasa.gov/citations/19800004788

Little, J. W., & Russell, R. E. (1976, March 21-15). *Status report: Subsonic aircraft noise reduction* [Conference paper]. ASME 1976 International Gas Turbine and Fluids Engineering Conference, New Orleans, Louisiana. https://doi.org/10.1115/76-GT-116

Lui, J. (2021, August 2-6). *Supersonic jet noise reduction using micro vortex generators* [Conference presentation]. AIAA Aviation 2021 Forum, virtual. https://doi.org/10.2514/6.2021-2183

Liu, J., Khine, Y. Y., Saleem, M., Rodriguez, O. L., & Gutmark, E. (2022, June 14-17). *Comparison of the thrust-based noise reduction performance between micro-vortex generators and chevrons* [Conference presentation]. 28th AIAA/CEAS Aeroacoustics Conference, Southampton, United Kingdom. https://doi.org/10.2514/6.2022-2970

Marsh, A. H., Chapkis, R. L., & Blankenship, G. L. (1983). *Study of noise-certification standards for aircraft engines, volume 3: Selection and evaluation of engine-noise-certification concept*. Dytec Engineering Inc., Long Beach, California. https://apps.dtic.mil/sti/citations/ADA137805

McLean, J. D. (2012). *Understanding aerodynamics: Arguing from the real physics*. Wiley.

McPike, A. L. (1972). Community noise levels of the DC-10 aircraft. *Journal of Aircraft, 9*(8), 542-547. https://doi.org/10.2514/3.59033

Morris, P., McLaughlin, D., & Kuo, C-W. (2013). Noise reduction in supersonic jets by nozzle fluidic inserts. *Journal of Sound and Vibration, 332*(17), 3992-4003.

Nicolai, L. M., & Carichner, G. E. (2013). Turbine engine inlet design (Ch. 15). In *Fundamentals of Aircraft and Airship Design: Volume 1*. American Institute of Aeronautics and Astronautics (AIAA).

Rodriguez, O. L., Saleem, M., Gutmark, E., & Liu, J. (2022, January 3-7*). Implementation of chevrons as a noise reduction system for a supersonic tactical nozzle* [Conference presentation]. AIAA SciTech 2022 Forum, San Diego, California, & virtual. https://doi.org/10.2514/6.2022-0682

Seddon, J., & Goldsmith, E. L. (1999). *Intake aerodynamics*. Blackwell Science.

Seddon, J., & Goldsmith, E. L. (1993). *Practical intake aerodynamic design*. AIAA Education Series.

Seiner, J., & Gilinsky, M. (1995, June 19-22). *Nozzle thrust optimization while reducing jet noise* [Conference paper]. Fluid Dynamics Conference, San Diego, California. https://doi.org/10.2514/6.1995-2191

Slater, J. W. (2020, August 24-28). *A study of the internal aerodynamics of the Concorde inlet* [Conference presentation]. AIAA Propulsion and Energy 2020 Forum, virtual.

Stone, J. R. (2001). *Separate flow nozzle jet noise source separation and correlation extension to enhanced mixing configurations*. MTC Report to GE Aircraft Engines.

Stone, J. R., Krejsa, E. A. and Clark, B. J. (2003, January 6-9). *Semi-empirical model for coannular nozzle component noise extraction and correlation including the effects of noise reduction devices* [Conference paper]. 41st Aerospace Sciences Meeting and Exhibit, Reno, Nevada. https://doi.org/10.2514/6.2003-1060

Stone, J. R., Krejsa, E. A., & Clark, B. J. (2004). *Jet noise modeling for supersonic business jet application* (NASA/CR-2004-212984). Modern Technologies Corporation, Middleburg Heights, Ohio. https://ntrs.nasa.gov/api/citations/20040050631/downloads/20040050631.pdf

Stone, J. R., Krejsa, E. A., & Clark, B. J. (2009). *Jet noise modeling for suppressed and unsuppressed aircraft in simulated flight* (NASA/TM-2009-215524). NASA Glenn Research Center. https://ntrs.nasa.gov/api/citations/20090015381/downloads/20090015381.pdf

Tinney, C. E., Valdez, J., & Murray, N. (2020). Aerodynamic performance of augmented supersonic nozzles. Experiments in Fluids, 61(2). https://link.springer.com/article/10.1007/s00348-019-2866-3